UNIVERSITÀ DI PADOVA
DIPARTIMENTO DI FISICA E ASTRONOMIA GALILEO GALILEI
CORSO DI DOTTORATO DI RICERCA IN FISICA
XXXII CICLO

TESI DI DOTTORATO

HIKING THE ALPS: SIGNATURES AND MODELS

CANDIDATO
FEDERICO POBBE

COORDINATORE
CH.MO PROF. FRANCO SIMONETTO
RELATORE
CH.MO PROF. STEFANO RIGOLIN

ANNO ACCADEMICO 2018/2019

CONTENTS

Part I

AXIONS AND ALPS

1 INTRODUCTION

In 1977 Roberto Peccei and Helen Quinn published the paper "*CP conservation in the presence of instantons*" [1]. In this ground-breaking paper, the authors proposed an innovative and original solution to the problem of the CP conservation in the strong sector of the Standard Model (SM), one of the most compelling challenges of particle physics. The QCD Lagrangian *a priori* contains a topological term commonly called the "θ-term":

$$\mathcal{L}_{QCD} \supset \frac{\widetilde{\theta}_{QCD}}{32\pi^2} \mathrm{Tr}\, G_{\mu\nu}\widetilde{G}^{\mu\nu}\,, \tag{1.1}$$

where $G_{\mu\nu}$ is the gluon field strength tensor and $\widetilde{G}^{\mu\nu} = \epsilon^{\mu\nu\alpha\beta}G_{\alpha\beta}/2$ is its dual. The parameter $\widetilde{\theta}_{QCD}$ in Eq. 1.1 is the bare quantity due to $SU(3)$ gauge group, but another source of CP violation can arise from the eletroweak (EW) sector due to the mass of the quarks. The physical parameter we will refer to from now on is:

$$\theta_{QCD} = \widetilde{\theta}_{QCD} + \arg\det M_u M_d\,, \tag{1.2}$$

where M_u and M_d are the quark mass matrices.

In abelian gauge theories this term is usually not considered because it is equivalent to a total derivative, but in this case it must be taken into account due to the particular structure of the $SU(3)$ vacuum [2]. The θ-term violates CP and, as a direct consequence, it should give rise to an electric dipole moment (EDM) for the neutron [3]. The expression for the EDM is [3]:

$$d_n \approx 3.6 \times 10^{-16}\,\theta_{QCD}\, e\,\mathrm{cm}\,, \tag{1.3}$$

where e is the charge of the electron. Experimentally, the static dipole moment is constrained to be $|d_n| < 3.0 \times 10^{-26}\, e\,\mathrm{cm}$ (90% C.L.) [4], which implies that $\theta_{QCD} \leq 10^{-10}$. This tension represents a true fine-tuning problem since θ_{QCD}, which is a fundamental parameter of the theory, is expected to be $\mathcal{O}(1)$ and there is no justification for its smallness within the SM.

The solution developed by Peccei and Quinn is based on the idea that if an unnaturally small parameter of a theory is promoted to be a dynamical field, then it can be naturally driven to the experimental value by a symmetry breaking potential. This basic concept is the core of the axion solution to the strong-CP problem. The name "axion" is due to Frank Wilczek, who named the field after an American laundry detergent using the axial anomaly to clean up the mess of CP violation in the strong sector. In this framework, the axion field, generated as a Goldstone boson of an extra global group, called $U(1)_{PQ}$, exploits the instanton QCD potential to naturally drive the CP-violating term to zero.

The consequences sprung from this single idea were incredible. Immediately after the publication of the first paper, the idea was developed by Wilczek and Weinberg, creating a framework for the axion mechanism to take place consistently within the SM, known as the Peccei-Quinn-Weinberg-Wilczek model (PQWW) [5,6]. With the introduction of a second Higgs doublet, the model provides a clean realisation of the

axion mechanism. In this context, the instantonic QCD potential plays a fundamental role in the solution of the strong-CP problem because it is necessary to drive the axion field to the CP-conserving minimum. However, this potential is non-perturbative and the presence of the quark masses explicitly breaks the residual shift-symmetry associated to the axion field (as a Goldstone boson). The explicit breaking is responsible for the mass of the axion m_a which is correlated to the $U(1)_{PQ}$ breaking scale by the relation:

$$m_a f_a \approx m_\pi f_\pi \tag{1.4}$$

where m_π and f_π are the mass and the decay constant of the pions. The dynamics of the PQWW model, connected with the scale f_a, is bound to be at the EW scale and, unfortunately, it was ruled out by the so called "beam-dump" experiments [7] in the late '80. At the same time, other implementations of the axion mechanism were developed trying to avoid the existing experimental bounds. The two most famous are the Kim-Shifman-Vainshtein-Zakharov model (KSVZ) [8, 9], characterised by a PQ dynamics is associated to a heavy fermionic sector plus an extra scalar singlet, and the Dine-Fishler-Srednicki-Zhitnitsky model [10, 11], where PQWW is equipped with an extra scalar singlet coupled to SM fermions. In these two models the PQ breaking scale f_a is not bound to be at the EW scale so the experimental constraints can be avoided. Moreover, the coupling of the axion with SM particles is always proportional to the inverse of f_a and, as a consequence, the large value of f_a required to avoid experimental bounds is translated into a very weak coupling. Indeed, these models are usually referred to as "*invisible axions*". A clarification is necessary at this point: KSVZ and DFSZ are not the only possibilities to have an invisible axion compatible with experiments and observations. Models with a higher degree of complexity are widely studied in current literature and they can involve the presence of extra $SU(N)$ colour groups or extra massless fermions living at the PQ breaking scale (see for example [12, 13]). As it will be clear in the next chapter, KSVZ and DFSZ are nowadays considered more like two categories of specific axion models, depending whether the PQ dynamics is mainly associated to an extra fermionic sector or directly to the SM quarks.

Finally, in its invisible realisation, the axion is a great dark matter (DM) candidate. It is a stable particle which interacts very weakly with the ordinary matter and it can easily reproduce the current DM abundance of our universe through vacuum re-alignment (see [14] for more details). A general summary of the most important experimental and observational bounds on the axion parameter space can be found in Fig. 1.1.

Besides the solution of the strong-CP problem, the axion mechanism can be used in many other applications. One of the most famous is the so called "*Natural Inflation*" [15], where the scalar field driving our universe through the inflationary era is the axion itself. The word "natural" refers to the mass of the Higgs boson, which is naturally driven to its experimental value (well below the Plank scale) the same way the CP-violating term in the QCD Lagrangian is driven to zero.

The axion mechanism and all its features have a wide field of applications in particle physics and the previous examples are just hints at the zoology of models. As a consequence, QCD axions are just a small subgroup of a larger category that includes models where the solution of the strong-CP problem is not mandatory anymore. That is why it is convenient use the expression "*Axion-Like Particles*" (ALP), which addresses the whole category. In this context, QCD axions are ALPs that solve the strong-CP problem. The direct consequence is that the relation of Eq. (1.4) does not hold anymore so m_a and f_a can be considered independent parameters.

However, not all that glisters is gold, and the even the axion mechanism has its pros and cons. To avoid experimental bounds, the PQ breaking scale f_a can be *a priori* very large, well above the EW scale. In the specific case of the QCD axion, astrophysical observations bound the scale to be at least of the order of 10^8 GeV [16, 17]. The presence of an extra scalar sector at the scale f_a, responsible for the symmetry breaking, can be troublesome. If not taken care of properly, it can create a tension with the scalar potential of the Higgs field worsening the hierarchy problem. Moreover, the presence of a "wanna-be fundamental" new symmetry at such a large scale is difficult to justify. Indeed, because of its global nature, the $U(1)_{PQ}$ cannot be included in a quantum gravity contest, where all the symmetries must be local (see [18] for a detailed discussion).

These are just two examples of the open debates around the axion/ALP world, which are still taking the time of the scientific community nowadays. However, the main problem has not been mentioned yet: fourty-two years after the famous Peccei and Quinn article, there are no experimental proofs of the existence of axions or ALPs. After PQWW model was ruled out, the experimental quest for axions and ALPs took many different roads. Concerning axion dark matter, where the scale f_a is so large that the axion field is almost decoupled from the SM, the search is still going on with experiments like CAST [19] and ADMX [20]. On the ALP side, where the scale f_a can be much lower, collider experiments can contribute to the cause. While in the low-energy regime required for DM cavity experiments the (almost) only relevant coupling of the axion is the one with photons, in colliders, where the energy at disposal is much higher, the coupling with the heavy gauge bosons becomes relevant triggering, for example, searches for mono-W and mono-Z final states [17, 21]. Currently, the increased sensitivity of flavour experiments, like Belle-II [22] and LHCb [23], opens new channels where to look for ALPs. The hermeticity of the detectors and the high event production rate make this kind of experiments suitable to search for such elusive particles.

In this context, ALPs are long to be a closed topic in particle physics, both from a theoretical and an experimental point of view. As mentioned above, they can arise in many different areas of particle physics and touching every of these fields in one single work would be unrealistic. However, given that all ALP models have their roots in that paper of 1977, a general way to approach the problem can be found. This idea of moving from a general phenomenological perspective on ALPs to the peculiarity of specific models is the guideline of this thesis work. In the remainder of part i a detailed introduction to the axion mechanism will be presented. Even if QCD axion is not specifically the central topic of this work, the functioning of the axion mechanism is fundamental to understand the dynamics related to the whole ALP category. In part ii an effective field theory (EFT) approach is adopted to deal with experimental searches for ALPs. We focused on how B-factories can be a suitable environment where to search for ALPs associated to a dynamics around the TeV scale. Starting from an effective theory, we will discuss how ALP searches can be consistently performed at these facilities taking into account their peculiarities: axion-like particles are not just simple pseudo-scalars and should not be treated as they were. In particular, the focus of our work will be in the interplay between the ALP coupling with photons and with b-quarks, which in principles can play an important role in the interpretation of the result of B-factories. In part iii the discussion is shifted to model building. In chapter 7, we investigate the possibility for an axion/ALP to arise in a composite Higgs scenario. In particular, the Minimal Linear σ Model [24] is chosen due to the extra fermionic sector which makes it suitable for an KSVZ-like axion. In chapter 8 the scalar sector of this set up is studied analytically (where possible) and numerically to see how the presence of the extra scalar field associated to the axion mechanism can affect the SM Higgs sector and its dynamics. Finally, in chapter 9 a

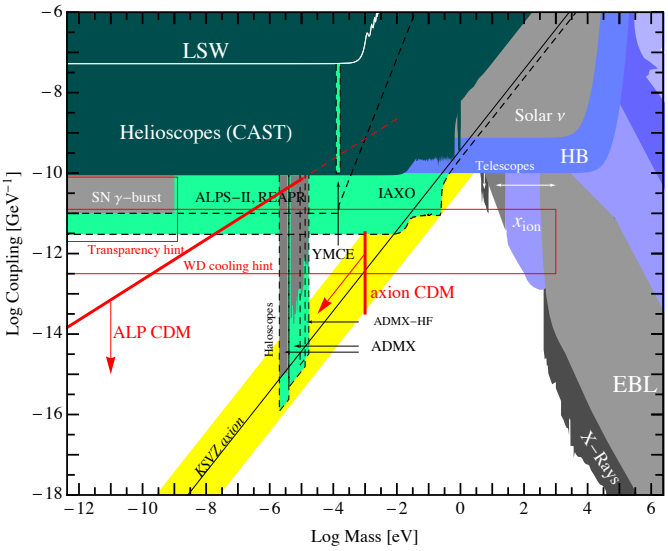

Figure 1.1: *The figure, taken from [25], represents the axion parameter space, with the mass m_a on the horizontal axis and the effective coupling to photons on the vertical one. Colored regions are: generic prediction for the QCD axion, relating its mass with its coupling to photons (yellow), experimentally excluded regions (dark green), constraints from astronomical observations (grey) or from astrophysical or cosmological arguments (blue), and sensitivity of planned experiments(light green). Shown in red are boundaries where axions and ALPs can account for all the cold dark matter produced either thermally or non-thermally by the vacuum realignment mechanism.*

phenomenologically viable solution, where the PQ scale coincide with the compositness one, is presented and discussed. Lowering the value of f_a to the TeV region forces us to discard the QCD axion option, remaining within a more general ALP frame. At the end of this chapter the analysis tools discussed in part ii will be used to bound the ALP parameter space of the model, closing the circle.

The intention of the author is to shed some light on specific aspects that can apparently seem secondary, but that can still play an important role in terms of consistency. In times when the evidence of new physics, if there is any, is anything but manifest, it is fundamental to understand properly what we already have.

2

AXION SOLUTION TO THE STRONG–CP PROBLEM

As anticipated in the introduction, the strong CP problem is one of the most compelling challenges of particle physics and it was approached with different perspectives along the years. In the remainder of the chapter the axion solution to the strong-CP problem will be discussed in details, following the approach of [26]. After discussing briefly the origin of the problem, the different implementations and the most peculiar aspects of the axion mechanism will be revised. Although most of the work of this thesis is about ALPs which does not explicitly QCD axions, understanding the underlying mechanism is fundamental to contextualise properly every discussion about the topic.

2.1 THE STRUCTURE OF THE VACUUM

A brief discussion on the peculiarity of the QCD vacuum structure is necessary to understand the CP-violation puzzle in the strong sector. However, the complexity of the topic is well beyond the scope of this work, so just a brief general introduction to the problem will be discussed here. The approach of [27] will be adopted.

Quantum field theories depend on the Euclidean functional integral, where the field configurations of the finite Euclidean action dominate the path integrals. These dominant contributions to the semi-classical approximation are known as instantons. In general, the action for a field theory with a gauge group G ($G = SU(N)$, for definiteness) in a 4-D Euclidean space is:

$$S = \frac{1}{4g_G^2} \int d^4x \, \mathrm{Tr}\left[F_{\mu\nu} F^{\mu\nu}\right] . \tag{2.1}$$

For the action S to be finite, every possible field configuration must have a proper behaviour at the boundaries, namely $F \sim \mathcal{O}(1/r^3)$ as $r \to \infty$. The gauge field then must be of the form:

$$A_\mu = g \partial_\mu g^{-1} + \mathcal{O}(1/r^2) \, , \tag{2.2}$$

for some gauge transformation $g(x)$, which is a function mapping G to the variables of the Euclidean space. A gauge transformation must not alter the asymptotic behaviour in the radial variable r and, to do so, $g(x)$ must map G only to the angular variables. Therefore, the field configurations are defined up to a mapping of G to the space-time boundary, which in this case is topologically equivalent to the three-dimensional hypersphere, S^3.

The key point of the situation can be summed up by the following question: how many different mappings are there, and how can they be classified? An important result in [28] states that only the $SU(2)$ subgroups of our G need to be considered. $SU(2)$ is topologically S^3, so we can consider the trivial mapping:

$$g^{(1)}(x) = \left(x_4 + i \mathbf{x} \cdot \boldsymbol{\sigma}\right) / r \, , \tag{2.3}$$

where $\sigma_{1,2,3}$ are the Pauli matrices. It is also proven that all mappings from S^3 to S^3 are homotopic to a family of mappings

$$g^{(\nu)}(x) = \left[g^{(1)}(x)\right]^{\nu} , \tag{2.4}$$

where ν is an integer called *winding number*. A simple example is necessary to better understand this statement. Suppose to have a $U(1)$ group and to wrap its elements around a circle S^1. The trivial mapping in this case would be:

$$g^{(1)}(\theta) = e^{i\theta} , \tag{2.5}$$

where the dependence is just on θ because $U(1)$ has one angular variable. All the mappings on the circle S^1 can be obtained simply elevating $g^{(1)}(\theta)$ to an integer power:

$$g^{(\nu)}(\theta) = \left[g^{(1)}(\theta)\right]^{\nu} = e^{i\nu\theta} . \tag{2.6}$$

The winding number ν labels the representations of $U(1)$ as number of laps around the circle S^1 in the form $e^{i\nu\theta}$, where θ is the only angular variable[1].

Finally, it is possible to show that the winding number of a field configuration is given by the integral

$$\nu = \frac{1}{32\pi^2} \int d^4x \, \mathrm{Tr}\left[F_{\mu\nu}\widetilde{F}^{\mu\nu}\right] , \tag{2.7}$$

where $\widetilde{F}$ is the dual field strength as defined below Eq. (1.1). Therefore, the winding number is a topological invariant of the field configuration and, as a consequence, it provides directly a finite contribution to the Euclidean action proportional to the θ-term.

For a general $SU(N)$ group, different values of ν represent different possible vacuum states. The vacuum state of the theory will be a superposition of all these states:

$$|\theta\rangle = \sum_{\nu} e^{i\nu\theta} |\nu\rangle , \tag{2.8}$$

such that

$$\langle\theta|e^{HT}|\theta\rangle \propto \int [dA]\, e^{-S} e^{i\nu\theta} . \tag{2.9}$$

By definition, the θ-vacua are topologically distinct, therefore transitions between them are forbidden as they involve discontinuous changes in the gauge field boundary conditions. The energy of the vacuum state is estimated in [27] to be

$$E(\theta) \propto e^{-S_0} \cos(\theta) , \tag{2.10}$$

where $S_0 = 8\pi^2/g_G^2$ is the one-instanton action. This result will be extremely useful in the computation of the axion non-perturbative potential needed to solve the strong-CP problem in 2.4.

1 The $U(1)$ gauge theory has no instantons in $3+1$ dimensions. $U(1)$ is topologically equivalent to the circle S^1 which, when wrapped around the hypersphere S^3 can always be continuously deformed to a point: the trivial mapping

2.2 THE PQ SOLUTION

There are many ways to approach the strong-CP problem. A massless up quark can be a simple solution: if $m_u = 0$ then also $\det M_u M_d = 0$, and θ_{QCD} can be simply removed with a chiral field redefinition. However, this solution is almost ruled out by the measurements of light quarks' masses and the scientific community by now agrees on their massive nature ($m_u, m_d \sim \mathcal{O}(\text{MeV})$) [29].

A very elegant solution to the strong-CP problem is provided by the QCD axion mechanism, proposed in 1977 by Peccei and Quinn [1]. The idea is to promote θ_{QCD} to be a dynamical field which would naturally drive the θ-term to zero via QCD non-perturbative effects. This field is the axion. The requirement for the axion mechanism to work are:

- a global, chiral $U(1)_{PQ}$ symmetry spontaneously broken at the scale f_a. The axion is the wanna-be Goldstone boson of this symmetry breaking;
- a coupling between the field a and the gluon field strength in the form:

$$\mathcal{L}_a \supset \frac{1}{32\pi^2}\frac{\mathcal{C}a}{f_a}\text{Tr}\, G_{\mu\nu}\widetilde{G}^{\mu\nu}\,, \tag{2.11}$$

  where $\mathcal{C}$ is the color anomaly factor (discussed in 2.3);
- a shift symmetry for the field a: $a \to a' = a + \text{const.}$. This symmetry can be violated only by QCD non-perturbative effects;
- a potential $V_{NP}(a)$ minimised for $\mathcal{C}a/f_a = 0$.

With these ingredients the solution of the strong-CP problem is easily achieved: θ_{QCD} is absorbed by a redefinition of a through the shift symmetry

$$\left(\frac{\mathcal{C}a}{f_a} + \theta_{QCD}\right)\text{Tr}\, G_{\mu\nu}\widetilde{G}^{\mu\nu} \qquad \xrightarrow{\text{shift}} \qquad \frac{\mathcal{C}a'}{f_a}\text{Tr}\, G_{\mu\nu}\widetilde{G}^{\mu\nu}\,. \tag{2.12}$$

At this point, the potential generated by non-perturbative effects of QCD, drives naturally the field to a zero vacuum expectation value ($\mathcal{C}\langle a\rangle/f_a = 0$), erasing dynamically the CP-violation induced by the θ-term. A theorem of Vafa and Witten [30] guarantees that the instanton QCD potential is minimised at the CP-conserving value. A residual interaction between the axion and the gluons is mantained, giving birth to a rich phenomenology. The pseudo-scalar nature of the axion ensures CP-conservation of these residual interactions.

Summing up, the axion mechanism provides an effective solution to the strong-CP problem. The dynamics takes place at two (in principle different) energy scales: the $U(1)_{PQ}$ scale f_a and the QCD scale Λ_{QCD}. As the energy falls below f_a, $U(1)_{PQ}$ breaks spontaneously generating the axion as a Goldstone boson; at this point the axion is massless and it enforces the shift symmetry. Approaching Λ_{QCD}, the instanton non-perturbative potential grows, driving the axion field to its CP conserving minimum and solving the strong-CP problem. The non-perturbative potential violates explicitly the shift symmetry generating a small mass for the axion.

The whole axion mechanism is at this point largely model-independent. However, the discussion on how the mechanism is realised, the field content and the symmetry breaking patterns is still an open topic. In the following sections, three general types of QCD axions model will be presented.

2.2.1 *PQWW*

The Peccei-Quinn-Weinberg-Wilczek model [1, 5, 6] introduces a single additional complex scalar field, φ, to the SM as a second Higgs doublet. One Higgs field will give a mass to the up-type quarks, while the other to the down-type. As a consequence, the representation of φ in $SU(2)_L \times U(1)_Y$ is fixed. The Lagrangian is equipped with the global $U(1)_{PQ}$, which acts as a chiral rotation (i.e. proportional to γ_5). These chiral rotations shift the angular part of φ by a constant. The PQ field now is coupled to the SM via the Yukawa interactions, which give the mass to the SM fermions. The PQ charges of the fermions are fixed by the invariance of these terms under $U(1)_{PQ}$.

The new field φ, like the Higgs, requires a symmetry breaking potential:

$$V(\varphi) = \lambda \left(|\varphi|^2 - \frac{f_a^2}{2} \right)^2 , \tag{2.13}$$

and takes a vacuum expectation value $\langle \varphi \rangle = f_a/\sqrt{2}$. The field φ is co-responsible for the mass generation of the fermions, therefore the symmetry breaking must take place at the EW phase transition, as the standard Higgs doublet. This forces f_a to be approximately 250 GeV. The angular degree of freedom appears as $\langle \varphi \rangle e^{ia/f_a}$ after the kinetic term is canonically normalised. The relevant terms in the Yukawa sector then take the form:

$$\mathcal{L}_y \supset -\frac{v}{\sqrt{2}} \left(Y_u \, \overline{u}_L e^{ia/f_a} u_R + Y_d \, \overline{d}_L e^{ia/f_a} d_R \, + \text{h.c.} \right) , \tag{2.14}$$

where Y_u, Y_d are the matrices of the Yukawa coefficients and $v = 246$ GeV is the EW vev. Expanding in powers of $1/f_a$ the quark coupling is:

$$\mathcal{L}_y \sim m_q \left(\frac{a}{f_a} \right) \overline{q} \, i\gamma_5 \, q \, , \tag{2.15}$$

where we identified $m_q = y_q v/\sqrt{2}$. The chiral anomaly, which will be discussed treated in 2.3, induces 1-loop couplings to the gauge bosons $\propto a/f_a \, G\widetilde{G}$ and $\propto a/f_a \, F\widetilde{F}$, where F is the EM field strength. The coupling with the gluon is the desired term and leads to the PQ solution to the strong-CP problem.

For any axion models, the axion couplings are proportional to $1/f_a$. In the PQWW f_a is forced to be at the EW scale, meaning that the axion coupling with SM particle is rather important. For this reason, the PQWW set-up is ruled out by *beam-dump* experiments [7]. One way to avoid these experimental bounds is to untie f_a from the EW scale. The decay constant is thus a free parameter of these models and it can be large enough such that they can be avoided. These categories of axion models, characterised by a large value of f_a which makes the axion very light, stable and weakly coupled, are called *Invisible Axion Models*. The two most famous types are the KSVZ and DFSZ.

2.2.2 *KSVZ*

The Kim-Shifman-Vainshtein-Zakharov model [8, 9] introduces a heavy quark doublet Q_L, Q_R, triplet of $SU(3)_C$. The PQ scalar field φ is now a complex SM singlet. The two new fields interact via the PQ-invariant Yukawa term, which provides the heavy quark mass:

$$\mathcal{L}_Y = -\lambda_Q \, \varphi \, \overline{Q}_L Q_R \, , \tag{2.16}$$

where the Yukawa coupling λ_Q is a free parameter in the model. The $U(1)_{PQ}$ charges are fixed in order to make the Lagrangian invariant. The potential is the same of Eq. 2.13 and the symmetry breaking pattern makes the axion arise as a Goldstone boson. A peculiarity of the this model is that no SM field is charged under $U(1)_{PQ}$; all the PQ dynamics lives in the BSM sector. Nevertheless, at the quantum level, chiral rotations on Q affect the $G\widetilde{G}$ term via the chiral anomaly:

$$\mathcal{L} \to \mathcal{L} + \frac{1}{32\pi^2}\frac{a}{f_a} G\widetilde{G}\,. \tag{2.17}$$

In the simple KSVZ model the value of the color anomaly is equal to unity (just the one heavy quark Q runs into the loop).

At low energies (below the PQ breaking), φ takes a vev and, as a consequence, the quark Q obtains a mass proportional to $\lambda_Q f_a$. At this point, the field Q can be integrated out. The coupling of the axion to $G\widetilde{G}$ acts as a "memory" of the chiral rotation applied at high energy. At the level of EFT, the induced topological term is the only reminiscence of the PQ dynamics. Besides the axion-gluon coupling, usually the coupling with the photons is present in this type of models. It can be calculated via loops through the EM anomaly and it depends on the EM charge of the extra quark field.

2.2.3 *DFSZ*

In the Dine-Fishler-Srednicki-Zhitnitsky model [10, 11] the axion is coupled to the SM via the Higgs sector. As in the PQWW model, two Higgs doublets (H_u, H_d) are required and of top of them the complex scalar φ is introduced as a SM singlet. The global $U(1)_{PQ}$ is imposed and spontaneously broken by the potential of Eq. (2.13). The field φ and the Higgs doublets interact via the potential:

$$V = \lambda_H\, \varphi^2\, H_u H_d\,. \tag{2.18}$$

When the PQ symmetry is broken and φ acquires a vev, the parameters in the potential and the coupling constant λ_H must be chosen in order to keep the Higgs field light, consistent with the observed 125 GeV SM Higgs [31, 32], and the EW vev, $v = \sqrt{\langle H_u\rangle^2 + \langle H_d\rangle^2}$. The Higgs provides the masses to the SM fermions, as usual, trough the Yukawa couplings:

$$\mathcal{L}_Y \supset Y_u\, \overline{q}_L u_R H_u + \text{h.c.}\,. \tag{2.19}$$

Therefore, the SM fields must be charged under $U(1)_{PQ}$ for this term to be invariant under the PQ symmetry. After the EW symmetry breaking, the Higgs is replaced by its vev, inducing the usual axial coupling between the axion and the SM fermions from the mass term, the same of Eq. (2.15). At this point, the main difference between KSVZ and DFSZ is that in the DFSZ the $G\widetilde{G}$ is induced by a light SM quarks loops at low energies, rather than via the integration of the heavy degrees of freedom Q. In the DFSZ model all of the standard model quarks are charged under the PQ symmetry and, as a consequence, the color anomaly factor is larger ($\mathcal{C} = 6$).

The fermion loop induces, in the same way, the coupling with the photons. In this model there is freedom on choosing whether it is H_u or H_d that give mass to leptons via $H_{u,d}\,\bar{l}_L e_R$. As the axion-photon coupling is the sum of quark and lepton loops, different values of their PQ charge give different contribution to the EM anomaly, and thus to the coupling.

These are two good illustrations on how a UV complete axion model can be built. However, these are not the only possibilities. Models where the PQ charge is distributed between the SM fields and the BSM sector are common in literature: an example of this approach is thoroughly described in part iii of this work.

2.3 QUARK MASSES AND THE CHIRAL ANOMALY

A key role in the axion mechanism is played by the chiral anomaly [33], which is strictly connected with CP violation in the quark mass term. A simple example is the best way to explain the interplay between these two apparently different topics. Let's suppose to have a single quark splitted in its chiral components q_L, q_R. The mass term is in general:

$$\mathcal{L}_M = \overline{q}_L M q_R + \overline{q}_R M^\dagger q_L \,. \tag{2.20}$$

The mass matrix can be *a priori* complex, generating a source of CP violation, and it can be parametrised as $M \equiv m e^{i\alpha}$, where m is the absolute value of the fermion mass and α is the CP-violating phase. The Lagrangian of Eq. (2.20) takes the form:

$$\mathcal{L}_M = m\,\overline{q}q \;+\; im\alpha\overline{q}\gamma_5 q + \mathcal{O}(\alpha^2)\,, \tag{2.21}$$

where we expanded for small α and regrouped the chiralities of q. The second piece is CP-violating and in principle it can be reabsorbed by an axial $U(1)$ field redefinition of q. The rotations of $U(1)_A$ are:

$$\begin{aligned} q_L &\to e^{i\beta} q_L \,, \\ q_R &\to e^{-i\beta} q_R \,, \end{aligned} \tag{2.22}$$

where β is the parameter of the transformation. It is easy to check that the CP-violating term is cancelled if $\beta = \alpha/2$. However, the $U(1)_A$ group is anomalous, so this symmetry is not conserved at quantum level. The anomalous contribution deriving from the transformation in Eq. (2.22) can be computed via loop or with the Fujikawa method [34]. In any case, the four-divergence of the axial current is proportional to the $G\widetilde{G}$ term, and the additional term in the Lagragian due to the anomaly is:

$$\mathcal{L} \to \mathcal{L} + \frac{\alpha}{32\pi^2} \mathrm{Tr}\, G_{\mu\nu}\widetilde{G}^{\mu\nu} \,, \tag{2.23}$$

where the relation $\beta = \alpha/2$ is imposed. The anomalous behaviour of $U(1)_A$ does not allow the CP-violating phase to be completely removed from the theory if a quark mass term is included. CP-violation effects, proportional to the parameter α, is always present in the Lagrangian either in the form of Eq. (2.20) or of Eq. (2.23). For the sake of completeness, in the case of more than one quark field, like the SM, the CP-violating phase is proportional to $\arg\det M$, explaining the expression of Eq. (1.2).

In spite of that, this duality is a fundamental feature for the axion mechanism. The group $U(1)_{PQ}$ acts on the Lagrangian as a chiral rotation where the angle is proportional to the axion field $\alpha = a/f_a$. As a consequence, the $G\widetilde{G}$ term is generated whenever a field redefinition of this kind is performed on a quark mass term. In the computation of the axial anomaly, the $G\widetilde{G}$ term is always proportional to a numerical

factor, the anomaly factor, which depends on the specific model. In the case of the PQ symmetry the *colour anomaly* is given by [35]:

$$\mathcal{C}\delta_{ab} = 2\beta \,\mathrm{Tr}\, T_a T_b \,, \tag{2.24}$$

for the trasformation of Eq. (2.22). The trace is all over the fermions of the theory, and T_a are the generators of the $SU(3)_c$ representations of the fermions.

2.4 INSTANTONS AND THE AXION POTENTIAL

Even though the topological term in Eq. (1.1) does not affect the classical equation of motion, it does affect the vacuum structure and, as a consequence, the vacuum energy depends on θ_{QCD}. This is because of the presence of instantons in the so called θ-vacua configuration of QCD [27], discussed in 2.1. These happens because the group of the space-time boundary, onto which $SU(3)_c$ is mapped, allows for topologically distinct field configurations. A many-vacua structure emerges from this situation, each one labelled by a value of θ_{QCD}. The vacuum energy is [36]:

$$E_{vac} \propto \cos\left(\theta_{QCD}\right) . \tag{2.25}$$

The different θ-vacua are topological distinct, so any transition between two different vacuum states is not allowed. On the other hand, introducing a field that couples to $G\widetilde{G}$, as the axion does, means that the vacuum energy now depends on the linear combination $E_{vac}(\theta_{QCD} + \mathcal{C}a/f_a)$. Through the shift symmetry of the axion, the contribution of θ_{QCD} can be reabsorbed:

$$E_{vac} \propto \cos\left(\frac{\mathcal{C}a}{f_a}\right) . \tag{2.26}$$

The vacuum energy now depends on a dynamical field and it can be interpreted as a non-perturbative potential for the axion. The dynamics of a sends it to one of these vacua, which is the essence of the PQ mechanism.

The Goldstone boson nature of the axion forces it to be massless. However, when the energy approaches Λ_{QCD} the instantonic potential becomes important, explicitly breaking the shift symmetry and generating a small mass for the axion. The process can be easily sketched using the single quark approach of 2.3. The relevant terms in the Lagrangian are:

$$m\bar{q}q + \frac{1}{32\pi^2}\frac{\mathcal{C}a}{f_a}\mathrm{Tr}\, G\widetilde{G} . \tag{2.27}$$

Applying a $U(1)_{PQ}$ chiral rotation of angle $\alpha = \mathcal{C}a/f_a$ and expanding the exponential in sines and cosines we get:

$$\mathcal{L} \supset m\,\cos\left(\frac{\mathcal{C}a}{f_a}\right)\bar{q}q + im\sin\left(\frac{\mathcal{C}a}{f_a}\right)\bar{q}\gamma_5 q \,. \tag{2.28}$$

If the energy is below Λ_{QCD} the quark bi-linear condensates to $\langle\bar{q}q\rangle$. Remembering that for almost every viable axion model the condition $f_a \gg \Lambda_{QCD}$ is verified, the wanna-be potential in Eq. (2.28) can be expended in powers of $1/f_a$:

$$m\,\langle\bar{q}q\rangle\,\cos\left(\frac{\mathcal{C}a}{f_a}\right) \simeq \frac{1}{2}\frac{m\langle\bar{q}q\rangle}{f_a^2}a^2 + \ldots \tag{2.29}$$

where the first term of the expansion is the mass term for the axion. In any case, a general expression commonly used for the axion potential is:

$$V_{NP}(a) = m_u \Lambda_{QCD}^3 \left[1 - \cos\left(\frac{\mathcal{C}a}{f_a}\right)\right] \tag{2.30}$$

where a constant shift is applied such the the minimum of the potential is in zero.

In the general QCD case, this mass can be calculated in chiral perturbation theory [5, 6]:

$$m_a^2 = \frac{m_\pi^2 f_\pi^2}{(\frac{f_a}{\mathcal{C}})^2} \frac{m_u m_d}{(m_u + m_d)^2} \left\{1 + \frac{m_\pi^2}{m_\eta^2}\left[-1 + \mathcal{O}\left(1 - \frac{m_\pi}{m_\eta}\right)\right]\right\} , \tag{2.31}$$

where m_π, f_π are the masses and the decay constant of the pion, m_u, m_d are the masses of the up and down quarks and m_η is the mass of the η meson. It is straight forward from Eq. (2.31) to see that, for the QCD axion, a particularly strict relation occurs between the mass m_a and the scale f_a:

$$m_a f_a \sim m_\pi f_\pi \, . \tag{2.32}$$

The mass and the scale are strongly correlated for QCD axions, the larger is f_a, the smaller is m_a. Putting some numbers into Eq. (2.31) a general formula for the value of m_a is obtained:

$$m_a \approx 6 \times 10^{-6}\,\text{eV} \left(\frac{10^{12}\,\text{GeV}}{f_a/\mathcal{C}}\right) . \tag{2.33}$$

This statement is completely general and in principle valid for any of the particular QCD models discussed.

2.5 COUPLING TO THE SM

The couplings of the axion with the SM fields depend on the model and on the PQ charge assignment. Nevertheless, a structure of the interaction terms can be outlined. A general expression for the interactions between the field a and the SM can be find in [37]:

$$\begin{aligned}\mathcal{L}_{int} = \frac{\partial_\mu a}{2f_a}\left(c_{aHH} H^\dagger i \overleftrightarrow{D}^\mu H + \frac{1}{2}\sum_f c_{aff}\overline{\psi}_f \gamma^\mu \gamma_5 \psi_f\right) + \\ - \frac{a}{f_a}\left\{c_{agg}\frac{g_3^2}{32\pi^2} G\widetilde{G} + c_{aWW}\frac{g^2}{32\pi^2} W\widetilde{W} + c_{aBB}\frac{g'^2}{32\pi^2} B\widetilde{B}\right\} ,\end{aligned} \tag{2.34}$$

where H is the Higgs doublet, ψ_f are the SM fermions and g_3, g and g' are the coupling constants of $SU(3)_c$, $SU(2)_L$ and $U(1)_Y$. As expected, the PQ invariant couplings contain only derivatives of a to preserve the shift symmetry. They depend on the model-dependent values of the PQ charges included in the coefficients c_{aff}, c_{aHH} assigned to the fields. On the other hand, the non derivative couplings of $aG\widetilde{G}$ form violate the PQ symmetry in the $U(1)_{PQ}$ anomaly framework.

Given the extraordinary adaptability of the QCD axion to be a dark matter candidate, usually its interaction are studied from a low-energy EFT approach. The most interesting coupling, from a phenomenologically point of view, is the one with the

photon, generated through the electromagnetic anomaly. In the effective approach, this coupling is usually parametrised as:

$$\mathcal{L}_{a\gamma\gamma} = -\frac{g_{a\gamma\gamma}}{4}\, a\, F_{\mu\nu}\widetilde{F}^{\mu\nu}\,, \tag{2.35}$$

where $g_{a\gamma\gamma}$ is the effective coefficient, it has mass-dimension -1 and is proportional to $1/f_a$. To link the EFT term with its PQ invariant origin it is convenient to define:

$$g_{a\gamma\gamma} = \frac{\alpha_{\rm em}}{2\pi}\frac{c_{a\gamma\gamma}}{f_a}\,, \tag{2.36}$$

where α_{em} is the EM coupling constant and $c_{a\gamma\gamma}$ is a dimensionless parameter that depends on the specific model. The factor $\alpha_{\rm em}/2\pi$ in front of the coefficient is the reminiscence of the "1-loop" origin of this coupling. As a consequence, even though the coefficient $c_{a\gamma}$ can be of $\mathcal{O}(1)$, the effective coupling of the axion with the photon (and in general with the SM vector bosons) is always suppressed by a loop factor. The dimensionless coupling receives contributions from above the $U(1)_{PQ}$ breaking scale, via the EM anomaly, and below it by mixing with the longitudinal component of the Z-boson [35]:

$$c_{a\gamma\gamma} = \frac{\mathcal{E}}{\mathcal{C}} - \frac{2}{3}\cdot\frac{4+m_u/m_d}{1+m_u/m_d}\,, \tag{2.37}$$

where $\mathcal{E} = 2\mathrm{Tr}\, n_{PQ}\mathcal{Q}_{EM}$ is the EM anomaly.

Here the difference between KSVZ and DFSZ is manifest. In KSVZ only the heavy quark Q has a PQ charge, so the value of $c_{a\gamma\gamma}$ depends on the EM charge assigned to Q. Introducing more than one heavy field can induce model dependence. On the other hand, in DFSZ models all the SM fermions carry a PQ charge. The model dependence here is due to the lepton PQ charges, i.e. whether H_u or H_d gives mass to the leptons. If H_u is responsible for lepton masses, $c_{a\gamma\gamma}$ also depends on the ratio of Higgs vevs, $\tan\beta = \langle H_u\rangle/\langle H_d\rangle$. Anyway, there is a canonical set-up, for both KSVZ and DFSZ, which represents the simplest case of a QCD axion solving the strong-CP problem. For KSVZ it consists in a single, EM neutral heavy quark Q. For DFSZ the H_d doublet gives mass to the leptons, allowing for a $SU(5)$ unification. In this two situation the value of the coefficient is:

$$c_{a\gamma\gamma} = -1.92\,(\text{KSVZ})\,; \qquad\qquad c_{a\gamma\gamma} = 0.75\,(\text{DFSZ})\,. \tag{2.38}$$

This brief discussion on the axion-photon coupling is useful to understand the interplay between the different energy scales involved in the axion mechanism. The relation between what is fundamental and what is effective will have a key role in all the remainder of this work. The general EFT Lagrangian, which can be associated both to a QCD axion or, more generally, to an axion-like particle, will be treated separately in the next chapter.

3

AXION LIKE PARTICLES (ALPS)

In the previous chapter the we discussed axion mechanism as a solution to the strong-CP problem. Although it represents an elegant and promising way to solve this long-standing problem of the SM, the requirements for it to take place strongly constrain the parameter space. In particular, to solve the strong-CP problem, the PQ scale f_a of a KSVZ or DFSZ model must satisfy the condition of Eq. (2.32). Given that astrophysical observations force f_a to be at least of the order of 10^9 GeV, the axion must be very light, of $\mathcal{O}(\mu\text{eV})$. Such a large value of f_a can be avoided if a greater degree of complexity is introduced in the complete model, like a larger dark group or a more complicated PQ dynamics (see [12, 13] as an example). Nevertheless, as it was briefly discusses in the introduction, the axion mechanism has been applied to many different areas of particle physics which go beyond the simple solution to the strong-CP problem. Without this requirement, the model is much less constrained and the allowed parameter space widens up. In what follows, some of this interesting situations will be discussed togheter with the general, low-energy, effective approach commonly used for ALP studies.

3.1 MOTIVATION FOR ALP SEARCHES

An interesting application where an ALP/axion can be an explanation for the flavour puzzle in the matter sector of the SM is the *Axiflavon* [38], or *Flaxion* [39]. The idea is to promote one of the residual $U(1)$, generated by the flavour group of the SM, to be the PQ symmetry. At this point, in a similar way of the DFSZ model, the PQ field φ is coupled to SM fermions:

$$\mathcal{L}_Y = -y^d_{ij}\left(\frac{\varphi}{M}\right)^{n^d_{ij}} \overline{Q}_i H d_R - y^u_{ij}\left(\frac{\varphi}{M}\right)^{n^u_{ij}} \overline{Q}_i \widetilde{H} u_R + \dots \tag{3.1}$$

where $y^{d,u}_{ij}$ are the Yukawa matrices, $n^{d,u}_{ij}$ are the PQ charges necessary to make the Lagrangian invariant, M is the scale of validity of the model and the dots stand for the leptonic sector. After the spontaneous breaking of $U(1)_{PQ}$, the field φ takes a vev $\langle\varphi\rangle$ and the ALP/axion is generated as the angular variable e^{ia/f_a}. The masses of the fermions generated by the EW symmetry breaking in this contest are:

$$m^d_{ij} = y^d_{ij}\left(\frac{\langle\varphi\rangle}{M}\right)^{n^d_{ij}} v; \qquad m^u_{ij} = y^u_{ij}\left(\frac{\langle\varphi\rangle}{M}\right)^{n^u_{ij}} v\,, \tag{3.2}$$

where $v = 246$ GeV is the EW vev. The masses of the SM fermions depend on the PQ charge assignment, with the charge of the top quark conventionally set to zero, and the large difference between them can be explained even with $\mathcal{O}(1)$ Yukawa couplings. Finally, as for DFSZ, the residual interaction with the field a can be in principle used to solve the strong-CP problem.

In [40] the ALP works as a portal between the SM and dark matter. The dark matter candidate χ is a Dirac fermion with mass m_{DM} which interacts with the SM fermions via a pseudoscalar a. The interaction Lagrangian is very simple:

$$\mathcal{L}_{\text{int}} = -i\,\frac{g_{a\chi\chi}}{2}\,a\,\overline{\chi}\gamma_5\chi - i\sum_f \frac{g_{aff}}{2}\,\overline{f}\gamma_5 f\,. \tag{3.3}$$

The field a can be an ALP in this scenario. This simple model can fit the gamma-ray energy burst from the center of the galaxy observed by the FERMI-LAT telescope [41].

A third possible field of application is the long-standing $g-2$ of the muon. In [42] the discrepancy between the SM model prediction and the data can be explained by an ALP coupled both to photon and to fermions, with interaction terms of the form of Eq. (2.34). The interesting result is that an ALP is a good candidate to solve the $(g-2)_\mu$ problem at the price of a relatively large coupling with photons.

Axion-like particles became a topic of great interest in the particle physics community even though the solution of the strong-CP problem is no more a mandatory condition. The possible applications are many, as we saw in the previous examples. Nevertheless, in every model containing ALPs the form of the interaction terms is usually very similar and this is due to a similar symmetry structure from where they arise and to the effective approach commonly used for the analysis.

3.2 EFT LAGRANGIAN FOR ALPS

The scale of the fundamental dynamics of the axion mechanism for simple KSVZ or DFSZ is bounded by observations to be extremely large. As a consequence, it is impossible by now to test directly these energies because they are way beyond the reach of any possible experiment. A viable way to prove experimentally these models is to study the low energy (EW scale and below) processes involving the axion. Therefore, it is useful to adopt an effective approach, which will be valid even in the ALP case, where the scale f_a is not bound to be so large (but still larger than the EW scale). The dimension-five effective Lagrangian describing ALP interactions, above the electroweak symmetry breaking scale, can be generically written as [43]:

$$\begin{aligned}\delta\mathcal{L}_{\text{eff}} = &\frac{1}{2}(\partial^\mu a)\,(\partial_\mu a) - \frac{m_a^2}{2}a^2 - \frac{g_{aBB}}{4}\,a\,B^{\mu\nu}\widetilde{B}_{\mu\nu} - \frac{g_{aWW}}{4}\,a\,W^{\mu\nu}\widetilde{W}_{\mu\nu}\\ &- \frac{g_{agg}}{4}\,a\,G_a^{\mu\nu}\widetilde{G}^a_{\mu\nu} - \frac{\partial_\mu a}{2}\sum_f g_{aff}\,\overline{f}\gamma^\mu\gamma_5 f\,,\end{aligned} \tag{3.4}$$

where $\widetilde{V}^{\mu\nu} = \frac{1}{2}\,\varepsilon^{\mu\nu\alpha\beta}V_{\alpha\beta}$, g_{aff} and g_{aVV} denote the ALP effective couplings to fermions and to the SM gauge bosons, $V \in \{g, B, W\}$, respectively. The dependence on the scale is absorbed in the effective coupling:

$$g_{aVV} = \frac{\alpha_V}{2\pi}\frac{c_{aVV}}{f_a}\,, \qquad\qquad g_{aff} = \frac{c_{aff}}{f_a}\,; \tag{3.5}$$

where c_{aVV} are the adimensional coefficients. The same argument holds for fermionic couplings. If the ultraviolet completion of Eq. (3.4) is not specified, the ALP couplings are independent parameters, which can be of the same order of magnitude and which should be simultaneously considered in phenomenological analyses.

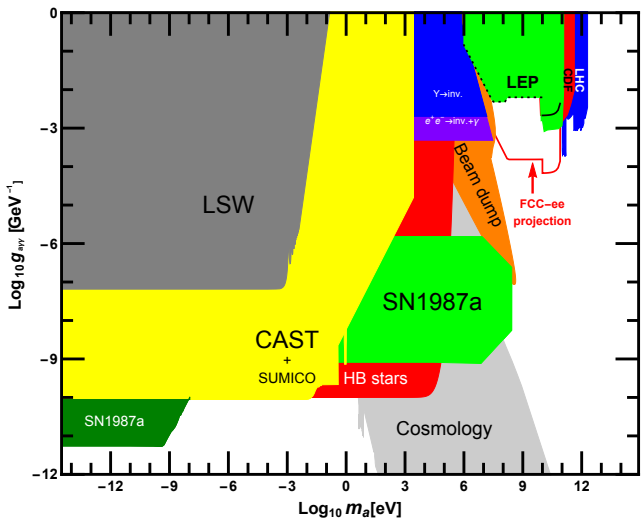

Figure 3.1: *The figure, taken from [16], gives a general overview on the bounds of the ALP parameter space, where just the coupling with photons is considered.*

Below the EW symmetry breaking the relevant couplings for collider studies are the following:

$$\begin{aligned}\delta\mathcal{L}_{\text{eff}} = &\frac{1}{2}(\partial^\mu a)\,(\partial_\mu a) - \frac{m_a^2}{2}a^2 - \frac{g_{a\gamma\gamma}}{4}\,a\,F^{\mu\nu}\widetilde{F}_{\mu\nu} - \frac{g_{agg}}{4}\,a\,G^{\mu\nu}\widetilde{G}_{\mu\nu} + \\ &- \frac{g_{aWW}}{4}\,a\,W^{\mu\nu}\widetilde{W}_{\mu\nu} - \frac{g_{aZZ}}{4}\,a\,Z^{\mu\nu}\widetilde{Z}_{\mu\nu} - \frac{g_{aZ\gamma}}{4}\,a\,Z^{\mu\nu}\widetilde{F}_{\mu\nu} + \\ &+ \frac{\partial_\mu a}{2}\sum_f g_{aff}\,\overline{f}\gamma^\mu\gamma_5 f\,,\end{aligned} \tag{3.6}$$

where $g_{a\gamma\gamma} = \mathrm{c}_W^2\, g_{aBB} + \mathrm{s}_W^2\, g_{aWW}$, $g_{aZZ} = \mathrm{s}_W^2\, g_{aBB} + \mathrm{c}_W^2\, g_{aWW}$ and $g_{aZ\gamma} = 2\mathrm{c}_W\mathrm{s}_W\,(g_{aWW} - g_{aBB})$. This effective Lagrangian is widely used to study processes involving axions or ALPs in the energy range relevant for collider searches.

For low-energy experiments such as direct detection, besides the ubiquitous axion-photon coupling, the focus is shifted to the couplings with nucleons and electrons:

$$\begin{aligned}\delta\mathcal{L}_{\text{eff}} = &\frac{1}{2}(\partial^\mu a)\,(\partial_\mu a) - \frac{m_a^2}{2}a^2 - \frac{g_{a\gamma\gamma}}{4}\,aF_{\mu\nu}\widetilde{F}_{\mu\nu} + \frac{g_{aNN}}{2}\,\partial_\mu a\,\left(\overline{N}\gamma^\mu\gamma_5 N\right) + \\ &+ \frac{g_{aee}}{2}\,\partial_\mu a\,(\overline{e}\gamma^\mu\gamma_5 e) - \frac{i}{2}\,g_d\,a\,\overline{N}\sigma_{\mu\nu}\gamma_5 N F^{\mu\nu}\,,\end{aligned} \tag{3.7}$$

where $\sigma_{\mu\nu} = \frac{i}{2}[\gamma_\mu, \gamma_\nu]$, and N is a nucleon (proton or neutron). While the coupling $g_{a\gamma\gamma}$ is the usual effective axion photon coupling, the situation is a bit different for the other coefficients. The coupling g_d, which parametrises the axion-gluon coupling that generates an electric dipole moment (EDM) for a nucleon, has mass-dimension -2 and is proportional to $1/f_a$ [44]. The couplings g_{aee} and g_{aNN} represent the axial coupling of the ALP with electrons and nucleons, which can be tested in "direct detection-like" experiments.

Nevertheless, the experimental search for axions and ALPs is long to be concluded. In Fig. 3.1 some general experimental constraints on the effective ALP coupling with photons are depicted. Reminding that $g_{a\gamma\gamma} \propto 1/f_a$, once the model is specified,

bounds on the PQ scale can be obtained. The allowed parameter space for $m_a > 1$ GeV is of particular interest because it can be accessible by collider experiments while the down-left part can be explored both by cosmological and astrophysical observation and by precision axion dark matter experiments, such ADMX [20] and CAST [19].

Part II

ALP AT B-FACTORIES

4

ALP PRODUCTION @ B-FACTORIES

Light pseudoscalar particles naturally arise in many extensions of the Standard Model (SM), including the ones endowed with an approximate global symmetry spontaneously broken at a given scale, f_a. Sharing a common nature with the QCD axion [1,5,6], (pseudo) Nambu-Goldstone bosons are generically referred to as Axion-Like Particles (ALPs). The ALP mass m_a can, in general, be much lighter than the symmetry breaking scale f_a, as it is paradigmatically exemplified in the KSVZ and DFSZ invisible axion models [8–11]. Therefore, it may be not inconceivable that the first hint of new physics at (or above) the TeV scale could be the discovery of a light pseudoscalar state.

The ALP parameter space has been intensively explored in several terrestrial facilities, covering a wide energy range [16, 17, 21, 43, 45–47], as well as by many astrophysical and cosmological probes [48–50]. The synergy of these experimental searches allows to access several orders of magnitude in ALP masses and couplings, cf. e.g. Ref. [51] and references therein. While astrophysics and cosmology impose severe constraints on ALPs in the sub-KeV mass range, the most efficient probes of weakly-coupled particles in the MeV-GeV range come from experiments acting on the precision frontier [52]. Fixed-target facilities such as NA62 [53] and the proposed SHiP experiment [54] can be very effective to constrain long-lived particles. Furthermore, the rich ongoing research program in the B-physics experiments at LHCb [55, 56] and the B-factories [22, 57] offers several possibilities to probe yet unexplored ALP parameter space.

The main goal of this chapter is to re-examine existing BaBar and Belle flavor-conserving constraints on ALPs, and to identify the most promising experimental searches to be performed at the forthcoming Belle-II experiment. While there have been several studies discussing signatures of ALPs at B-factories [23, 58–60], many clarifications are still needed. Firstly, the resonant contributions to the ALP production, via the $e^+e^- \to \Upsilon(nS) \to a\gamma$ process, have been overlooked before. As will be shown, these effects can induce numerically significant corrections to experimental searches performed at $\sqrt{s} = m_{\Upsilon(nS)}$, with $n = 1, 2, 3$. Another improvement concerns the theoretical expression for the $\Upsilon \to \gamma a$ branching fraction. Previous studies estimate this quantity by considering either the ALP coupling to b-quarks [61], or to gauge bosons [59]. In this chapter, it will be shown that the simultaneous presence of both interactions, as expected in the most general framework, gives rise to new interesting phenomenological features.

In order to assess the limits on ALP couplings, one should specify not only the ALP production mechanism, but also its decay products. In this paper, it will be assumed that the ALP does not decay into visible particles. Such a scenario can be easily achieved by assuming a sufficiently large ALP coupling to a stable dark sector, as motivated by several dark matter models. The conclusions related to ALP production are, however, general and they can also be applied to the reinterpretation of experimental searches with visible decays in the detector, as will be discussed in the following.

4.1 B-FACTORIES

B-factories are particle collider experiments designed and built to study the physics of the B mesons at the intensity frontier. Originally, the target of these experiments was to measure the CP violating phase in the $B^0 - \overline{B}^0$ system, which was expected to be significantly larger than in the Kaons decay. The idea was to study the decay of the $B^0\bar{B}^0$ mesons into the same final state: an asymmetry between the two decay rates would be directly proportional to che CP violating phase in the CKM matrix. The so called "golden observable" is the CP asymmetry between $B^0 \to J/\psi K_s^0$ and $\overline{B}^0 \to J/\psi K_s^0$. At the B-factories, neutral B mesons are produced in pairs at a center of mass energy corresponding to the $\Upsilon(4S)$, which decays almost 100% into a $B\overline{B}$ pair.

To reach the sufficient sensitivity and precision to measure such an effect of CP violation both the colliders and the detector had to satisfy some technical requirements:

- **High Luminosity:** due to a relatively branching fraction for the $B^0 \to J/\psi K_s^0$ and $\overline{B}^0 \to J/\psi K_s^0$ (around 0.04%), tens of millions of $B\overline{B}$ pairs are required. For an e^+e^- collider operating at the $\Upsilon(4S)$, this means an integrated luminosity of ~ 30 fb^{-1} or more.

- **Boosted $\mathbf{B^0\overline{B}^0}$ pairs:** the propagation in time of the B mesons decays is fundamental to measure the CP violation effect. As a consequence, the $B\overline{B}$ pair must be boosted to ensure a sufficient decey length in the laboratory frame. This is achieved thanks to the asymmetric colliders, where the center od mass frame is boosted by a factor of $\beta \sim 0.5$ with respect to the lab frame.

- **High-resolution and large-coverage detector:** the interesting decays considered and their flavour dependence require precision in the particle type identification and the ability to reconstruct displaced vertices with an extremely high accuracy. Moreover, hermeticity is fundamental to avoid misidentification of events and loss of signal.

Moreover, a sophisticated data acquisition system was necessary to handle the huge event rate associated with the available luminosities, precision tracking and and vertexing devices in addition to software and storage technologies required to deal with those large samples. These requirements were fulfilled for the first time at the end of the '90s by the two machines: PEP-II at SLAC in Stanford (USA), and KEKB at the KEK facility in Tsukuba (Japan). They were able to produce routinely more than one million $B\overline{B}$ meson pairs per day. Two different detectors were designed for the two experiments: BaBar for PEP-II and Belle for KEKB [57].

All these features make B-factories suitable also to search for new physics on top of SM precision measurements. In particular, the high luminosity of the machine and the hermeticity of the detector are very important to study elusives particles such as ALPs. For this reason, Babar and Belle collaborations decided to acquire data also at different energies ($\Upsilon(nS)$ with $n = 1, 2, 3$). In the following chapter, these data will be very useful to our analysis to set bounds on the ALP parameter space.

Regarding the future, the scientific community is waiting for the beginning of the data taking of Belle-II [22] experiment, an update of the Belle detector and of the KEKB collider (now SUPER KEKB). The new machine will be able to provide an even larger luminosity that will probably reach the 50 ab^{-1} at the end of the data taking and, on top of this, the new detector is designed to improve even more the coverage and the sensibility. Differently from the previous two experiments, Belle-II will exploit the $B\overline{B}$ system to search for new physics, especially regarding the so called

"B-anomalies" and the Lepton Flavour Universality Violation (LFUV) [62–78], already spotted by BaBar, Belle and LHCb but still below the significance threshold. For this reason, the machine will not run at resonances below the $\Upsilon(4S)$: as it will be discussed in the following, this will have an impact on the type of searches for ALPs one can perform at B-factories.

4.2 ALP EFFECTIVE LAGRANGIAN

The dimension-five effective Lagrangian describing ALP interactions, above the electroweak symmetry breaking scale, is the one of Eq. 3.4:

$$\begin{aligned}\delta\mathcal{L}_{\text{eff}} = &\frac{1}{2}(\partial^\mu a)\,(\partial_\mu a) - \frac{m_a^2}{2}a^2 - \frac{g_{aBB}}{4}\,a\,B^{\mu\nu}\widetilde{B}_{\mu\nu} - \frac{g_{aWW}}{4}\,a\,W^{\mu\nu}\widetilde{W}_{\mu\nu} \\ &- \frac{g_{agg}}{4}\,a\,G_a^{\mu\nu}\widetilde{G}^a_{\mu\nu} - \frac{\partial_\mu a}{2}\sum_f g_{aff}\,\overline{f}\gamma^\mu\gamma_5 f\,,\end{aligned} \tag{4.1}$$

where $\widetilde{V}^{\mu\nu} = \frac{1}{2}\,\varepsilon^{\mu\nu\alpha\beta}V_{\alpha\beta}$, g_{aff} and g_{aVV} denote the ALP effective couplings to fermions and to the SM gauge bosons, $V \in \{g, B, W\}$, respectively. The dependence on the scale is, as usual, hidden inside the effective coupling:

$$g_{aVV} = \frac{\alpha_V}{2\pi}\frac{c_{aVV}}{f_a}\,, \tag{4.2}$$

where c_{aVV} are the adimensional coefficients. The same argument holds for fermionic couplings. The ALP mass m_a and the scale f_a are assumed to be independent parameters, in contrast to the QCD-axion paradigm, which is characterised by the relation $m_a\,f_a \approx m_\pi\,f_\pi$ [79]. Moreover, if the ultraviolet completion of Eq. (4.1) is not specified, the ALP couplings to gauge bosons and fermions are described by independent parameters, which can be of the same order of magnitude and which should, therefore, be simultaneously considered in phenomenological analyses.

At the energy-scales relevant at B-factories, the ALP interactions with the Z boson can be safely neglected, due to the Fermi constant suppression. Furthermore, the ALP couplings to the top-quark and $W^\pm$ boson are relevant only to the study of flavor-changing neutral currents observables, which are complementary to the probes discussed here – see e.g. Refs. [80–83] for a recent discussion. The only relevant couplings in Eq. (4.1) at low-energies are

$$\begin{aligned}\delta\mathcal{L}_{\text{eff}} \supset &\frac{1}{2}(\partial^\mu a)\,(\partial_\mu a) - \frac{m_a^2}{2}a^2 \\ &- \frac{g_{a\gamma\gamma}}{4}\,aF_{\mu\nu}\widetilde{F}_{\mu\nu} - \frac{g_{agg}}{4}\,a\,G_a^{\mu\nu}\widetilde{G}^a_{\mu\nu} - \frac{\partial_\mu a}{2}\sum_f g_{aff}\,\overline{f}\gamma^\mu\gamma_5 f\,,\end{aligned} \tag{4.3}$$

where $g_{a\gamma\gamma} = g_{aBB}\,\cos^2\theta_W + g_{aWW}\,\sin^2\theta_W$. The couplings relevant to ALP production are $\{g_{a\gamma\gamma}, g_{abb}\}$, while the other couplings only contribute to the ALP branching fractions.

Light pseudoscalar particles can also act as portals to a light dark sector [40, 84]. In this case, to describe these additional interactions, new couplings are customarily introduced. By assuming, for instance, an extra light and neutral dark fermion state χ, the following term should be considered in the effective Lagrangian:

$$\delta\mathcal{L}_{\text{eff}} \supset -g_{a\chi\chi}\,\frac{\partial_\mu a}{2}\,\overline{\chi}\gamma^\mu\gamma_5\chi\,, \tag{4.4}$$

where $g_{a\chi\chi}$ denotes a generic coupling, which can induce a sizable ALP decay into invisible final states, as will be considered in the following.

In the remained of this paper, $c_{aii} \equiv c_{aii}^{\rm eff}(\mu = m_b)$ will be assumed, and the ALP mass will be taken in the range $m_a \in (0.1 - 10)$ GeV, for which B-factories provide some of the most stringent bounds on its couplings.

4.3 B-FACTORIES PROBES OF INVISIBLE ALPS

In this Section, the potential of B-factories to probe ALP couplings in the $e^+e^- \to \gamma a$ channel will be discussed. Two main scenarios are typically considered in the literature, depending on the relative strength of the ALP coupling to SM and dark sector particles: either $|g_{a\chi\chi}| \ll |g_{a\rm SM}|$, or $|g_{a\chi\chi}| \gg |g_{a\rm SM}|$. In the first case, for m_a values in the GeV range, the ALP would typically decay in the detector, leaving the signatures $\gamma a(\to jj)$ [85, 86], $\gamma a(\to \gamma\gamma)$ [87–89] and $\gamma a(\to \ell\ell)$ [90–92], with $\ell = \{e, \mu, \tau\}$. This scenario is dubbed the *visible* ALP. If, however, the coupling to the dark sector $g_{a\chi\chi}$ is large, in comparison to the SM couplings, then the ALP will decay predominantly into an invisible channel, providing the mono-γ plus missing energy signature. This scenario will be referred to as the *invisible* ALP, [1] which also covers the possibility of a sufficiently long-lived ALP that does not decay in the detector.

In this chapter, the *invisible ALP* scenario will be considered for the sake of illustration. The main goal will be (i) to revisit the theoretical expressions available in the literature, including ALP coupling to bottom quarks, as well as previously unaccounted experimental uncertainties, and (ii) to propose an optimal strategy for future ALP analyses. Even though the main focus will be the minimalistic *invisible* ALP scenario, most of the observations that will be made in this paper can be translated *mutatis mutandis* to the *visible* case. After explaining the strategy for the invisible ALP case, some results on possible ALP decay channels will be shown in the following chapter.

NON-RESONANT ALP PRODUCTION: The most straightforward way of producing ALPs in e^+e^- facilities is via the non-resonant process $e^+e^- \to \gamma a$, as illustrated in Fig. 4.1. If the ALP does not decay inside the detector, as assumed throughout the chapter, this process would result in an energetic γ plus missing energy. The differential cross-section for this process, keeping explicit the ALP mass dependence, can be expressed as [42]

$$\left(\frac{{\rm d}\sigma(s)}{{\rm d}\cos\theta_\gamma}\right)_{\rm NR} = \frac{\alpha_{\rm em}}{128}\, g_{a\gamma\gamma}^2\, (3 + \cos 2\theta_\gamma) \left(1 - \frac{m_a^2}{s}\right)^3 , \tag{4.5}$$

where $s = E_{\rm cm}^2$, and θ_γ is the angle of photon emission with respect to the collision axis, in the center-of-mass frame. In this expression, the contributions coming from the exchange of an off-shell Z boson, which are also induced by c_{aWW} in Eq. (4.1), have been neglected, since they are suppressed, at low-energies, by $s/m_Z^2 \ll 1$. The integrated cross-section then gives:

$$\sigma_{\rm NR}(s) = \frac{\alpha_{\rm em}}{24}\, g_{a\gamma\gamma}^2 \left(1 - \frac{m_a^2}{s}\right)^3 . \tag{4.6}$$

While the non-resonant contribution to ALP production given above is unavoidable in any experiment relying on e^+e^- collisions [58], the situation at B-factories is more intricate since these experiments operate at specific $\Upsilon(nS)$ resonances. Therefore, it is crucial to account for the resonantly enhanced contributions, which can be

1 The *invisible* ALP case should not be confused with the traditional *invisible* QCD axion [8–11].

numerically significant, as will be shown in the following. Taking into account the resonant enhancement of this process will require some assumptions on the calculation of the non-perturbative contributions due to the hadronic nature of the $\Upsilon(nS)$ meson.

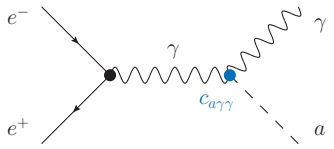

Figure 4.1: *Non-resonant contribution to the process $e^+e^- \to \gamma a$ produced via the effective coupling $g_{a\gamma\gamma}$ defined in Eq. (4.3).*

RESONANT ALP PRODUCTION: Vector quarkonia can produce significant resonant contributions to the mono-γ channel, $e^+e^- \to \Upsilon \to \gamma a$, since they are very narrow particles coupled to the electromagnetic current. Assuming a fixed center-of-mass energy $\sqrt{s} \approx m_\Upsilon$, as is the case at B-factories, and using the Breit-Wigner approximation, one finds for the resonant cross-section

$$\sigma_{\rm R}(s) = \sigma_{\rm peak} \frac{m_\Upsilon^2 \Gamma_\Upsilon^2}{(s-m_\Upsilon^2)^2 + m_\Upsilon^2 \Gamma_\Upsilon^2} \mathcal{B}(\Upsilon \to \gamma a)\,, \tag{4.7}$$

where m_Υ and Γ_Υ are the mass and width of a specific Υ resonance, and $\sigma_{\rm peak}$ is the peak cross-section defined as

$$\sigma_{\rm peak} = \frac{12\pi \mathcal{B}(\Upsilon \to ee)}{m_\Upsilon^2}\,, \tag{4.8}$$

with $\mathcal{B}(\Upsilon \to ee)$ being the leptonic branching fraction, experimentally determined for the different $\Upsilon(nS)$ resonances [29]. The effective couplings defined in Eq. (4.3) appear, instead, in the $\mathcal{B}(\Upsilon \to \gamma a)$ branching fraction, as illustrated in Fig. 4.2, which will be computed in full generality in Secs. 4.3.1 and 4.3.2.

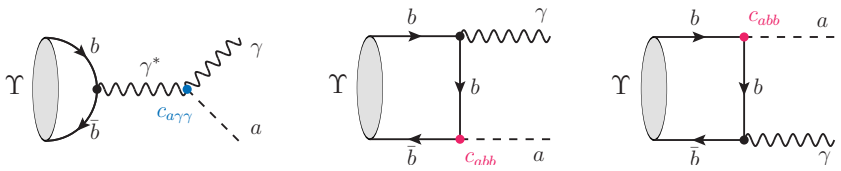

Figure 4.2: *Contributions to the $\Upsilon(nS) \to \gamma a$ decays from the effective couplings introduced in the Lagrangian or Eq. ((4.3)).*

RESONANT VS NON-RESONANT: Naively, one would expect that the resonant cross-section (Eq. (4.7)) clearly dominates over the non-resonant one (Eq. (4.6)) for the very narrow $\Upsilon(1S)$, $\Upsilon(2S)$ and $\Upsilon(3S)$ resonances, since $\Gamma_\Upsilon/m_\Upsilon \ll 1$. Nevertheless, this turns out to not be the case at B-factories, since these experiments are intrinsically limited by the energy spread of the e^+e^- beam, which is of order $\sigma_W \approx 5$ MeV at current facilities. [2] This value is considerably larger than the width of these resonances, which therefore cannot be fully resolved at B-factories. The only exception is the $\Upsilon(4S)$ resonance, for which $\Gamma_{\Upsilon(4S)} = 20.5$ MeV [95]. Therefore,

2 More specifically, the energy spread was $\sigma_W = 5.5$ MeV at BaBar (PEP) [29] and $\sigma_W = 5.24$ MeV at Belle (KEKB) [93], and it is expected to be $\sigma_W = 5.45$ MeV at Belle-II (SuperKEKB) [94].

one should expect a sizable reduction of the estimation in Eq. (4.7) for the lightest quarkonia resonances, due to this intrinsic experimental uncertainty.

To account for the beam-energy uncertainties in Eq. (4.7), the procedure presented in Ref. [96] has been adopted by performing a convolution of $\sigma_{\rm R}(s)$ with a Gaussian distribution, with spread σ_W,

$$\langle\sigma_{\rm R}(s)\rangle_{\rm vis} = \int {\rm d}q\, \frac{\sigma_{\rm R}(q^2)}{\sqrt{2\pi}\sigma_W} \exp\left[-\frac{(q-\sqrt{s})^2}{2\sigma_W^2}\right] . \tag{4.9}$$

At the very narrow $\Upsilon(nS)$ resonances, with $n = 1, 2, 3$, one finds $\Gamma_\Upsilon \ll \sigma_W$, in such a way that the previous expression can be simplified by writing [96]

$$\langle\sigma_{\rm R}(m_\Upsilon^2)\rangle_{\rm vis} = \rho\, \sigma_{\rm peak}\, \mathcal{B}(\Upsilon \to \gamma a) , \tag{4.10}$$

where the parameter ρ, defined as

$$\rho = \sqrt{\frac{\pi}{8}}\frac{\Gamma_\Upsilon}{\sigma_W} , \tag{4.11}$$

accounts for the cross-section suppression at the peak due to the finite beam-energy spread. These effects will be quantified in the following in two scenarios: (i) ALP with predominant couplings to photons, $|g_{a\gamma\gamma}| \gg |g_{abb}|$, and (ii) the general case with both $g_{a\gamma\gamma}$ and g_{abb} nonzero.

4.3.1 *The Photo-Philic Scenario:* $|g_{a\gamma\gamma}| \gg |g_{abb}|$

The scenario most commonly considered in the literature is the one with predominant ALP couplings to photons [59]. In this case, by neglecting g_{abb}, the first diagram in Fig. (4.2) leads to

$$\mathcal{B}(\Upsilon \to \gamma a)\Big|_{g_{abb}=0} = \frac{m_\Upsilon^2}{32\pi\alpha_{\rm em}}\, g_{a\gamma\gamma}^2 \left(1-\frac{m_a^2}{m_\Upsilon^2}\right)^3 \mathcal{B}(\Upsilon \to ee) , \tag{4.12}$$

which agrees with Ref. [58] in the massless ALP limit. Note that this expression does not require assumptions on hadronic uncertainties, since the hadronic matrix element appearing in this computation, namely $\langle 0|\bar{b}\gamma^\mu b|\Upsilon(p)\rangle$, also enters the process $\Upsilon \to ee$ which has been accurately measured experimentally [29]. Alternatively, $\mathcal{B}(\Upsilon \to ee)$ can be expressed in terms of the Υ decay constant, defined as

$$\langle 0|\bar{b}\gamma^\mu b|\Upsilon(p)\rangle \equiv m_\Upsilon\, f_\Upsilon\, \varepsilon^\mu(p) , \tag{4.13}$$

which encapsulates the QCD dynamics of this process and which has been independently computed, for the lighter Υ resonances, by means of numerical simulations of QCD on the lattice [97–99]. The previous definition allows to recast Eq. (4.12) in the more convenient form,

$$\mathcal{B}(\Upsilon \to \gamma a)\Big|_{g_{abb}=0} = \frac{\alpha_{\rm em}}{216\,\Gamma_\Upsilon} m_\Upsilon f_\Upsilon^2\, g_{a\gamma\gamma}^2 \left(1-\frac{m_a^2}{m_\Upsilon^2}\right)^3 . \tag{4.14}$$

The Lattice QCD (LQCD) determinations of $f_{\Upsilon(nS)}$ are summarized in Tab. 4.1 along with the values extracted from the experimentally determined $\mathcal{B}(\Upsilon(nS) \to e^+e^-)$ [29], showing a reasonable agreement.

In Table 4.2, Eq. (4.12) is combined with Eqs. (4.6) and (4.10) to estimate the resonant and non-resonant cross-section, for each Υ resonance, along with the peak cross-section $\sigma_{\rm peak}$ and the suppression parameter ρ. This computation has been performed with the Belle-II (KEKB) energy-spread for illustration, which is similar to the ones

$\Upsilon(nS)$	$f_\Upsilon^{\text{latt.}}$ (MeV)	$f_\Upsilon^{\text{exp.}}$ (MeV)
$\Upsilon(1S)$	680(14)	659(17)
$\Upsilon(2S)$	494(15)	468(27)
$\Upsilon(3S)$	539(84)	405(26)
$\Upsilon(4S)$	–	349(23)

Table 4.1: $\Upsilon(nS)$ *decay constants computed by means of numerical lattice simulations [97–99] or determined experimentally from* $\mathcal{B}(\Upsilon(nS) \to e^+e^-)$ *[29].*

$\Upsilon(nS)$	m_Υ [GeV]	Γ_Υ [keV]	σ_{peak} [nb]	ρ	$\langle\sigma_R(m_\Upsilon^2)\rangle_{\text{vis}}/\sigma_{\text{NR}}$
$\Upsilon(1S)$	9.460	54.02	$3.9(18)\times10^3$	6.1×10^{-3}	0.53(5)
$\Upsilon(2S)$	10.023	31.98	$2.8(2)\times10^3$	3.7×10^{-3}	0.21(3)
$\Upsilon(3S)$	10.355	20.32	$3.0(3)\times10^3$	2.3×10^{-3}	0.16(3)
$\Upsilon(4S)$	10.580	20.5×10^3	2.10(10)	0.83	$3.0(3)\times10^{-5}$

Table 4.2: *Estimated visible cross-section at Belle-II for* $e^+e^- \to \Upsilon \to \gamma a$ *compared to the non-resonant one,* $e^+e^- \to \gamma^* \to \gamma a$*. Here, vanishing ALP couplings with b-quarks have been assumed,* $c_{abb} = 0$*. Experimental inputs are taken from Ref. [29]. Belle-II machine parameter have been considered [94], namely* $\sigma_W = 5.45$ *MeV for the beam-energy spread.*

from BaBar (PEP) and Belle (KEK). From this table, one learns that even though the peak cross-section is large for the $\Upsilon(nS)$ resonances ($n = 1, 2, 3$), the beam-energy uncertainties entail a considerable suppression of the *visible* cross-section. These effects are milder for the $\Upsilon(4S)$ resonance, but in turn the cross-section at the peak is much smaller in this case. The final results are summarized in the last column of Table 4.2, which shows that the effective resonant cross-section is smaller than the non-resonant one, but it still contributes with numerically significant effects. For the (very) narrow resonances $\Upsilon(nS)$ ($n = 1, 2, 3$), the resonant contribution amounts to corrections between 20% and 50% to the non-resonant one, which should be included when reinterpreting experimental searches. [3] On the other hand, for the $\Upsilon(4S)$ resonance, the resonant contribution turns out to be negligible, due to its larger width, as expected.

4.3.2 *The General case:* $g_{a\gamma\gamma} \neq 0$ *and* $g_{abb} \neq 0$

The previous discussion implies that the resonant contributions are not only important to correctly assess limits on the ALP coupling to photons, $g_{a\gamma\gamma}$, but they also open the window to probe the ALP coupling to b-quarks, g_{abb}, cf. Fig. 4.2. The simultaneous presence of these contributions gives rise to a rich phenomenology which will be discussed in the following.

Firstly, the hadronic matrix element needed to estimate the g_{abb} contribution to $\mathcal{B}(\Upsilon \to \gamma a)$ is far more intricate than the one given in Eq. (4.13), since this is a QCD-structure dependent emission, as depicted in the last two diagrams in Fig. (4.2). This contribution was first computed by Wilczek for a SM-like Higgs by using a non-

3 Interference effects between the non-resonant and resonant $c_{a\gamma\gamma}$ terms turn out to be negligible due to the small width of the $\Upsilon(nS)$ resonances.

relativistic approximation [5, 100], see also Ref. [101–104]. [4] By using a similar approach, the total $\mathcal{B}(\Upsilon \to \gamma a)$ branching fraction reads

$$\mathcal{B}(\Upsilon \to \gamma a) = \frac{\alpha_{\rm em}}{216\,\Gamma_\Upsilon} m_\Upsilon f_\Upsilon^2 \left(1 - \frac{m_a^2}{m_\Upsilon^2}\right) \left[g_{a\gamma\gamma} \left(1 - \frac{m_a^2}{m_\Upsilon^2}\right) - 2\, g_{abb} \right]^2 . \tag{4.15}$$

This expression includes, the most general $g_{a\gamma\gamma}$ and g_{abb} contributions, as well as their interference. Note, however, that the computation of the g_{abb} contributions are done within a first approximation that considerably simplifies the QCD structure-dependent emission of this decay. If a new physics signal is indeed observed in such observable, a more accurate theoretical calculation would be needed to fully assess the (non-perturbative) effects associated to the last two diagrams in Fig. 4.2.

Eq. (4.15) shows that the $g_{a\gamma\gamma}$ and g_{abb} couplings can induce comparable contributions to the non-resonant cross-section in Eq. (4.7). Often, in QCD axion models such as DFSZ, the fermionic coupling of the axion are tree-level while the bosonic is generated by the axial anomaly, and as a consequence should be suppressed by a loop factor. However, once a more general ALP scenario is considered, from a purely effective point of view the situation is no more so clear. The magnitude of the effective couplings are highly dependent on the underlying UV model and they cannot be determined in the EFT, so in principle they should be considered of the same order. For example, for a general KSVZ-like model, the axion coupling with photons is proportional to the number of heavy extra fermions, which can be very large, increasing significantly the relative weight of $g_{a\gamma\gamma}$. Depending on the relative sign of these two couplings, they can interfere destructively or constructively, as will be illustrated with a concrete example in Chap. 5. Finally, note that Eq. (4.15) shows a different dependence on m_a and $\{g_{a\gamma\gamma}, g_{abb}\}$ than the non-resonant cross-section in Eq. (4.6). A comparison between $\langle\sigma_{\rm R}\rangle_{\rm vis}$ and $\langle\sigma_{\rm NR}\rangle_{\rm vis} \approx \sigma_{\rm NR}$ is postponed to Chap. 5 where a concrete scenario will be considered.

4.4 SUMMARY OF EXPERIMENTAL SEARCHES

From the previous discussion, one learns that the non-resonant cross-section, via the coupling $g_{a\gamma\gamma}$, is the largest one, but it can be of the same order of the resonant one, cf. Tab. 4.2. Moreover, the latter searches have the advantage of being sensitive to both $g_{a\gamma\gamma}$ and g_{abb} couplings. Based on these observations, ALP searches at B-factories can be classified in the following three categories:

- **Resonant searches**: Excited quarkonia states $\Upsilon(nS)$ (with $n > 1$) can decay into lighter $\Upsilon(nS)$ resonances via pion emission, as for example $\Upsilon(2S) \to \Upsilon(1S)\,\pi^+\pi^-$ and $\Upsilon(3S) \to \Upsilon(1S)\,\pi^+\pi^-$. By exploiting the kinematics of these processes one can reconstruct the $\Upsilon(1S)$ meson and then study its decay into a specific final state, which can, for instance, be the invisible Υ decay [106], or the Υ decay into photon and a light (pseudo)scalar particle [87, 88]. These searches are dubbed *resonant*, since they allow to directly probe $\mathcal{B}(\Upsilon \to \gamma a)$ in a *model-independent* way, regardless of the non-resonant contribution from Fig. 4.1. In other words, reported limits on $\mathcal{B}(\Upsilon(1S) \to \gamma a)$ can be used to constrain both $g_{a\gamma\gamma}$ and g_{abb} via Eq. (4.15). Searches along these lines have been performed, for instance, by BaBar [87] and, more recently, by Belle [88], under the assumption that the ALP does not decay into visible particles inside the detector.

4 Compatible results have also been obtained in Ref. [105] for small pseudoscalar masses by using a QCD sum-rules approach.

- **Mixed (non-)resonant searches**: Alternatively, experimental searches could be performed at $\Upsilon(nS)$ (with $n = 1, 2, 3$) without identifying the Υ decay from a secondary vertex. Example of such experimental searches are the ones performed at $\sqrt{s} = m_{\Upsilon(3S)}$ [89], where limits on $\mathcal{B}(\Upsilon(3S) \to \gamma a) \times \mathcal{B}(a \to \text{inv})$ are extracted from the total $e^+e^- \to \gamma a(\to \text{inv})$ cross-section. From the above discussion, however, it is clear that this method is probing both resonant (Eq. (4.10)) and non-resonant (Eq. (4.6)) cross-sections and therefore model-independent limits on $\mathcal{B}(\Upsilon(3S) \to \gamma a)$ could not be extracted from these experimental results. The only scenarios for which such limits can be derived are the ones with $|g_{a\gamma\gamma}| \ll |g_{abb}|$, as predicted in models with an extended Higgs sector [107–109], since the non-resonant cross-section vanishes in this case.

  In the most general ALP scenario, instead, the limits on $\{g_{a\gamma\gamma}, g_{abb}\}$ can be obtained from Ref. [89] via a rescaling factor,

$$\frac{\langle \sigma_{\rm R}(s) + \sigma_{\rm NR}(s) \rangle_{\rm vis}}{\langle \sigma_{\rm R} \rangle_{\rm vis}} \approx 1 + \frac{\sigma_{\rm NR}}{\langle \sigma_{\rm R} \rangle_{\rm vis}} \,, \tag{4.16}$$

  which accounts for the non-resonant contributions (Eq. (4.9)) that have been overlooked experimentally in the total cross-section. For instance, in the case where $g_{abb} = 0$, one obtains constraints on $g_{a\gamma\gamma}$ which are a factor of ≈ 3 more stringent than the estimation that overlooks the latter effects, cf. Table 4.2. Note, also, that similar effects have also been overlooked in reinterpretations of other experimental limits, as for example the ones on $\mathcal{B}(\Upsilon(3S) \to \gamma a) \times \mathcal{B}(a \to \text{hadrons})$ [85] to constrain the product of ALP couplings to photons and gluons [23].

  The reinterpretation described above, for the results from Ref. [89] and similar searches, has a possible caveat related to the treatment of the background. In these experimental analyses, the background is determined by considering an independent data sample collected outside the resonance region, typically ≈ 30 MeV below $m_{\Upsilon(3S)}$. While this strategy allows for a robust determination of the SM background in scenarios with $g_{a\gamma\gamma} = 0$, this is not an efficient method if $g_{a\gamma\gamma}$ is non-negligible. In the latter case, the background sample also receives contributions from the non-resonant diagram in Fig. 4.1, which turns out to be the dominant effect. For that reason, it is important that future experimental searches determine the background without relying on off-resonance samples, as performed, for instance, in dark photon searches [110]. Furthermore, it would be helpful to also report the limits on the $e^+e^- \to \gamma a$ cross-section instead of the $\Upsilon(nS)$ branching fraction, as these results contain the full information on both resonant and non-resonant contributions.

- **Non-resonant searches**: The resonant cross-section is negligible at the $\Upsilon(4S)$ resonance, as can be seen from Table 4.2, since its mass lies just above the $B\overline{B}$ production threshold. Therefore, experimental searches at the $\Upsilon(4S)$ resonance can only probe the $g_{a\gamma\gamma}$ coupling via the non-resonant ALP production illustrated in Fig. 4.1. To our knowledge, no such ALP search has been performed yet at B-factories. For the future, this type of search could exploit the large luminosity collected at $\Upsilon(4S)$ Belle-II, providing the most stringent limits on $g_{a\gamma\gamma}$ for a GeV ALP mass. See Ref. [59] for a recent discussion on Belle-II prospects.

In summary, ALP production receives both resonant and non-resonant contributions at B-factories. The interplay between these production mechanisms allows to classify three complementary experimental strategies: (i) *resonant* searches of

$\Upsilon \to \gamma a$, from which one could infer bounds on g_{abb} and $g_{a\gamma\gamma}$, (ii) *mixed (non-)resonant* searches which are sensitive to a different combination of g_{abb} and $g_{a\gamma\gamma}$, and (iii) *non-resonant* searches which depend solely on $g_{a\gamma\gamma}$. Before deriving constraints on the ALP couplings from existing BaBar and Belle data, it is important to stress once again that the conclusions outlined above are general and that they apply, for instance, to searches for ALP decaying into visible particles, such as hadrons [85, 86], $\mu\mu$ [90, 91] and $\tau\tau$ [92].

5

CONSTRAINING THE ALP PARAMETER SPACE

In this Chapter, constraints on the ALP parameter space are derived from existing BaBar and Belle data, and prospects for the Belle-II experiment are discussed. The arguments explained in the previous Chapter will be used to compute the bounds on the parameter space in a consistent and robust way. In the first Section, the *invisible* ALP scenario will be considered, by assuming that $\mathcal{B}(a \to \text{inv}) = 1$, or equivalently, that the ALP does not decay inside the detector, while in the second Section, the possibility for the ALP to decay into a visible final state will be taken into account.

5.1 THE INVISIBLE ALP SCENARIO

Firstly, separate constraints on $g_{a\gamma\gamma}$ and g_{abb} are derived by assuming that the other Wilson coefficient vanishes. These couplings are subject to the limits on $\mathcal{B}(\Upsilon(1S) \to \gamma a) \times \mathcal{B}(a \to \text{inv})$ reported by BaBar [87] and Belle [88], in which the quarkonia state is produced via the $\Upsilon(2S) \to \Upsilon(1S)\pi^+\pi^-$ decay, cf. discussion in Sec. 4.4. Limits on $\mathcal{B}(\Upsilon(3S) \to \gamma a) \times \mathcal{B}(a \to \text{inv})$ reported by BaBar [89] are also considered by including the non-resonant contribution overlooked in the experimental analysis, cf. Eq. (4.16). These constraints are combined in Fig. 5.1 to constrain $g_{a\gamma\gamma}$ and g_{abb} as a function of the ALP mass. While the limits on g_{abb} from the different experimental searches turn out to be similar, the recast described above of $\Upsilon(3S)$ data provides the most stringent limit on $g_{a\gamma\gamma}$. For comparison, the limits obtained by neglecting the non-resonant contribution are also depicted in the same plot by the dashed-dotted line, which turn out to be weaker, as expected. It should be stressed that this reinterpretation is not strictly correct due to the background treatment in Ref. [89], but it can be seen as the expected sensitivity of such searches if the background is determined without relying on off-resonance samples, as discussed in Sec. 4.4.

Next, the allowed parameter space in the plane $\{g_{a\gamma\gamma}, g_{abb}\}$ when both couplings are simultaneously considered is shown in Fig. 5.2. To this purpose, two fixed values of m_a are taken, namely 1 GeV (left panel) and 7 GeV (right panel), and $g_{abb}/g_{a\gamma\gamma} > 0$ is assumed, in such a way that both couplings interfere destructively in Eq. (4.15). In this case, it can be seen from Fig. 5.2 that the $\Upsilon(1S)$ constraints have an unconstrained direction that cannot be resolved by only relying on resonant ALP searches. [1] The combination of couplings that lead to this cancellation depends on the ALP mass, especially for m_a values near the kinematical threshold, as depicted in the right panel of Fig. 5.2. BaBar results obtained at the $\Upsilon(3S)$ resonance, which is not reconstructed, depicts a different sensitivity to $\{g_{a\gamma\gamma}, g_{abb}\}$, as shown by the blue regions in the same plot. While a cancellation between $g_{a\gamma\gamma}$ and g_{abb} is possible for resonant cross-section, this cannot occur for the non-resonant one (4.6), which depends only on the $g_{a\gamma\gamma}$ coupling. The combination of these complementary searches allows one to corner the ALP parameter space as depicted in Fig. 5.2. Moreover, projections for searches performed at Belle-II, operating at the $\Upsilon(4S)$ resonance, as

1 A similar observation has been recently made for ALP produced in the rare decays $K^+ \to \pi^+ a$ and $B \to K^{(*)} a$, for which the top-quark and W loops can interfere destructively [83].

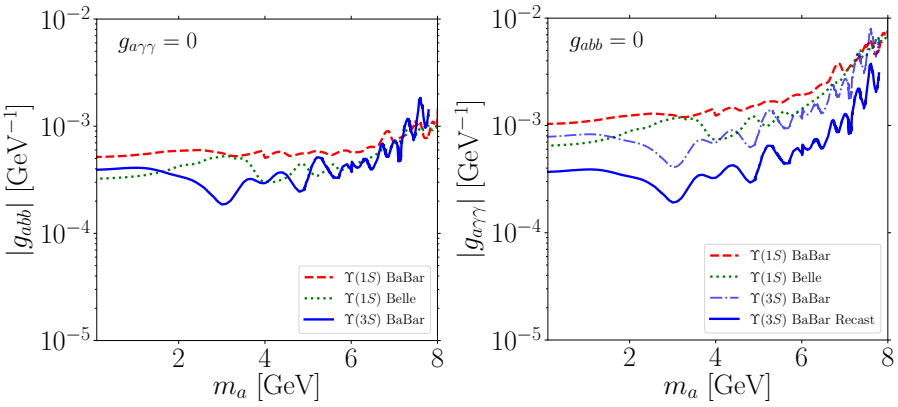

Figure 5.1: *Upper limits on g_{abb} (left panel) and $g_{a\gamma\gamma}$ (right panel) as a function of m_a for the invisible ALP scenario. Experimental limits on $\mathcal{B}(\Upsilon(nS) \to \gamma A) \times \mathcal{B}(a \to \text{inv})$ obtained by BaBar [87, 89] and Belle [88] are considered. For the constraint on $g_{a\gamma\gamma}$ obtained from data collected at $\Upsilon(3S)$ resonance [89], the reinterpretation of BaBar limits that neglects the non-resonant ALP production (blue dashed-dotted line) is also considered, along with the rescaled limit that accounts for both resonant and non-resonant ALP production (solid blue line), cf. Eq. (4.16). The latter results provide the most stringent limits on the ALP photon coupling from searches at B-factories.*

computed in Ref. [59], are displayed in the same plot for an expected luminosity of 20 fb^{-1}.

Before concluding, comments on studies providing similar constraints on ALP couplings are needed. The authors of Ref. [59] have performed a reinterpretation of the BaBar dark-photon search in the $e^+e^- \to \gamma + \text{inv}$ channel [110]. The constraints on $g_{a\gamma\gamma}$ they obtain, by only considering the non-resonant process from Fig. 4.1, are a factor of ≈ 2 better than the limits derived in this paper. Nonetheless, such reinterpretation should be performed with caution for two reasons. Firstly, the kinematical distribution of this process is different for ALPs and dark photons scenarios, as can be inferred from the comparison between Eq. (4.6) with the expressions given in Ref. [111]. Therefore, to translate the dark photon constraints into limits on ALP couplings, one should correct for the different detector efficiencies for the two cases. Another important issue is the fact that the dark photon analysis from Ref. [110] combine off-resonance data with data collected at the $\Upsilon(2S)$, $\Upsilon(3S)$ and $\Upsilon(4S)$ resonances. While the photons accompanied by dark photons cannot be produced via $\Upsilon(nS)$ decays, this is not the case for ALPs, as discussed above. Therefore, it is important to account for the resonant ALP production estimated in Tab. 4.2, which is different for each data set considered by BaBar and which can amount to corrections of $\mathcal{O}(50\%)$ to the total cross-section.

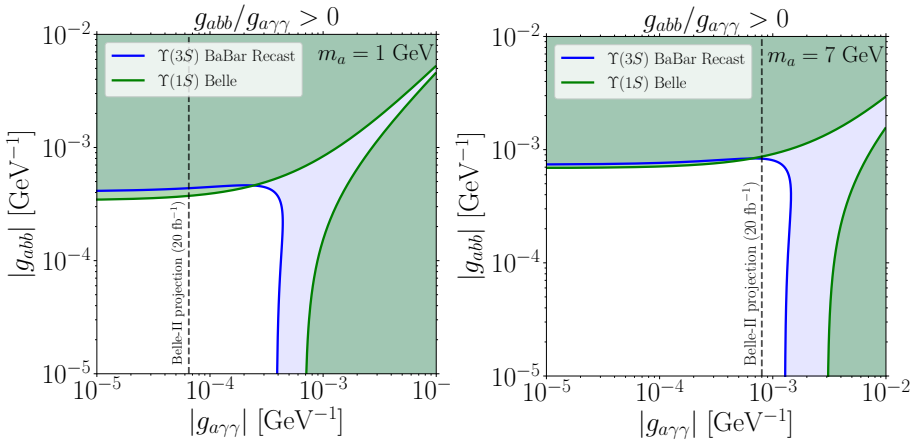

Figure 5.2: *Excluded $\{g_{a\gamma\gamma}, g_{abb}\}$ parameter space for the invisible ALP scenario when two couplings are simultaneously present. Belle constraints [88] at $\Upsilon(1S)$ (green line) and our recast of BaBar constraints [89] at $\Upsilon(3S)$ (blue line) are superimposed for the illustrative cases with $m_a = 1$ GeV (left panel) and $m_a = 7$ GeV (right panel). Projections for Belle-II sensitivity are depicted by the dashed lines. See text for details.*

6

CONCLUSIONS

In this part, ALP production in association with photons at B-factories is revisited. In particular, the contributions to the $e^+e^- \to \gamma a$ cross section are derived, assuming generic non-vanishing ALP couplings with both photons and b-quarks. The production of ALPs can proceed through the non-resonant channel, $e^+e^- \to \gamma a$, as well as the resonant one, $e^+e^- \to \Upsilon(nS) \to \gamma a$, which has the unique potential to probe the ALP coupling to b-quarks. After computing the relevant cross-sections and accounting for the effects stemming from the beam-energy uncertainty at B-factories, three distinct and complementary experimental searches have been identified:

i) *Resonant searches* that exploit decays such as $\Upsilon(2S) \to \Upsilon(1S)\,\pi^+\pi^-$ and/or $\Upsilon(3S) \to \Upsilon(1S)\,\pi^+\pi^-$ to directly probe the $\Upsilon(1S)$ decays [87, 88], which turn out to be equally sensitive to ALP couplings to photons and bottom quarks, as shown in Eq. (4.15);

ii) *Mixed (non-)resonant searches* that use, instead, the primarly produced $\Upsilon(nS)$ resonance, with $n = 1, 2, 3$, as in the analysis performed in Ref. [89]. These searches can probe both resonant and non-resonant ALP production, and hence are more sensitive to the ALP coupling to photons than to the one with b-quarks, cf. Sec. 4.4;

iii) *Non-resonant searches*, as the ones performed at $\sqrt{s} = m_{\Upsilon(4S)}$, that can provide information only on the ALP coupling to photons, cf. Table 4.2. Note, in particular, that neither Babar or Belle have reported such an analysis thus far.

Previous phenomenological analyses overlooked the distinction between these types of experimental searches and the optimal experimental strategies have also been discussed.

To illustrate the phenomenological implications of the effects mentioned above, the scenario with an ALP decaying into invisible final states has been considered. Constraints on the parameter space $\{m_a;\, g_{a\gamma\gamma}, g_{abb}\}$ have been derived from existing BaBar and Belle data, and projections for Belle-II have been discussed. In particular, constraints from resonant searches have a flat direction due to possible cancellations between $g_{a\gamma\gamma}$ and g_{abb} contributions in $\mathcal{B}(\Upsilon(1S) \to \gamma a)$. These flat directions, however, can be removed by existing mixed (non-)resonant searches performed at $\sqrt{s} = m_{\Upsilon(3S)}$, due to the interplay between resonant and non-resonant contributions described above. In the future, the Belle-II experiment has the great opportunity to perform a first search at $\sqrt{s} = m_{\Upsilon(4S)}$, probing solely the $g_{a\gamma\gamma}$ coupling, and providing a complementary piece of information to the aforementioned constraints.

Part III

ALPS IN A COMPOSITE HIGGS FRAMEWORK

7

THE MINIMAL AXION MLσM

The so-called Composite Higgs (CH) models provide an elegant solution to the Electroweak (EW) Hierarchy Problem. First introduced in the middle of the '80s [112–114], now they are experiencing a revival of interest with a more economical symmetry content [115–117]. The Minimal Composite Higgs Model (MCHM) [115] is based on the non-linear realisation of the $SO(5)/SO(4)$ spontaneous breaking, relying on a not well identified strong dynamics. The four Nambu-Goldstone bosons (GBs), arising from the global symmetry breaking, can be identified with the three longitudinal components of the SM gauge bosons and the Higgs. The Higgs field gains a mass term thanks to the gauging of the SM group and to the interactions with the SM fermions.

A general drawback of these CH models is represented by their effective formulation: the generality of the effective approach comes together with a limited range of validity in energy. Refs. [118–120] attempted to improve this aspect, providing a renormalisable description of the scalar sector. Following the treatment done in Ref. [24], the Minimal $SO(5)/SO(4)$ Linear σ model (MLσM) is constructed extending the SM spectrum by the introduction of an EW singlet scalar field σ and a set of vector-like fermions in the singlet and in the fundamental representations of $SO(5)$. In the limit of large mass the σ field is integrated out and the the model falls back onto the usual effective non-linear description of the MCHM [115,118,121–123], that represents a specific realisation of the so-called Higgs Effective Field Theory [124–144] Lagrangian describing the most general Higgs couplings to SM gauge bosons and fermions, which preserve the SM gauge symmetry.

The presence of a set of heavy extra fermions makes the MLσM an optimal framework where to look for a solution to the strong CP problem. A realisation of the KSVZ axion mechanism [8, 9] can be provided by extending the scalar spectrum with an additional scalar field s, $SO(5)$ and EW singlet, and by enlarging the symmetry content with an extra Peccei-Quinn $U(1)_{PQ}$ [1]. The angular component of the extra scalar s may indeed represent an axion. This idea has been firstly developed in Ref. [145] and this class of models will be dubbed Axion Minimal Linear σ Model (AMLσM). Even in this simple setup, the choice of the PQ charge assignment is not unique and different choices lead to physically distinct Lagrangians.

The aim of the following sections is to illustrate in details the minimal AMLσM and to analyse the phenomenological features. After introducing the full Lagrangian of the model, a "minimal" scenario will be identified by imposing some strong physical requirements and a "minimality" criteria in terms of number of parameters entering in the Lagrangian.

7.1 FIELD CONTENT AND LAGRANGIAN

The MLσM based on the linear $SO(5)/SO(4)$ symmetry breaking realisation has been analysed in Ref. [24]. In this class of minimal models, an additional $U(1)_X$ is introduced in order to ensure the correct hypercharge assignment. The field content of the original MLσM is the following:

1. The four SM gauge bosons associated to the SM gauge symmetry.

2. A real scalar field ϕ in the fundamental representation of $SO(5)$, which includes the three longitudinal components of the SM gauge bosons π_i, $i = 1, 2, 3$, the Higgs field h and the additional complex scalar field σ, singlet under the SM gauge group:

$$\phi = (\pi_1, \pi_2, \pi_3, h, \sigma)^T \qquad \xrightarrow{u.g.} \qquad \phi = (0, 0, 0, h, \sigma)^T \tag{7.1}$$

   where the last expression holds when selecting the unitary gauge, which will be used throughout the next sections.

3. Exotic vector fermions coupled directly to the $SO(5)$ scalar sector through $SO(5)$ invariant proto-Yukawa interactions. These fermions transform either in the fundamental of $SO(5)$, and they will be labelled as ψ, or in the singlet representation of $SO(5)$, dubbed χ. For both types of fermions, two distinct $U(1)_X$ assignments are considered, $2/3$ and $-1/3$. They are necessary to induce mass terms for both the SM up and the down quark sectors.

4. SM fermions, which do not couple directly to the Higgs field. SM fermion masses are originated through SM–exotic fermion interactions in the spirit of the fermion partial compositeness mechanism [146–149]. SM fermions do not come embedded in a complete representation of $SO(5)$, leading to a soft explicit $SO(5)$ symmetry breaking. Although the whole SM fermion sector could be considered, only the top and bottom quarks will be retained in what follows. This simplification does not have relevant consequences on the results presented here and the three generation setup can be easily included.

The AMLσM includes, in addition to the previous content:

5. A complex scalar field s, singlet under the global $SO(5) \times U(1)_X$ and the SM gauge group. Adopting an exponential notation,

$$s \equiv \frac{r}{\sqrt{2}} e^{ia/f_a} \tag{7.2}$$

   the degrees of freedom are defined as the radial component r and the angular one a, to be later identified with the physical axion. Following the philosophy adopted in Ref. [24] any direct coupling between the scalar s and the SM fermions is not introduced, as it will be discussed in more details in the following.

The complete renormalisable Lagrangian for the AMLσM can be written as the sum of three terms describing respectively the pure gauge, fermionic and scalar sectors,

$$\mathcal{L} = \mathcal{L}_{\rm g} + \mathcal{L}_{\rm f} + \mathcal{L}_{\rm s}\,. \tag{7.3}$$

The explicit expression for each piece will be detailed in the following subsections.

7.1.1 *The Gauge Lagragian*

The first piece of the Lagrangian, $\mathcal{L}_{\rm g}$, contains the SM gauge kinetic and the θ-term,

$$\mathcal{L}_{\rm g} = -\frac{1}{4} G^{a,\mu\nu} G^a_{\mu\nu} - \frac{1}{4} W^{a,\mu\nu} W^a_{\mu\nu} - \frac{1}{4} B^{\mu\nu} B_{\mu\nu} + \frac{\alpha_s}{8\pi} \theta G^{a,\mu\nu} \widetilde{G}^a_{\mu\nu} \tag{7.4}$$

with the indices summed over $SU(3)_c$ or $SU(2)_L$, and

$$\widetilde{G}_{\mu\nu} \equiv \frac{1}{2} \epsilon_{\mu\nu\rho\sigma} G^{\rho\sigma} \qquad (\text{with} \quad \epsilon_{1230} = +1) \tag{7.5}$$

The introduction of the axion can provide a natural explanation for the vanishing of the QCD-θ term.

7.1.2 *The Fermionic Lagrangian*

According to the spectrum and symmetries described in the previous section, the fermionic part of the renormalisable Lagrangian in agreement with Ref. [145], although with a slightly different notation, reads

$$\begin{aligned}
\mathcal{L}_{\rm f} = & \; \bar{q}_L i\not{D} q_L \, + \, \bar{t}_R i\not{D} t_R \, + \, \bar{b}_R i\not{D} b_R \\
& + \overline{\psi}\left[i\not{D} - M_5\right]\psi \, + \, \overline{\chi}\left[i\not{D} - M_1\right]\chi \, - \, \left[y_1\,\overline{\psi}_L\,\phi\,\chi_R + y_2\,\overline{\psi}_R\,\phi\,\chi_L + \text{h.c.}\right] \\
& - \left[z_1\,\overline{\chi}_R\,\chi_L\,s + \tilde{z}_1\,\overline{\chi}_R\,\chi_L\,s^* + z_5\,\overline{\psi}_R\,\psi_L\,s + \tilde{z}_5\,\overline{\psi}_R\,\psi_L\,s^* + \text{h.c.}\right] \\
& + \left[\Lambda_1\,(\bar{q}_L\Delta_{2\times 5})\,\psi_R + \Lambda_2\,\overline{\psi}_L\,(\Delta_{5\times 1} t_R) + \Lambda_3\,\overline{\chi}_L t_R + \text{h.c.}\right] \\
& + \overline{\psi}'\left[i\not{D} - M_5'\right]\psi' \, + \, \overline{\chi}'\left[i\not{D} - M_1'\right]\chi' \, - \, \left[y_1'\,\overline{\psi}_L'\,\phi\,\chi_R' + y_2'\,\overline{\psi}_R'\,\phi\,\chi_L' + \text{h.c.}\right] \\
& - \left[z_1'\,\overline{\chi}_R'\,\chi_L'\,s + \tilde{z}_1'\,\overline{\chi}_R'\,\chi_L'\,s^* + z_5'\,\overline{\psi}_R'\,\psi_L'\,s + \tilde{z}_5'\,\overline{\psi}_R'\,\psi_L'\,s^* + \text{h.c.}\right] \\
& + \left[\Lambda_1'\left(\bar{q}_L\Delta_{2\times 5}'\right)\psi_R' + \Lambda_2'\,\overline{\psi}_L'\left(\Delta_{5\times 1}' b_R\right) + \Lambda_3'\,\overline{\chi}_L' b_R + \text{h.c.}\right] .
\end{aligned} \tag{7.6}$$

The first line shows the kinetic terms for the 3^{rd} generation SM quarks, being q_L the left-handed (LH) $SU(2)_L$ doublet and t_R and b_R the right-handed (RH) singlet counterparts. The second line contains the kinetic and mass terms for the exotic vector fermions, ψ and χ (with $U(1)_X$ charge $2/3$). The direct mass terms for the heavy fermions are denoted by $M_{1,5}$ respectively for the fermions in the singlet and fundamental representations. The proto-Yukawa couplings between the heavy fermions and the real scalar quintuplet field ϕ are also included in the second line. The third line displays the Yukawa-like couplings of the exotic fermions with the complex scalar singlet s. Two different type of couplings, z and $\tilde{z}$, have been introduced reflecting the freedom in choosing the PQ charges of s and of the fermionic bilinears. The fourth line contains the interactions between the top quark and exotic fermions with $U(1)_X$ charge equal to $2/3$.

While, the second and third lines of the Lagrangian explicitly preserve $SO(5)$, the partial compositeness terms in the fourth line, proportional to $\Lambda_{1,2}$, explicitly break the global $SO(5)$ symmetry. The combinations $\Lambda_1\Delta_{2\times 5}$ and $\Lambda_2\Delta_{5\times 1}$ could play the role of spurions [150–154] that formally ensure the $SO(5)\times U(1)_X$ invariance of the operators. The exotic fermion spinors can be decomposed under the $SU(2)_L$ quantum numbers as follows:

$$\psi \sim (K,\, Q,\, T_5)\ , \qquad\qquad \chi \sim T_1\,, \tag{7.7}$$

where K and Q are doublets and $T_{1,5}$ singlets of $SU(2)_L$. The resulting interactions preserve the gauge EW symmetry, with the hypercharge defined as

$$Y = \Sigma_R^{(3)} + X\,, \tag{7.8}$$

with $\Sigma_R^{(3)}$ the third component of the global $SU(2)_R$ ($1/2$ for K and $-1/2$ for Q) and X the $U(1)_X$ charge of the spinor.

The last three lines describe the sector associated to the bottom quark. The exotic vector fermions, ψ' and χ' have $U(1)_X$ charge $-1/3$ in order to allow the direct partial compositness coupling with the bottom. Their decomposition in terms of $SU(2)_L$ representations, reads

$$\psi' \sim \left(Q',\, K',\, B_5'\right)\ , \qquad\qquad \chi' \sim B_1'\,, \tag{7.9}$$

being Q' and K' doublets of $SU(2)_L$ (with $\Sigma_R^{(3)}$ component $1/2$ and $-1/2$ respectively) and $B_{1,5}'$ singlets of $SU(2)_L$.

	$SO(5)\times U(1)_X$	$SU(3)_C\times SU(2)_L\times U(1)_Y$	$Q_{\rm em}$
ψ	$(\mathbf{5},\,2/3)$	$K=(\mathbf{3},\mathbf{2},7/6)$ $Q=(\mathbf{3},\mathbf{2},1/6)$ $T_5=(\mathbf{3},1,2/3)$	$5/3, 2/3$ $2/3, -1/3$ $2/3$
χ	$(1,\,2/3)$	$T_1=(\mathbf{3},1,2/3)$	$2/3$
ψ'	$(\mathbf{5},\,-1/3)$	$Q'=(\mathbf{3},\mathbf{2},1/6)$ $K'=(\mathbf{3},\mathbf{2},-5/6)$ $B_5=(\mathbf{3},1,-1/3)$	$2/3, -1/3$ $-1/3, -4/3$ $-1/3$
χ'	$(1,\,-1/3)$	$B_1=(\mathbf{3},1,-1/3)$	$-1/3$

Table 7.1: *Decomposition of the exotic fermions and their transformation properties under the SM gauge symmetry.*

A summary of the decomposition of the exotic fermions and their transformation properties under the SM gauge symmetry can be found in Tab. 7.1.

The Lagrangian in Eq. (7.6) can be rewritten for later convenience in terms of fermionic vectors regrouping all the spinors components ordered accordingly of their electric charge,

$$\Psi = \left(K^u,\, \mathcal{T},\, \mathcal{B}\,, K'^d\right)\,, \tag{7.10}$$

with

$$\mathcal{T} = \left(t,\, Q^u,\, K^d,\, T_5,\, T_1,\, Q'^u\right)\,, \qquad \mathcal{B} = \left(b,\, Q'^d,\, K'^u,\, B_5',\, B_1',\, Q^d\right)\,. \tag{7.11}$$

The fermion mass terms in Eq. (7.6) can then be written as

$$\mathcal{L}_{\mathcal{M}} = -\overline{\Psi}_L\, \mathcal{M}_f(h,\sigma,r)\, \Psi_R\,, \tag{7.12}$$

where the field dependent fermion mass matrix $\mathcal{M}_f$ is a 14×14 block diagonal matrix,

$$\mathcal{M}_f(h,\sigma,r) = \texttt{diag}\Big(M_5(r),\, \mathcal{M}_{\mathcal{T}}(h,\sigma,r),\, \mathcal{M}_{\mathcal{B}}(h,\sigma,r),\, M_5'(r)\Big)\,. \tag{7.13}$$

For the top sector one has explicitly

$$\mathcal{M}_{\mathcal{T}}(h,\sigma,r) = \begin{pmatrix} 0 & \Lambda_1 & 0 & 0 & 0 & \Lambda_1' \\ 0 & M_5(r) & 0 & 0 & y_1\frac{h}{\sqrt{2}} & 0 \\ 0 & 0 & M_5(r) & 0 & y_1\frac{h}{\sqrt{2}} & 0 \\ \Lambda_2 & 0 & & M_5(r) & y_1\sigma & 0 \\ \Lambda_3 & y_2\frac{h}{\sqrt{2}} & y_2\frac{h}{\sqrt{2}} & y_2\sigma & M_1(r) & 0 \\ 0 & 0 & 0 & 0 & 0 & M_5'(r) \end{pmatrix}\,, \tag{7.14}$$

with

$$M_1(r) = M_1 + (z_1+\tilde{z}_1)\, r\,, \qquad M_5(r) = M_5 + (z_5+\tilde{z}_5)\, r\,. \tag{7.15}$$

The corresponding matrix for the bottom sector, $\mathcal{M}_{\mathcal{B}}(h,\sigma,r)$ can be obtained from Eqs. (7.14) and (7.15) by substituting the unprimed couplings with the corresponding primed ones.

All the possible couplings invariant under the SM gauge group and $SO(5) \times U(1)_X$ global symmetry that can be constructed under the previous assumptions are included in Eqs. (7.6), (7.14), and (7.15). However, it is fundamental to notice that the Lagrangian actually describing the AMLσM can be defined only after the adoption of a specific PQ charge assignment, because not all the terms are simultaneously allowed. Indeed, only one between M_i, z_i and $\widetilde{z}_i$ (and corresponding primed) terms are allowed once a specific PQ charge assignment for the fermions is chosen, imposing a non-vanishing charge for the complex scalar s. This means that exotic fermions can gain a mass term either directly (M_i) or through the Yukawa-like coupling with s (z_i or $\widetilde{z}_i$) once the scalar field develops a VEV. Moreover, as the scalar quintuplet ϕ does not transform under the PQ symmetry, the fermion PQ charge assignment determines the presence (or absence) of the proto-Yukawa interactions (y_i).

Finally, taking a look at the interactions between exotic and SM fermions, in fourth and seventh lines of Eq. (7.6), if only the exotic fermions have non-vanishing charges, then these operators can be forbidden. This issue will be discussed in the next sections, where the conditions that lead to the minimal AMLσM charge assignment is studied.

7.1.3 *The Scalar Lagrangian*

The scalar part of the Lagrangian introduced in Eq. (7.3), describing scalar-gauge and scalar-scalar interactions, reads as follows:

$$\mathcal{L}_{\rm s} = \frac{1}{2}(D_\mu \phi)^T (D^\mu \phi) + (\partial_\mu s^*)(\partial^\mu s) - V(\phi, s)\,, \tag{7.16}$$

where the $SU(2)_L \times U(1)_Y$ covariant derivative of the quintuple ϕ is given by

$$D_\mu \phi = \left(\partial_\mu + i g \Sigma_L^{(i)} W_\mu^i + i g' \Sigma_R^{(3)} B_\mu\right) \phi\,, \tag{7.17}$$

and Σ_L^i and Σ_R^i denote respectively the generators of the $SU(2)_L \times SU(2)_R \sim SO(4)'$ subgroup of $SO(5)$, rotated with respect to the $SO(4)$ group preserved from the spontaneous breaking.

It is useful for later convenience to write the scalar Lagrangian in Eq. (7.16) in the unitary gauge, making use of Eqs. (7.1) and (7.2):

$$\begin{aligned}\mathcal{L}_{\rm s} = \;& \frac{1}{2}(\partial_\mu h)(\partial^\mu h) + \frac{1}{2}(\partial_\mu \sigma)(\partial^\mu \sigma) + \frac{h^2}{4}\left[g^2\, W_\mu^+ W^{-\mu} + \frac{g^2 + g'^2}{2} Z_\mu Z^\mu\right] + \\ & + \frac{1}{2}(\partial_\mu r)(\partial^\mu r) + \frac{r^2}{2 f_a^2}(\partial_\mu a)(\partial^\mu a) - V(h,\sigma,r)\,,\end{aligned} \tag{7.18}$$

The kinetic term of the axion field a will be canonically normalised as soon as the field r gets a VEV after the $U(1)_{PQ}$ spontaneous symmetry breaking, identifying:

$$f_a \equiv v_r \tag{7.19}$$

The scalar potential $V(\phi, s)$ can then be written as:

$$V(\phi, s) = V^{\rm SSB}(\phi, s) + V^{\rm CW}(\phi, s) + V^{\rm c.t.}(\phi, s)\,. \tag{7.20}$$

The first part, $V^{\rm SSB}(\phi, s)$, describes the most general potential built with ϕ and s, invariant under $SO(5) \times U(1)_{\rm PQ}$ symmetry, broken spontaneously to $SO(4)$:

$$V^{\rm SSB}(\phi, s) = \lambda(\phi^T\phi - f^2)^2 + \lambda_s(2\, s^* s - f_s^2)^2 - 2\lambda_{s\phi}\,(s^* s)\,\left(\phi^T\phi\right)\,, \quad (7.21)$$

where λ, λ_s and $\lambda_{s\phi}$ are the dimensionless quartic coefficients and the sign in front of $\lambda_{s\phi}$ has been chosen negative for future convenience. Notice that $\lambda_{s\phi}$ plays the role of portal between the $SO(5)$ and the PQ sectors: if $\lambda_{s\phi} \sim \mathcal{O}(1)$ then the $SO(5)/SO(4)$ and PQ breaking mechanisms would be linked and they would occur at similar scales; this would represent a possible tension between the naturalness of the AMLσM, which requires f not so much larger than EW scale $v = 246$ GeV, in order to reduce the typical fine-tuning in CH models, and the experimental data on the axion sector, which suggests very high values of f_s. As a consequence, values of $\lambda_{s\phi}$ smaller than 1 are favoured in the AMLσM.

The expression of $V^{\rm SSB}$ in the exponential notation will be useful in the following sections:

$$V^{\rm SSB}(h, \sigma, r) = \lambda(h^2 + \sigma^2 - f^2)^2 + \lambda_s(r^2 - f_s^2)^2 - \lambda_{s\phi}\, r^2\,(h^2 + \sigma^2)\,. \quad (7.22)$$

When the scalar fields h, σ and r take a non trivial VEV, repectively v_h, v_σ and v_r, the spontaneous symmetry breaking for the EW, the global $SO(5)$ and the PQ symmetry, is realised.

The second term $V^{\rm CW}(\phi, s)$ is the Coleman-Weinberg (CW) one-loop potential that provides an explicit and dynamical breaking of the original symmetries. Its form depends on the explicit structure of the fermionic and bosonic Lagrangians, in particular on the symmetry breaking terms, and it will be outlined in the following subsection.

Finally, the term $V^{\rm c.t.}(\phi, s)$, includes all the couplings that need to be introduced at tree-level in order to cancel the divergences potentially arising from the one-loop CW potential, in order to have a renormalisable theory.

7.1.4 *The Coleman-Weinberg Potential*

Explicit dynamical breaking of the tree-level symmetries can be introduced at one-loop level through the CW mechanism [155]. Indeed, the presence of $SO(5)$ breaking couplings in both the fermionic and the gauge sectors generates $SO(5)$ breaking terms at one-loop level in the potential. Explicit $U(1)_{\rm PQ}$ breaking contributions may also be generated, depending on the fermion PQ charge assignment.

We compute the one-loop fermionic contributions to the potential from the field dependent fermion mass matrix $\mathcal{M}_f(h,\, \sigma,\, r)$ in Eq. (7.13), using the usual CW expression:

$$\begin{aligned} V_f^{\rm CW} = -\frac{1}{64\pi^2}\Bigg(&{\rm Tr}\left[\mathcal{M}_f\mathcal{M}_f^\dagger\right]\Lambda^2 - {\rm Tr}\left[\left(\mathcal{M}_f\mathcal{M}_f^\dagger\right)^2\right]\log\left(\frac{\Lambda^2}{\mu^2}\right) + \\ &+{\rm Tr}\left[\left(\mathcal{M}_f\mathcal{M}_f^\dagger\right)^2\log\left(\frac{\mathcal{M}_f\mathcal{M}_f^\dagger}{\mu^2}\right)\right] - \frac{1}{2}{\rm Tr}\left[\left(\mathcal{M}_f\mathcal{M}_f^\dagger\right)^2\right]\Bigg)\,, \end{aligned} \quad (7.23)$$

where Λ is the ultraviolet (UV) cutoff scale while μ is a generic renormalisation scale. The two terms in the first line are divergent, quadratically and logarithmically

respectively, while those in the second line are finite. For the model under discussion the possible divergent contributions are

$$\begin{aligned}
\mathrm{Tr}\left[\mathcal{M}_f\mathcal{M}_f^\dagger\right] &= c_0 + c_1(s^*s) + c_2\,(\phi^T\phi)\,,\\
\mathrm{Tr}\left[\left(\mathcal{M}_f\mathcal{M}_f^\dagger\right)^2\right] &= d_0 + d_1\,(s^*s) + d_2\,(\phi^T\phi) + d_3\,(s^*s)^2 +\\
&\quad + d_4\,(\phi^T\phi)^2 + d_5\,(\phi^T\phi)(s^*s) + \tilde{d}_1\sigma + \tilde{d}_2 h^2 +\\
&\quad + \hat{d}_1\sigma(s+s^*) + \hat{d}_2(\phi^T\phi)(s+s^*) + \hat{d}_3(\phi^T\phi)(ss+s^*s^*)\,.
\end{aligned} \tag{7.24}$$

The terms in Eq. (7.24) are already present in the tree level potential $V^{\rm SSB}$ in Eq. (7.22) and therefore the quadratic divergences can be absorbed by a redefinition of the initial Lagrangian parameters. This is not the case for the logarithmic divergent term that contains five new couplings, denoted with $\tilde{d}_{1,2}$ and $\hat{d}_{1,2,3}$ in Eq. (7.24). The ones proportional to $\tilde{d}_{1,2}$ and $\hat{d}_1$ are $SO(5)$ breaking terms, while the ones proportional to $\hat{d}_{2,3}$ are $SO(5)$ preserving. On the other side, $\hat{d}_{1,2,3}$ terms also explicitly break the PQ symmetry. If in a specific setup these terms were not vanishing, renormalisability of the model would then require the introduction of the corresponding structure in the tree-level potential.

The expressions for the top sector CW coefficients that provide an explicit breaking of the $SO(5)$ and/or of the PQ symmetries are:

$$\begin{aligned}
\tilde{d}_1 &= 4(y_1M_1 + y_2M_5)\Lambda_2\Lambda_3\\
\tilde{d}_2 &= y_2^2\Lambda_1^2 - 2\,y_1^2\Lambda_2^2\\
\hat{d}_1 &= 2\,y_1(z_1+\tilde{z}_1)\Lambda_2\Lambda_3 + 2\,y_2(z_5+\tilde{z}_5)\Lambda_2\Lambda_3\\
\hat{d}_2 &= 2\,y_1y_2(z_1+\tilde{z}_1)M_5 + 2\,y_1y_2(z_5+\tilde{z}_5)M_1\\
\hat{d}_3 &= 2\,y_1y_2\,(z_1z_5 + \tilde{z}_1\tilde{z}_5)\,.
\end{aligned} \tag{7.25}$$

Similar contributions for the bottom sector are obtained by replaing the unprimed couplings in Eq.(7.25) with the corresponding primed ones. As stated before, assuming a specific PQ charge assignment forbids some of the couplings in the Lagrangian and consequently the corresponding CW coefficients vanish, as it will be explicitly discussed in the next section.

In a similar way the one-loop gauge boson contributions to the CW potential can be calculated through the CW formula given in Eq. (7.23) just replacing the fermion mass matrix $\mathcal{M}_f$ with the gauge boson one $\mathcal{M}_g$:

$$V_g^{CW} = -\frac{1}{64\pi^2}\left(\mathrm{Tr}\left[\mathcal{M}_g^2\right]\Lambda^2 - tr\left[\left(\mathcal{M}_g^2\right)^2\right]\log\left(\frac{\Lambda^2}{\mu^2}\right) + \dots\right). \tag{7.26}$$

The quadratic and logarithmic divergent terms are

$$\mathrm{Tr}\left[\mathcal{M}_g^2\right] = \tilde{a}_1 h^2 \qquad\qquad \mathrm{Tr}\left[\left(\mathcal{M}_g^2\right)^2\right] = b_0 + \tilde{b}_1\,h^4\,, \tag{7.27}$$

with

$$\tilde{a}_1 = \frac{1}{8}\left(g^2+g'^2\right) \qquad\qquad \tilde{b}_1 = \frac{1}{64}\left[2\,g^4 + \left(g^2+g'^2\right)^2\right], \tag{7.28}$$

both explicitly breaking the global $SO(5)$ symmetry.

The two divergences associated to $\tilde{a}_1$ and $\tilde{d}_2$ ask for the introduction of an h^2 term in the tree-level scalar potential, in order to ensure the renormalisability of the model, while the divergence proportional to the $\tilde{b}_1$ coefficient requires an additional h^4 term.

7.2 MINIMALITY CONDITIONS

There is a large zoology of possible $U(1)_{\rm PQ}$ charges that can be assigned to the spectrum discussed in the previous sections (see Ref. [145] for details on more general charge assignments). However, one single minimal scenario can be identified after requiring a few strong physical conditions. The requirements are the following:

1. Mass terms for the SM quarks are originated at tree-level. Generalising the result in Ref. [24], the leading order (LO) contribution to the third generation quark masses is given by

$$m_t = \frac{y_1 \Lambda_1 \Lambda_3 v_h}{M_1(v_r) M_5(v_r) - y_1 y_2 (v_h^2 + v_\sigma^2)} + \\ - \frac{y_1 y_2 \Lambda_1 \Lambda_2 v_h v_\sigma}{M_1(v_r) M_5^2(v_r) - y_1 y_2 M_5(v_r)(v_h^2 + v_\sigma^2)} \,, \tag{7.29}$$

   and similarly for the bottom mass. In this expression, $M_{1,5}(v_r)$ refers to the definitions in Eq. (7.14) replacing the dependence on r with its VEV, v_r. In order for this expression not to be vanishing, the conditions $y_1 \neq 0$ and $\Lambda_1 \neq 0$ should hold simultaneously. Then, either $\Lambda_3 \neq 0$ or $y_2 \neq 0 \wedge \Lambda_2 \neq 0$ should be verified, depending on whether the leading or sub-leading term in the v/M expansion is retained.

2. The dynamics that generate the partial-composite operators in the fourth line of Eq. (7.6) are associated only to the $SO(5)/SO(4)$ breaking sector. This implies that the scales f and f_s are distinct and independent.[1]

In a completely generic model a third condition can be also considered:

3. No PQ explicit breaking is generated at one-loop from the CW potential. This condition is satisfied by imposing $\hat{d}_i = 0$, for $i = 1, 2, 3$ (and the equivalent ones for the bottom sector).

This condition prevents the arising of large contributions to the axion mass, and it is automatically verified in the class of AMLσM constructions defined in Eq. (7.6), as it will be explicitly shown in the following.

If one requires additionally to solve the strong CP problem *à la* KSVZ a fourth condition is necessary:

4. The complex scalar field s needs to couple to at least one of the exotic fermions (not necessarily to all of them) and the net contribution to the QCD-θ term of the colour anomaly needs to be different from zero.

This last condition, when satisfied, implies condition 3 and therefore for a QCD axion no PQ explicit breaking contributions arise in the scalar potential, besides those due to non-perturbative QCD effects.

The model identified with the PQ charge assignments in Tab. 7.2 satisfies all the previous requirements: using the freedom to fix one of the charges, i.e. the charge of the complex scalar singlet $n_s = 1$, the two cases shown in the table are physically equivalent. This model is contained within the classes of constructions presented in Ref. [145].

The model presents a series of interesting features. No PQ charge is assigned to the SM particles and neither to the exotic fermions ψ_R and χ_L. The Yukawa-like terms proportional to $y_{1,2}$ are invariant under $U(1)_{\rm PQ}$, while the term proportional

1 The discussion the case where the $SO(5)/SO(4)$ and PQ symmetry breaking occur at the same scale is deferred to chap. 9

n_{q_L}	n_{t_R}	n_{ψ_L}	n_{ψ_R}	n_{χ_L}	n_{χ_R}	y_1	y_2	Λ_1	Λ_2	Λ_3	M_5	M_1	$z_1, \tilde{z}_5$	$\tilde{z}_1, z_5$
0	0	$+1$	0	0	$+1$	✓	✓	✓	✗	✓	✗	✗	✓	✗
0	0	-1	0	0	-1	✓	✓	✓	✗	✓	✗	✗	✗	✓

Table 7.2: *On the left-side, the PQ charge assignments where n_i refers to the i field, conventionally fixing the PQ charge of the complex scalar field s, $n_s = 1$. On the right-side, the parameters entering the fermionic Lagrangian, together with the information on whether they are compatible (✓) or not (✗) with the PQ symmetry. This assignment can be trivially extended to the bottom sector.*

to Λ_2 is not and then it cannot be introduced in the Lagrangian. In consequence, the subleading contribution to the SM fermion masses is identically zero and the top mass is given only by the leading term in Eq. (7.29) (similarly for the bottom mass). The Dirac mass terms $M_{1,5}$ are also forbidden and then the exotic fermions ψ and χ receive mass of the order $z_5 v_r$ (or $\tilde{z}_5 v_r$ depending on the specific sign of the PQ charge) and $z_1 v_r$ (or $\tilde{z}_1 v_r$), once r develops VEV. As v_r is typically expected to be of the order of f_s, these fermions decouple from the spectrum when $f_s \gg f$. Finally, condition 2 implies that the couplings Λ_i are neither promoted to spurions nor substituted by a dynamical field (i.e. s or s^*).

Accordingly to the charge assignment in Tab. 7.2, the PQ-breaking terms in the fermionic CW potential, $\hat{d}_i$, are vanishing, while the $SO(5)$ breaking terms are

$$\tilde{d}_1 = 0\,, \qquad \tilde{d}_2 = y_2^2 \Lambda_1^2\,. \tag{7.30}$$

In consequence, in this scenario, only a log-divergent $SO(5)$ breaking contribution to the h-mass term arises from the fermionic part of the CW potential, while no σ tadpole contribution is generated. This is different from the analysis performed in Ref. [24], where the only $SO(5)$ symmetry breaking terms considered have been the σ tadpole and the h^2 terms. To obtain a viable $SO(5)$ and EW spontaneous symmetry breaking at least two different $SO(5)$ breaking terms are necessary. Additional unavoidable sources of $SO(5)$ breaking comes from the gauge sector, as shown in Eq. (7.26). The minimal counter-term potential required at tree-level by renormalisability of the theory, once the charge assignment has been chosen, is then given in the unitary gauge by

$$V^{\text{c.t.}}(h,\sigma) = -\beta f^2 h^2 + \gamma h^4\,. \tag{7.31}$$

Other values for the PQ charges are possible by varying the explicit value of n_s, but they lead to the same physical model presented above, at least for what concerns the $SO(5)/SO(4)$ phenomenology and the analysis of the scalar potential. The physical dependence on the explicit value of n_s, and then of those of the exotic fermions, can be found in the couplings between the axion and the gauge field strengths, whose coefficients are determined by the chiral anomaly (see Refs. [38,39, 50, 156–163] for other studies where the axion couplings are modified with respect to those in the original KSVZ model).

The coefficients of the axion couplings with the gauge boson field strengths in the physical basis read

$$\begin{aligned}\delta\mathcal{L} \supset & -\frac{\alpha_s}{8\pi}\frac{a}{f_a} c_{agg} G^a_{\mu\nu}\tilde{G}^{a\mu\nu} - \frac{\alpha_{em}}{8\pi}\frac{a}{f_a} c_{a\gamma\gamma} F_{\mu\nu}\tilde{F}^{\mu\nu} - \frac{\alpha_{em}}{8\pi}\frac{a}{f_a} c_{aZZ} Z_{\mu\nu}\tilde{Z}^{\mu\nu} + \\ & - \frac{\alpha_{em}}{8\pi}\frac{a}{f_a} c_{a\gamma Z} F_{\mu\nu}\tilde{Z}^{\mu\nu} - \frac{\alpha_{em}}{8\pi}\frac{a}{f_a} c_{aWW} W^+_{\mu\nu}\tilde{W}^{-\mu\nu}\,.\end{aligned} \tag{7.32}$$

The values of the coefficients are reported in Tab. 7.3 for the PQ scenario under consideration[2]. It will be useful for the future discussion to introduce the notation of the effective couplings

$$g_{agg} \equiv \frac{\alpha_s}{2\pi}\frac{c_{agg}}{f_a} \qquad\qquad g_i \equiv \frac{\alpha_{\rm em}}{2\pi}\frac{c_i}{f_a}\,, \tag{7.33}$$

where $i = \{a\gamma\gamma,\, aZZ,\, a\gamma Z,\, aWW\}$.

c_{agg}	$c_{a\gamma\gamma}$	c_{aZZ}	$c_{a\gamma Z}$	c_{aWW}
8	$112/3$	49.3	17.8	108.1

Table 7.3: *The coefficients of the axion couplings to the gauge boson field strengths in the physical basis are reported, where the normalisation is defined in Eq. (7.32).*

The charge assignment in Tab. 7.2 corresponds to the minimal setup between all the possible AMLσM constructions, where the minimality refers to the number of new parameters introduced with respect to the MLσM. The number of parameters in the fermionic Lagrangian is the same, while in the scalar potential only three additional parameters are considered, corresponding to the PQ sector (f_s, λ_s and $\lambda_{s\phi}$), and in particular only two $SO(5)$ breaking terms are present (corresponding to β and γ). The PQ charges also represent degrees of freedom and the minimal model in Tab. 7.2 is determined by fixing n_s. Indeed, conditions 1 and 2 impose that the difference between the charges of the LH and RH components of the SM fermions is vanishing, $n_{q_L} - n_{t_R} = 0$, and in consequence it is always possible to redefine the whole set of PQ charges such that $n_{q_L} = n_{t_R} = 0$.

It is worth mentioning that an alternative charge assignment can be found satisfying to the conditions 1-4, but this scenario is not minimal in terms of number of parameters. In this case, the charges are such that $n_{t_R} = n_{\chi_L} = n_{\chi_R} = n_{\psi_L} = n_{\psi_R} \mp n_s = n_{q_L} \mp n_s$, where the "$-$" or "$+$" refer to the presence of z_5 or $\tilde{z}_5$ terms in the Lagrangian, respectively. As discussed in Ref. [145], SM fermions transform under the PQ symmetry differently from the minimal AMLσM in Tab. 7.2. In this particular set-up the Dirac mass term M_1 is allowed in the Lagrangian, while the ψ fermions receive mass from the Yukawa-like term proportional to z_5 (or $\tilde{z}_5$). Moreover, the terms proportional to $\Lambda_{1,2,3}$ and y_1 are allowed, while the one with y_2 is forbidden. As a consequence, the term $\tilde{d}_1$ in Eq. (7.25) is not vanishing and then we need to add a σ tadpole into the counter term potential $V^{\rm c.t.}(h,\sigma)$. The number of $SO(5)$ breaking parameters is now increased by one unit with respect to the minimal case discussed above. For this reason, this second scenario is not considered in what follows.

2 In the present discussion, only one fermion generation has been considered. Once extending this study to the realistic case of three generations, the values reported in Tab. 7.3 will be modified: for example, assuming that the same charges will be adopted for all the fermion generations, the numerical values in the table will be multiplied by a factor 3.

8

THE SCALAR SECTOR

As constructed in the previous chapter, the tree-level renormalisable scalar potential of the minimal AMLσM is

$$V(h,\sigma,r) = \lambda(h^2+\sigma^2-f^2)^2 - \beta f^2 h^2 + \gamma h^4 + \lambda_s (r^2-f_s^2)^2 - \lambda_{s\phi}\, r^2\,(h^2+\sigma^2)\,. \tag{8.1}$$

When $f^2 > 0$ and $f_s^2 > 0$, the minimum of the potential allows for the $SO(5)$, $U(1)_{\text{PQ}}$ and EW spontaneous symmetry breaking with non-vanishing VEVs,

$$\begin{aligned} v_h^2 &= \frac{\beta}{2\gamma} f^2 \\ v_\sigma^2 &= \left(1-\frac{\lambda_{s\phi}^2}{4\lambda\lambda_s}\right)^{-1} \left\{ f^2 \left[\left(1-\frac{\beta}{2\gamma}\right) + \frac{\beta}{2\gamma}\frac{\lambda_{s\phi}^2}{4\lambda\lambda_s}\right] + \frac{f_s^2}{2}\frac{\lambda_{s\phi}}{\lambda}\right\} \\ v_r^2 &= \left(1-\frac{\lambda_{s\phi}^2}{4\lambda\lambda_s}\right)^{-1} \left\{ f_s^2 + \frac{f^2}{2}\frac{\lambda_{s\phi}}{\lambda_s}\right\} \equiv f_a^2\,, \end{aligned} \tag{8.2}$$

where the condition $v_r \equiv f_a$ is imposed to have canonically normalised axion kinetic term, see Eqs. (7.18) and (7.19). For sake of definiteness we will indicate in the following with $\hat{h}$, $\hat{\sigma}$ and $\hat{r}$ the physical fields after SSB breaking. Assuming all parameters non-vanishing, the following conditions on the parameters must be imposed:

(i) $\lambda > 0$ and $\lambda_s > 0$ in order to have a potential bounded from below.

(ii) β and γ should have the same sign in order to guarantee a positive v_h^2 value. Following the sign convention adopted in Eq. (8.1), when both parameters are positive, the explicit symmetry breaking terms sum "constructively" to the quadratic and quartic terms in the potential in the broken phase, and a larger parameter space is allowed. Moreover, the ratio $\beta/2\gamma < 1$ leads to $v_h < f$, corresponding to the expected ordering in the symmetry breaking scales.

(iii) $\lambda_{s\phi}$ should satisfy the following condition:

$$\lambda_{s\phi}^2 < 4\lambda\lambda_s \tag{8.3}$$

in order to enforce positive v_σ^2 and v_r^2 values. For negative $\lambda_{s\phi}$ values, additional constraints could be enforced depending on the values of the other parameters. The sign convention chosen in Eq. (8.1) guarantees that no cancellation in v_σ^2 and v_r^2 occurs for $\lambda_{s\phi} > 0$.

After the SSB of the two symmetry groups, mass eigenvalues and eigenstates can be identified. While the general case can be studied only numerically (sect. 8.2), simple analytical expressions can be obtained in some specific limit cases:

1. Integrating out the heaviest scalar dof, whose largest component is the radial scalar field r, and studying the LO terms of the Lagrangian;
2. Assuming $f_s \sim f$, expanding perturbatively in the small β and $\lambda_{s\phi}$ parameters.

These two cases will be discussed in the following section.

8.1 APPROXIMATE SOLUTIONS

8.1.1 *Integrating Out The Heaviest Scalar Field*

A clear hierarchy between the three mass scalar eigenstates is achievable for large values of λ_s and/or f_s: the mass of the heaviest scalar dof receives a LO contribution proportional to

$$m_3 \propto \sqrt{8\lambda_s} f_s \,. \tag{8.4}$$

With increasing values of λ_s and/or f_s, the mixing of $\hat{h}$ and $\hat{\sigma}$ to the heaviest scalar dof, in this region of the parameter space, tend to vanish and the only relevant constituent is the radial component, $\hat{r}$. From the expression in Eq. (8.4), one can foresee two different ways for integrating out the heaviest dof, either taking the limit $\lambda_s \gg 1$ or taking $f_s \gg f \sim \sqrt{s_{\rm cm}}$, being $\sqrt{s_{\rm cm}}$ the typical centre of mass energy scale at LHC. These two cases represent two physically different scenarios that must be discussed separately.

The case for $\lambda_s \gg 1$, with f_s of the same order of f, corresponds to the $U(1)_{\rm PQ}$ non-linear spontaneous symmetry breaking framework[1]: this is the traditional axion framework where the only component of s in the low-energy spectrum is the axion, while $\hat{r}$ is integrated out. As the Yukawa-like couplings of the exotic fermions do not depend on λ_s, the decoupling of $\hat{r}$ does not have any impact on the spectrum of the exotic fermions, that depends exclusively of the specific value chosen for f_s. One can then consider in detail the two limiting cases: $f_s \sim f$ or $f_s \gg f$. Notice that in the second scenario, when f_s is much larger than any other mass scale, the exotic fermion sector decouples at the same time as the heavier scalar dof.

Considering the scalar sector, integrating out the $\hat{r}$ component, leads to an effective scalar potential that, at LO in the appropriate expansion parameter, reads

$$V_R^{LO}(h,\sigma) = \lambda_R(h^2+\sigma^2-f_R^2)^2 - \beta_R f_R^2 h^2 + \gamma h^4 \,, \tag{8.5}$$

in terms of conveniently renormalised couplings:

$$\lambda_R = k_\lambda \lambda \,, \qquad \beta_R = \frac{k_\lambda}{k_f}\beta \,, \qquad f_R^2 = \frac{k_f}{k_\lambda} f^2 \,. \tag{8.6}$$

The finite renormalisation constants k_λ and k_f are going to be different in the two limiting cases as it will be detailed in the following paragraphs.

The minimum of the effective scalar potential in Eq. (8.5) corresponds to the following VEVs for the lighter dofs $\hat{h}$ and $\hat{\sigma}$:

$$v_h^2 = \frac{\beta_R}{2\gamma} f_R^2 \,, \qquad v_\sigma^2 = f_R^2\left(1-\frac{\beta_R}{2\gamma}\right) \,, \tag{8.7}$$

satisfying to

$$v_h^2 + v_\sigma^2 = f_R^2 \,. \tag{8.8}$$

The restrictions on the parameters that follow from Eq. (8.2) hold for the expressions just obtained: β_R/γ needs to be positive in order to guarantee $v_h^2 > 0$; f_R is required to be larger than v_h to ensure $v_\sigma^2 > 0$. Moreover, if $v_\sigma > v_h$ then the field $\hat{h}$ is the largest component of the mass eigenstate interpreted as the physical Higgs particle.

From Eq. (8.5) and using the relations of Eq. (8.7) one derives the following mass matrix:

$$\mathcal{M}_s^2 = 8\,\lambda_R \begin{pmatrix} (1+\gamma/\lambda_R)v_h^2 & v_h v_\sigma \\ v_h v_\sigma & v_\sigma^2 \end{pmatrix} \,, \tag{8.9}$$

1 In the case where an UV strong interacting dynamics is responsible of the largeness of λ_s, new resonances are expected at the scale $\lesssim 4\pi f_s$ (see the naive dimensional analysis [164]).

that can be diagonalised by performing an $SO(2)$ rotation,

$$\texttt{diag}\left(m_1^2,\, m_2^2\right) = U(\vartheta)^T \mathcal{M}_s^2 U(\vartheta) \qquad \text{with} \qquad U(\vartheta) = \begin{pmatrix} \cos\vartheta & \sin\vartheta \\ -\sin\vartheta & \cos\vartheta \end{pmatrix} . \tag{8.10}$$

The expressions for the masses and the mixing obtained from the LO potential of Eq. (8.5) are given by

$$m_{1,2}^2 = 4\lambda_R \left[\left(1 + \frac{\gamma}{\lambda_R}\right) v_h^2 + v_\sigma^2 \pm \right. \\ \left. \pm \sqrt{\left(1 + \frac{\gamma}{\lambda_R}\right)^2 v_h^4 + 2\left(1 - \frac{\gamma}{\lambda_R}\right) v_h^2 v_\sigma^2 + v_\sigma^4} \right] \tag{8.11a}$$

$$\tan 2\vartheta = \frac{2 v_h v_\sigma}{v_\sigma^2 - (1 + \gamma/\lambda_R) v_h^2} \,. \tag{8.11b}$$

The positivity of the two mass square eigenvalues is guaranteed imposing that both the trace and the determinant of the mass matrix in Eq. (8.9) are positive: this leads to

$$\lambda_R > 0 \,, \qquad \gamma > 0 \,, \qquad \beta_R > 0 \,, \tag{8.12}$$

where the last condition follows from the requirement that γ and β_R should have the same sign in order to guarantee a positively defined v_h^2 value, as discussed below Eq. (8.2).

The two limits $\lambda_s \gg 1$ and $f_s \gg f \sim \sqrt{s_{\rm cm}}$ will be described in details in what follows, focusing on the scalar sector.

THE LARGE PQ QUARTIC COUPLING: for λ_s in the strongly interacting regime, the radial component r can be expanded in inverse powers of λ_s (see Ref. [120] for a similar analysis): at the NLO, one has

$$r = f_s + \frac{1}{\lambda_s} r_1 \,. \tag{8.13}$$

Solving the Equations Of Motion (EOMs) perturbatively allows to determine r_1:

$$r_1 = \frac{\lambda_{s\phi}}{4 f_s} \left(h^2 + \sigma^2\right) + \frac{1}{8 f_s^3} \left(\partial_\mu a\right) \left(\partial^\mu a\right) \,. \tag{8.14}$$

The effective Lagrangian at the NLO reads

$$\mathcal{L}_s = \frac{1}{2}(\partial_\mu h)(\partial^\mu h) + \frac{1}{2}(\partial_\mu \sigma)(\partial^\mu \sigma) - \frac{h^2}{4} \mathrm{Tr}\left(\mathbf{V}^\mu \mathbf{V}_\mu\right) + \tag{8.15}$$

$$+ \frac{1}{2}(\partial_\mu a)(\partial^\mu a) - \lambda_R \left(h^2 + \sigma^2 - f_R^2\right)^2 + \beta_R f_R^2 h^2 - \gamma h^4 + \delta\mathcal{L}_s^{\rm NLO} \tag{8.16}$$

with λ_R, β_R and f_R^2 defined as in Eq. (8.6) with

$$k_\lambda = 1 \,, \qquad k_f = \left(1 + \frac{1}{2} \frac{\lambda_{s\phi}}{\lambda} \frac{f_s^2}{f^2}\right) \,, \tag{8.17}$$

and where the NLO correcting term is given by

$$\delta\mathcal{L}_s^{\rm NLO} = \frac{4}{\lambda_s} f_s^2 r_1^2 = \frac{\lambda_{s\phi}^2}{4\lambda_s} \left[\left(h^2 + \sigma^2\right) + \frac{1}{2 f_s^2} \left(\partial_\mu a\right) \left(\partial^\mu a\right) \right]^2 \,. \tag{8.18}$$

In this scenario, f_R is the new effective $SO(5)/SO(4)$ breaking scale, while the $SO(5)$ quartic coupling $\lambda = \lambda_R$ remains unchanged. The positivity of f_R^2 translates into a constraint on the couplings $\lambda_{s\phi}$:

$$\lambda_{s\phi} > -2\lambda \frac{f^2}{f_s^2}\,, \tag{8.19}$$

where λ, f^2 and f_s^2 are all positive (see the discussion at the beginning of Chap. 8). The value $\lambda_{s\phi} = 0$ is special: $\lambda_{s\phi}$ represents the portal between the $SO(5)$ and the PQ sectors, and therefore once it is vanishing the two sectors are completely decoupled.

An interesting limit that will be used to compare with the numerical analysis, is when $\lambda_s \gg \lambda_R \gtrsim 1$ and small β, for which the expressions in Eqs. (8.11a) and (8.11b), reduce to

$$\begin{aligned} m_1^2 &= 4\beta f^2 \left(1 - \frac{\beta}{2\gamma}\right) \\ m_2^2 &= 8\lambda f^2 \left(1 + \frac{\beta^2}{4\gamma\lambda}\right) + 4\lambda_{s\phi} f_s^2 \end{aligned} \tag{8.20}$$

with the mixing angle defined as

$$\tan 2\vartheta = \left(1 - \frac{\beta}{\gamma}\right)^{-1} \sqrt{\frac{2\beta}{\gamma}\left(1 - \frac{\beta}{2\gamma}\right)}\,. \tag{8.21}$$

THE LARGE PQ SSB SCALE: In the limit $f_s \gg f \sim \sqrt{s_{\rm cm}}$, being λ_s in either the perturbative or strongly interacting regimes, a similar expansion as in the previous subsection can be performed on the field r, adopting as new dimensionless expanding parameter f/f_s. Within this setup r at NLO reads

$$r = f_s + \frac{f}{f_s}\, r_1\,. \tag{8.22}$$

Solving the EOMs in this case, one gets

$$r_1 = \frac{\lambda_{s\phi}}{4\lambda_s f}\left(h^2 + \sigma^2\right)\,. \tag{8.23}$$

Once replacing these expressions in Eq. (7.18), the effective Lagrangian in Eq. (8.16) is obtained with

$$\begin{aligned} \delta\mathcal{L}_s^{\rm NLO} = &\frac{\lambda_{s\phi}}{4\lambda_s}\frac{\left(h^2+\sigma^2\right)}{f_s^2}\left[\left(\partial_\mu a\right)\left(\partial^\mu a\right) + \frac{\lambda_{s\phi}^2}{4\lambda_s}\left(h^2+\sigma^2\right)^2\right] + \\ &+ \frac{\lambda_{s\phi}^2}{32\lambda_s^2 f_s^2}\partial_\mu\left(h^2+\sigma^2\right)\partial^\mu\left(h^2+\sigma^2\right)\,, \end{aligned} \tag{8.24}$$

and λ_R and f_R^2 defined in Eq. (8.6), with k_λ and k_f explicitly given by

$$k_\lambda = \left(1 - \frac{1}{4}\frac{\lambda_{s\phi}^2}{\lambda\lambda_s}\right)\,, \qquad k_f = \left(1 + \frac{1}{2}\frac{\lambda_{s\phi}}{\lambda}\frac{f_s^2}{f^2}\right)\,. \tag{8.25}$$

An increasing value of f_s corresponds to an increasing value of f_R. However, caution is necessary in the case when $\lambda_{s\phi}$ is exactly vanishing, as the $SO(5)$ and PQ sectors are decoupled: in this specific case $f_R = f$ and the $SO(5)$ SSB sector is not affected by the integration out of the radial dof r.

Differently from the previous case, here also a new renormalised quartic couplings $\lambda_R \neq \lambda$ is introduced. To ensure a potential bounded from below both f_R^2 and λ_R need to be positive, leading to the following constraints on $\lambda_{s\phi}$,

$$\lambda_{s\phi} > -2\lambda\frac{f^2}{f_s^2} \qquad \wedge \qquad \lambda_{s\phi}^2 < 4\lambda\lambda_s \,. \tag{8.26}$$

In the case under discussion, the explicit values for the two lightest mass eigenvalues and for their mixing in Eqs. (8.11a) and (8.11b), assuming for simplicity $\lambda_{s\phi}^2 \ll \lambda\lambda_s$, simplify to

$$m_1^2 = 4\beta f^2\left(1 - \frac{\beta}{\gamma}\frac{\lambda}{\lambda_{s\phi}}\frac{f^2}{f_s^2}\right), \qquad m_2^2 = 4\lambda_{s\phi}f_s^2\left(1 + 2\frac{\lambda}{\lambda_{s\phi}}\frac{f^2}{f_s^2}\right) \tag{8.27}$$

with the mixing angle given by

$$\tan 2\vartheta = 2\sqrt{\frac{\beta}{\gamma}\frac{\lambda}{\lambda_{s\phi}}}\frac{f}{f_s}\,. \tag{8.28}$$

8.1.2 *The Small Couplings Case:* $\beta,\ \lambda_{s\phi} \ll 1$

For $f_s \sim f \sim \sqrt{s_{\rm cm}}$, all the three scalar dofs are retained in the low energy spectrum and in general a stronger mixing between the three eigenstates is expected, compared to the previous setups. Complete analytical expression for the masses and mixings cannot be written in particularly elegant and condensed form. Nevertheless, simple analytic results can be obtained under the assumption that $\beta,\ \lambda_{s\phi} \ll 1$, which are natural conditions in the AMLσM. The first condition comes from the requirement that v_h coincides with the EW scale v, defined by $v \equiv 2M_W/g = 246$ GeV, and it is much smaller than the $SO(5)$ SSB scale, i.e. $v_h < f$. The smallness of $\lambda_{s\phi}$ follows, instead, from the assumption that the $SO(5)$ and PQ sectors are determined by two distinct dynamics and therefore the two breaking mechanisms have to occur independently. A large $\lambda_{s\phi}$ would indicate, instead, a unique origin for the two symmetry breaking mechanisms and would mean the impossibility of disentangling the two sectors.

Expanding the expressions for the generic VEVs found in Eq. (8.2) for small β and $\lambda_{s\phi}$, it leads to the following simplified expressions:

$$\begin{aligned} v_h^2 &= \frac{\beta}{2\gamma}f^2 \\ v_\sigma^2 &= \left(1 - \frac{\beta}{2\gamma}\right)f^2 + \frac{\lambda_{s\phi}}{\lambda}\frac{f_s^2}{2} + \mathcal{O}\left(\beta^2, \beta\lambda_{s\phi}, \lambda_{s\phi}^2\right) \\ v_r^2 &= f_s^2 + \frac{\lambda_{s\phi}}{\lambda_s}\frac{f^2}{2} + \mathcal{O}\left(\beta^2, \beta\lambda_{s\phi}, \lambda_{s\phi}^2\right), \end{aligned} \tag{8.29}$$

where in the brackets the dependence on β and $\lambda_{s\phi}$ of the higher order corrections is reported. The scalar squared mass matrix is given by the following expression

$$\mathcal{M}_s^2 = 2\begin{pmatrix} 4(\gamma+\lambda)v_h^2 & 4\lambda v_h v_\sigma & -2\lambda_{s\phi}v_h v_r \\ 4\lambda v_h v_\sigma & 2\lambda(v_h^2 + 3v_\sigma^2 - f^2) - \lambda_{s\phi}v_r^2 & -2\lambda_{s\phi}v_\sigma v_r \\ -2\lambda_{s\phi}v_h v_r & -2\lambda_{s\phi}v_\sigma v_r & -\lambda_{s\phi}(v_h^2 + v_\sigma^2) + 6\lambda_s v_r^2 - 2\lambda_s f_s^2 \end{pmatrix}$$

that can be diagonalised with an orthogonal transformation,

$$\texttt{diag}\left(m_1^2,\, m_2^2,\, m_3^2\right) = U(\vartheta_{12}, \vartheta_{23})^T \mathcal{M}_s^2 U(\vartheta_{12}, \vartheta_{23}) \tag{8.30}$$

with

$$U(\vartheta_{12},\vartheta_{23}) = U(\vartheta_{12})U(\vartheta_{23})\,, \tag{8.31}$$

the product of a rotation in the 12 sector and in the 23 sector respectively, of angles ϑ_{12} and ϑ_{23}. The resulting mass eigenvalues read

$$\begin{aligned} m_1^2 =& 4\beta f^2\left(1-\frac{\beta}{2\gamma}\right)+\mathcal{O}\left(\beta^3,\beta^2\lambda_{s\phi}\right)\\ m_2^2 =& 8\lambda f^2\left(1+\frac{1}{2}\frac{\lambda_{s\phi}}{\lambda}\frac{f_s^2}{f^2}\right)+\mathcal{O}\left(\beta^2,\beta\lambda_{s\phi},\lambda_{s\phi}^2\right)\\ m_3^2 =& 8\lambda_s f_s^2\left(1+\frac{1}{2}\frac{\lambda_{s\phi}}{\lambda_s}\frac{f^2}{f_s^2}\right)+\mathcal{O}\left(\beta\lambda_{s\phi},\lambda_{s\phi}^2\right)\,, \end{aligned} \tag{8.32}$$

while the mixing angles are given by

$$\tan 2\vartheta_{12} = \sqrt{\frac{2\beta}{\gamma}}\left(1+\mathcal{O}(\beta,\lambda_{s\phi})\right)\,,\quad \tan 2\vartheta_{23} = \frac{f f_s}{\lambda_s f_s^2-\lambda f^2}\,\lambda_{s\phi}\left(1+\mathcal{O}(\beta,\lambda_{s\phi})\right)\,. \tag{8.33}$$

As for Eq. (8.29), only the first two relevant terms in the expansion are reported in the expressions in Eqs. (8.32), while the powers in β and $\lambda_{s\phi}$ of the expected next order terms are shown in the brackets. Instead, in the formula for the mixing angles in Eq. (8.33), only the first term is indicated. Notice that, once considering the next order terms in the masses expressions, a rotation in the 13 sector is also necessary to exactly diagonalise the squared mass matrix.

8.2 THE NUMERICAL ANALYSIS

This section provides the numerical analysis on the parameter space of the scalar potential. The analytic results of the specific cases presented in the previous section will be used to discuss the numerical outcome. To this aim, a more general notation with respect to the one previously adopted is introduced. The scalar mass matrix $\mathcal{M}_s$ is real and can be diagonalised by an orthogonal transformation,

$$\texttt{diag}(m_1^2,m_2^2,m_3^2) = U(\vartheta_{12},\vartheta_{23},\vartheta_{13})^T\mathcal{M}_s^2\,U(\vartheta_{12},\vartheta_{23},\vartheta_{13})\,, \tag{8.34}$$

where $U(\vartheta_{12},\vartheta_{23},\vartheta_{13}) \equiv U(\vartheta_{23})U(\vartheta_{13})U(\vartheta_{12})$ is the product of three rotations in the 23, 13, and 12 sectors respectively, of angles ϑ_{23}, ϑ_{13} and ϑ_{12}. The scalar mass eigenstates φ_1, φ_2, and φ_3 are defined by

$$\begin{pmatrix}\varphi_1\\ \varphi_2\\ \varphi_3\end{pmatrix} = U(\vartheta_{12},\vartheta_{23},\vartheta_{13})^T\begin{pmatrix}\hat{h}\\ \hat{\sigma}\\ \hat{r}\end{pmatrix} \tag{8.35}$$

in terms of the three physical shifts around the vacua. Unless explicitly indicated, in the analysis that follows, φ_1 will be identified with the Higgs particle and the deviations of its couplings from the SM predicted values are interesting observables at colliders. The φ_1 couplings to the SM gauge bosons can be computed from the couplings of $\hat{h}$, as $\hat{\sigma}$ and $\hat{r}$ are singlets under the SM gauge group. The composition of $\hat{h}$ in terms of φ_i is explicitly given by

$$\hat{h} = c_{12}c_{13}\varphi_1 + c_{13}s_{12}\varphi_2 + s_{13}\varphi_3 \equiv C_1\varphi_1 + C_2\varphi_2 + C_3\varphi_3\,, \tag{8.36}$$

where c_{ij} and s_{ij} stand for $\cos\theta_{ij}$ and $\sin\theta_{ij}$, and the coefficients C_i in the last equality were introduced for shortness. The couplings with the SM gauge bosons can be written as

$$\begin{aligned}\frac{g^2}{4}(\hat{h}+v_h)^2 W_\mu^+ W^{-\mu} &= m_W^2 \left(C_1\frac{\varphi_1}{v_h}+C_2\frac{\varphi_2}{v_h}+C_3\frac{\varphi_3}{v_h}+1\right)^2 W_\mu^+ W^{-\mu}\,,\\ \frac{g^2+g'^2}{8}(\hat{h}+v_h)^2 Z_\mu Z^\mu &= \frac{m_Z^2}{2}\left(C_1\frac{\varphi_1}{v_h}+C_2\frac{\varphi_2}{v_h}+C_3\frac{\varphi_3}{v_h}+1\right)^2 Z_\mu Z^\mu\,.\end{aligned} \tag{8.37}$$

Finally, the φ_1 couplings to the longitudinal components of W and Z are modified with respect to the SM predictions for the Higgs particle by factor of C_1.

To have a clear comparison with CHM predictions, one can write the expression for the C_1 parameter obtained integrating out all the scalar dofs of our model, but the physical Higgs. The fastest way to obtain such a result is to start from Eq. (8.11b) and expanding it for $\lambda_R \gg 1$, giving

$$C_1 \simeq 1-\frac{1}{2}\frac{v_h^2}{v_\sigma^2} \equiv 1-\frac{\xi}{2}\,, \tag{8.38}$$

The last term on the right-hand side introduces the parameter ξ, that customary defines the tension between the EW and the composite scales. This parameter often appears in CHMs to quantify the level of non-linearity of the model. The expression in Eq. (8.38) agrees with previous MCHM results present in literature, see for example Ref. [165]. Therefore, the corresponding bounds on ξ, as the ones from Refs. [122, 166],

$$\xi \lesssim 0.18 \quad @\, 2\sigma\,, \tag{8.39}$$

strictly apply to the model presented here only in the MCHM limit, i.e. when all the scalar fields, but the Higgs, are extremely massive and can be safely integrated out. If this is not the case, the coefficient C_1 is a complicate function of all the scales and parameters effectively present in the model.

8.2.1 *The Scalar Potential Parameter Space*

The parameter space of the scalar sector is spanned by seven independent parameters: five dimensionless coefficients λ, λ_s, β, γ, $\lambda_{s\phi}$, and two scales f and f_s. By using the known experimental values of the Higgs VEV, $v_h = v \equiv 246$ GeV, and mass $m_1 = m_h \equiv 125$ GeV, two of these coefficients can be rewritten in terms of the remaining five. The adopted procedure for the numerical analysis is to express γ as function of β and f, by inverting the v_h^2 expression in Eq. (8.2):

$$\gamma = \left(\frac{f}{v_h}\right)^2 \frac{\beta}{2}\,. \tag{8.40}$$

and then extract β, in terms of the remaining five parameters, by numerically solving the equation $m_1(\beta, \lambda, \lambda_s, \lambda_{s\phi}, f, f_s) = m_h$. Consequently, predictions for all the remaining observables can be obtained by choosing values for $(\lambda, \lambda_s, \lambda_{s\phi}, f, f_s)$.

In Fig. 8.1 the bounds on the $|C_1|$ parameter in the (f_s, f) plane for $\lambda = \lambda_s = 1$ and $\lambda_{s\phi} = 0.1$ are shown. The dark green region corresponds to $|C_1| < 0.90$, while the light green one to $0.90 < |C_1| < 0.95$. In the white region $|C_1| > 0.95$. From this plot one can have an order of magnitude comparison with present/future experimental bound on the Higgs-gauge boson interaction. The following bounds on

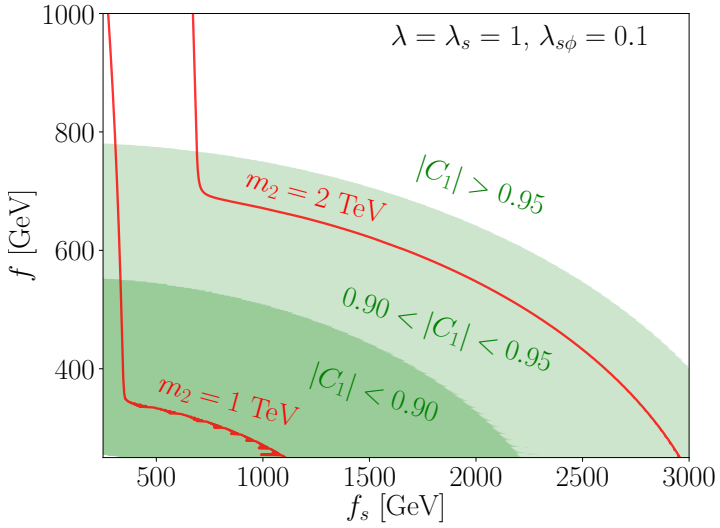

Figure 8.1: *C_1 contours in the (f_s, f) plane, for $\lambda = \lambda_s = 1$ and $\lambda_{s\phi} = 0.1$. The dark green region corresponds to $|C_1| < 0.90$, while the light green one to $0.90 < |C_1| < 0.95$. In the white region $|C_1| > 0.95$. The two red curves correspond to values for the next to lightest scalar $m_2 = 1$ TeV and $m_2 = 2$ TeV respectively, being the Higgs mass fixed to the reference value $m_h = 125$ GeV.*

hZZ and hWW couplings are obtained by [167], using the so called κ-framework[2]:

$$|\kappa_Z| = 0.89 + 0.09 - 0.08 \quad @ \quad 1\sigma$$
$$|\kappa_W| = 1.00 + 0.00 - 0.05 \quad @ \quad 1\sigma$$

The expressions in Eq. (8.37) enforce the relation $\kappa_Z = \kappa_W = C_1$.

Fig. 8.1 gives the idea of the interplay between the two scales f and f_s for fixed values of the remaining parameters. For $f_s = 1$ TeV, LHC can already start to exclude values of $f \lesssim 0.7$ TeV. However, for the larger value $f_s = 3$ TeV, even values of $f \approx 0.5$ TeV will lie outside LHC exclusion reach and no precise bound separately on f or f_s can be inferred from the sole measurement of the Higgs couplings to gauge bosons, for most of the parameter space. Only when $\lambda, \lambda_s \gg 1$ are taken, the extra scalar dofs decouple and the CHM relation of Eq. (8.38) can be exploited. These results are compatible with the ones of Ref. [24], where a detailed study on the allowed range for f has been performed in the context of the MLσM. For completeness in Fig. 8.1 also the curves corresponding to two values of the mass of the next to lightest scalar, $m_2 = 1$ TeV and $m_2 = 2$ TeV, have been shown.

In the following analysis the value $f = 2$ TeV was chosen as benchmark. We studied the parameter space for the remaining four variable, $\lambda, \lambda_s, \lambda_{s\phi}, f_s$, plotting the behaviour of the scalar mass eigenvalues m_i and of the mixing coefficients squared C_i^2.

In Fig. 8.2, the masses m_2 and m_3 are shown as a function of $\lambda_{s\phi}$ (upper left), or $\lambda = \lambda_s$ (upper right), or λ (lower). The mass m_1 is fixed at m_h, while the scale f is taken at 2 TeV. Three distinct values for f_s are considered, $f_s = 1$ TeV, 10^3 TeV, 10^6 TeV, and are shown in the same plot spanning a different region of the parameter space. In the plot in the upper left, the values for λ and λ_s are taken to be equal to 10; in the plot in the upper right, $\lambda_{s\phi} = 0.1$; in the lower plot, $\lambda_{s\phi} = 0.1$ and $\lambda_s = 10$.

2 Notice that in the κ-framework one assumes that there are no new particles contributing to the ggH production or $H \to \gamma\gamma$ decay loops.

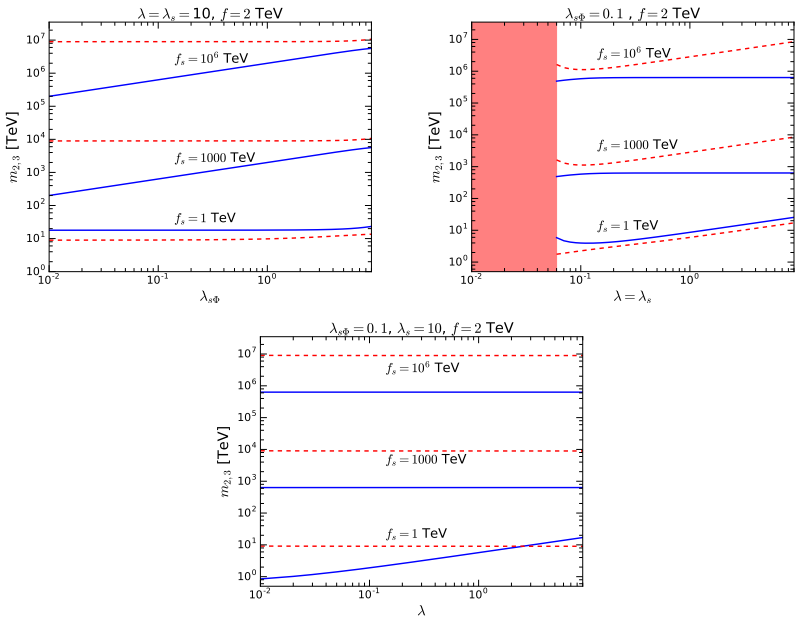

Figure 8.2: *The profiles of the scalar masses m_2 and m_3 as a function of $\lambda_{s\phi}$ (upper left), $\lambda = \lambda_s$ (upper right), and λ (lower). The other parameters are chosen at fixed values: $f = 2$ TeV; $f_s = 1$ TeV, 10^3 TeV, 10^6 TeV; $\lambda = \lambda_s = 10$ (upper left); $\lambda_{s\phi} = 0.1$ (upper right); $\lambda_s = 10$ and $\lambda_{s\phi} = 0.1$ (lower). The red-dashed line represents the heaviest dof with mass m_3, while the blue-continue line the next-to-heaviest dof with mass m_2. The lightest dof is identified with the Higgs particle with mass $m_1 = m_h$. The red area is excluded from the constraint in Eq. (8.3).*

All these plots present features discussed in the different limiting cases of the previous section. In the three plots, the lines corresponding to $f_s = 10^3$ TeV and $f_s = 10^6$ TeV represent the expressions for the masses in Eq. (8.27). In the upper left plot, the red-dashed line represents the heaviest dof with a constant mass according with Eq. (8.4). The blue-continue line corresponds to the second heaviest dof and it shows an increasing behaviour with a constant slope, corresponding to the expression for m_2^2 that in first approximation is proportional to $\lambda_{s\phi}$. In the upper right plot, the red area is excluded according to Eq. (8.3): close to this region, the analytic expressions do not closely follow the numerical results, as it appears in the behaviour of the red-dashed line that increases with a constant slope according to Eq. (8.4) only for $\lambda = \lambda_s \gtrsim 0.1$. The blue-continue line is almost constant, as expected from the expression of m_2^2 in Eq. (8.27), except for the region with small $\lambda = \lambda_s$. In the lower plot, both the red-dashed and the blue-continue lines are horizontal, as expected having fixed both λ_s and $\lambda_{s\phi}$.

When $f_s = 1$ TeV, the numerical results agree with the analytic expressions in Eqs. (8.20) and (8.32). In the upper left plot, the red-dashed and the blue-continue lines are exchanged with respect to the lines for $f_s = 10^3$ TeV and $f_s = 10^6$ TeV: this agrees with Eq. (8.32), as indeed for $f > f_s$ the heaviest dof is φ_2 and the next-to-heaviest is φ_3. Furthermore, the two lines are almost horizontal as the dependence on $\lambda_{s\phi}$ only enters at higher orders. In the upper right plot, both the lines increase with a constant slope, as expected from Eq. (8.32), except for small values of $\lambda = \lambda_s$, that is close to the excluded region. In the lower plot, the red-dashed line is almost horizontal, according to m_3^2 in Eq. (8.32), while the blue-continue line increases with λ, as shown by the expression for m_2^2. For $\lambda = 2.5$ the two lines cross and φ_2 becomes the heaviest dof. The same conclusions are expected by analysing the expressions in Eq. (8.20), where φ_3 is integrated out: the comparison is however more difficult as m_2^2 depends explicitly on β and γ, which are only numerically

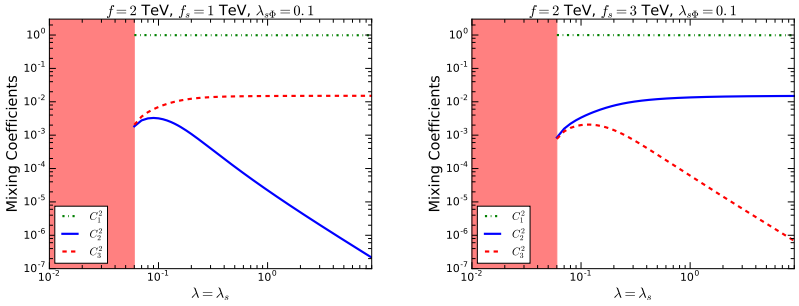

Figure 8.3: *The profiles of the coefficients squared C_1^2, C_2^2 and C_3^2, as a function of $\lambda = \lambda_s$. The other parameters are chosen at fixed values: $f = 2$ TeV; $\lambda_{s\phi} = 0.1$; $f_s = 1$ TeV on the left and $f_s = 3$ TeV on the right. The green-dot-dashed line describes C_1^2, the blue-continue line C_2^2 and the red-dashed line C_3^2. The red area is excluded from the constraint in Eq. (8.3).*

computed in terms of $\lambda, \lambda_s, \lambda_{s\phi}, f_s$. Moreover, when $\lambda > 2.5$, φ_2 should also be integrated out from the low-energy spectrum as its mass reaches the value of the one of φ_3, and not consistent description is expected for these values of λ.

The mixing coefficients C_1, C_2 and C_3 are shown in Fig. 8.3: the green-dot-dashed line describes C_1^2, the blue-continue line C_2^2 and the red-dashed line C_3^2. Both plots clearly show that the largest component to $\hat{h}$ is φ_1, that is identified to the physical Higgs particle. The contaminations from φ_2 and φ_3 are much smaller and at the level of $\sim 1\%$ at most. This is a typical feature in almost all the parameter space, and in particular for $f_s \gg f$, whose corresponding plots are very similar to the one in Fig. 8.3 on the right. The only important difference between the two plots shown is the exchange behaviour between C_2^2 and C_3^2: as far as $f_s > f$ the largest contamination is given by φ_2, while for $f < f_s$ it is given by φ_3, as it is confirmed by Eq. (8.33).

The results on the mixing coefficients can be compared to the ones for the equivalent quantities in the MLσM: in the latter, only two scalar states are present and then only one mixing can be defined, that is between $\hat{h}$ and $\hat{\sigma}$; for increasing masses of φ_2, which almost coincides with $\hat{\sigma}$, the sibling of C_2^2 asymptotically approaches the ratio v^2/f^2 and a benchmark value of 0.06 has been taken in the phenomenological analysis. From Fig. (8.3), the maximal value that C_2^2 (or C_3^2) can take is of 0.015: this means that some differences are expected between the two models when discussing the EW precision observables (EWPO) and the impact of the exotic fermions.

In a tiny region of the parameter space, φ_2 can be lighter than φ_1, with m_1 still fixed at the value m_h. This is consistent with the results in Ref. [24]. Although this possibility is experimentally viable, from the theoretical perspective it is not appealing as $m_2 < m_1$ requires $\lambda_{s\phi} \lesssim 10^{-7}$, corresponding to a highly tuned situation. Similarly, mixing parameters larger than the typical values shown in Fig. 8.3, for example $C_2^2 \sim 0.1$, can only be achieved for $\lambda_{s\phi} \lesssim 10^{-4}$, another tuned region of the parameter space. Another possibility for relatively large mixing parameters is for $f \sim 100$ GeV and $f_s \lesssim 1$ TeV, that is very unlikely as it would correspond to the case with the EWSB occurring before the $SO(5)/SO(4)$ symmetry breaking. In consequence, only the case with φ_2 heavier than φ_1 and values of $\lambda_{s\phi} \gtrsim 0.01$ will be considered in the following.

8.2.2 *Collider Phenomenology and Exotic Fermions*

Within a specific CH model setup, defined by a coset, the Higgs couplings to fermions depend on the kind of exotic fermions that enrich the spectrum and the chosen symmetry representations. A recent review on the $SO(5)/SO(4)$ context has been pre-

sented in Ref. [122] and the impact at colliders of different realisations has been analysed in Ref. [168]. The MLσM, and therefore also the AMLσM, seems an interpolation between the so-called $MCHM_4$ and $MCHM_5$ scenarios considered in Ref. [168], once only the physical Higgs is retained in the low-energy theory. Typical observables of interest at colliders are the EWPO, the $Zb\bar{b}$ coupling, couplings of the scalar dofs to gluons and photons [118, 119], and the interactions with fermions. As they have been studied for the MLσM in Refs. [24, 120], the aim of this section is to extend those results to the AMLσM.

EWPO: Deviations to the SM predictions for the T and S parameters [169] (or equivalently ϵ_1 and ϵ_3 [170]) are expected to be relevant. In the MLσM, the mixing between $\hat{h}$ and $\hat{\sigma}$ can reach relatively large values, ~ 0.1, and important scalar contributions to T and S are indeed expected. However, these contributions can always be compensated, in some allowed region of the parameters space, by including the exotic fermion contributions.

In the AMLσM, for the benchmark values chosen in the previous section, the values of the scalar sector mixing parameters result very small, see Fig. 8.3, and then the contributions to T and S are expected to be much less relevant. For smaller values of f consistent with Fig. 8.1, the $\hat{h}$-$\hat{\sigma}$ mixing slightly increases, and then larger contributions to T and S are expected. In addition, relevant contributions to the EWPO from the fermionic sector can also be present. However, exactly as happens in the MLσM case, it is always possible to avoid the T and S bounds in a non negligible part of the full (fermionic + bosonic) parameter space.

$Z\bar{b}b$ COUPLING: The modification of the Z couplings to $b\bar{b}$ is a very interesting observable to test a model. The most relevant contributions arise from the top-partner fermion, while the ones from the heavier scalar dofs turn out to be negligible. The top-partner induces deviations from the SM prediction of this coupling only at the one-loop level, and the effect of these contributions is soften with respect to those to the EWPO previously discussed. This result holds for both the MLσM and the AMLσM. As illustrated in Ref. [24], it is easy to accommodate the experimental measure of the $Zb\bar{b}$ coupling in a large part of the parameter space, and therefore no relevant constraint can be deduced from this observable.

GAUGE BOSONS AND σ PRODUCTION AT COLLIDERS: As in the SM, no tree level $\hat{h}gg$ and $\hat{h}\gamma\gamma$ couplings are present in the AMLσM. However, effective interactions with gluons and with photons may arise at the one-loop level. In consequence, all the three scalar mass eigenstates, $\varphi_{1,2,3}$, do couple with gluons and photons, with their interactions weighted by the corresponding mixing coefficients C_i^2, according to Eq. (8.36).

As worked out in details in Ref. [24], the Higgs coupling with two gluons, $\varphi_1 gg$, is mainly due to the top contribution, as the bottom one is negligible and the exotic fermion ones almost cancel out (due to their vector-like nature). On the other hand, the $\varphi_2 gg$ and $\varphi_3 gg$ couplings are suppressed by C_2^2 and C_3^2 respectively, and therefore are typically at least 10^{-2} smaller than $\varphi_1 gg$. Moreover, as the top quark is lighter than φ_2 and φ_3, its contribution to their couplings is also suppressed, and the dominant terms arise from the exotic fermion sector.

The couplings to photons receive relevant contributions not only from loops of top quark and of exotic fermions, but also from loops of massive gauge bosons. The latter are the dominant ones in the case of the physical Higgs particle, i.e. for $\varphi_1\gamma\gamma$, while they are suppressed by C_2^2 and C_3^2 for the heavier scalar dofs and the most relevant contributions to $\varphi_2\gamma\gamma$ and $\varphi_3\gamma\gamma$ are those from the exotic fermions.

These results impact on the production mechanisms of the heavier dofs at collider, that are gluon fusion or vector boson fusion. From Fig. 8.2, the masses for φ_2 and φ_3 are typically larger than the TeV scale, within the whole range of values for f and f_s shown in Fig. 8.1. The lowest mass values are then potentially testable at colliders, although it strongly depends on the couplings with gluons and the massive gauge bosons. Ref. [24] concluded that, in the presence of only two scalar dofs, the heaviest one would be constrained only for masses lower than 0.6 TeV and mixing coefficient $C_2^2 > 0.1$. Extending this result to the three scalar dofs described in the AMLσM and considering the results presented in Fig. 8.2, the present LHC data and the future prospects (LHC run-2 with total luminosity of $3ab^{-1}$) will not be able to put any relevant bound, or in other words the heavier scalar dofs have production cross sections too small to lead to any signal in the present and future run of LHC.

IMPACT OF THE EXOTIC FERMIONS: The exotic fermion masses partially depend on a distinct set of parameters with respect to those entering the scalar potential. While this is particularly true for the MLσM, where two arbitrary mass parameters $M_{1,5}^{(\prime)}$ are introduced in the Lagrangian, in the minimal AMLσM the exotic fermion masses are controlled by f_s, through the parameters $z_{1,5}^{(\prime)}$ (and/or $\tilde{z}_{1,5}^{(\prime)}$). The largeness of f_s corresponds to large masses for these exotic fermions, consistent with the fermion partial compositeness mechanism. Direct detections would be probably very unlikely, while their effect would manifest in deviations from the SM predictions of SM field couplings. In Ref. [24], the exotic fermions have been integrated out and the induced low-energy operators have been identified. The mayor expected effects consist in decorrelations between observables that are instead correlated in the SM, and the appearance of anomalous couplings: these effects are very much typical of the HEFT setup, where the EWSB is non-linearly realised and the Higgs originates as a GB. For an overview of these analyses see Refs. [131–133, 139, 142, 171, 172].

Besides the effects discussed above, it is worth to mention the possibility to investigate the Higgs nature through the physics of the longitudinal components of the SM massive gauge bosons. As the MLσM and AMLσM deal with the same symmetry of the SM, no additional effects are expected with respect to the analyses carried out in Refs. [173–177].

8.3 QCD AXION OR AXION-LIKE-PARTICLE?

The nature of the field a is necessarily linked to the origin of its mass term (as a GB it should be massless unless $U(1)_{PQ}$ is explicitly broken, as it happens in any axion model). There are two distinct contributions to the axion mass (gravitational and/or Planck-scale sources [178–181] will not be discussed here). The first is due to purely QCD effects (axion mixing with neutral pions), which is estimated to be [9, 182, 183]

$$m_a \sim 6\ \mu\text{eV} \left(\frac{10^{12}\ \text{GeV}}{f_a / c_{agg}} \right) , \tag{8.41}$$

for values of f_a typically taken to be larger than 10^6 GeV. The second is due to the extra fermions that couple to the axion, such as in the KSVZ invisible axion model [8, 9]:

$$m_a = \frac{\sqrt{Z}}{1+Z} \frac{\alpha_s^2}{\pi^2} \frac{f_\pi}{f_a} m_\pi \ln \left(\frac{m_\psi^2}{m_u m_d} \right) , \tag{8.42}$$

where $Z \simeq m_u/m_d$ and $f_\pi \sim 94$ MeV is the pion decay constant and m_ψ is the generic mass of the exotic fermions.

In Sect. 8.2.1, three values for f_s have been considered: $f_s = 1$ TeV, $f_s = 10^3$ TeV and $f_s = 10^6$ TeV. Eq. (7.19) links the axion scale f_a to the VEV of the radial component of s, and as a consequence $f_a \simeq f_s$ in first approximation. The corresponding induced axion mass belongs to the window from tens of meV to the keV. For this range of values, the strongest constraints on f_a come from the axion coupling to two photons $g_{a\gamma\gamma}$: specifying the value of $c_{a\gamma\gamma}$ for the minimal AMLσM charge assignment as reported in Tab. 7.3, one gets

$$f_s \gtrsim 3.7 \times 10^8 \text{ GeV} . \tag{8.43}$$

As a consequence, a QCD axion consistent with all the present data can only be generated in the minimal AMLσM if the scale f_s, associated to the PQ breaking, is of the order of 10^8 GeV or larger. As discussed in Ref. [145], the resulting axion falls into the category of the so-called invisible axions [8–11], as such a large f_s scale strongly suppresses all the couplings with SM fermions and gauge bosons, preventing any possible detection at colliders or at low-energy (flavour) experiments.

The difference with respect to the traditional invisible axion models resides partly in the axion couplings to photons and gluons, and in the EWSB sector. As underlined in Ref. [145], adding a KSVZ axion to the MLσM narrows the range of possible values that the ratio $c_{a\gamma\gamma}/c_{agg}$ may take: the minimal AMLσM presented here provides a very sharp prediction for this ratio,

$$\frac{c_{a\gamma\gamma}}{c_{agg}} = \frac{14}{3} . \tag{8.44}$$

Moreover, in the minimal AMLσM with $f_s \gtrsim 10^8$ GeV the low-energy theory is not exactly the SM, but the EWSB mechanism is non-linearly realised and the Higgs particle originates as a GB. This model may be confirmed, or excluded, by a precise measure of $c_{a\gamma\gamma}/c_{agg}$ and by a dedicated analysis of the EW sector. In particular, this case corresponds to the scenario where only the physical Higgs remains in the low-energy spectrum, while the other two scalar dofs are very heavy. In consequence, only indirect searches on Higgs couplings or the physics associated to the longitudinal components of the SM gauge bosons may have the potential to constrain the minimal AMLσM.

For much lighter values of the f_s scale, instead, the astrophysical bounds on $g_{a\gamma\gamma}$ coupling can be satisfied only assuming that the axion mass and its characteristic scale f_s are not correlated. This corresponds to the ALP scenario: differently from the QCD axion, an ALP has a mass which is independent from its characteristic scale f_s, due to additional sources of soft shift symmetry breaking with respect to those in Eqs. (8.41) and (8.42), and does not necessarily solve the strong CP problem[3]. As an example, a benchmark point that passes all the previous bounds corresponds to a 1 GeV axion with $f_s \sim 200$ TeV. The most sensitive observables for this particle are its couplings with two W's, two Z's and $Z\gamma$ than can be analysed in collider searches.

By increasing the axion mass, its decay length decreases and this may open up to another class of observables: if the axion decays inside the detector, then it would not show up as missing energy, but as a couple of gauge bosons, as discussed in Refs. [17, 43, 81]. The distance travelled by the axion after being produced may be casted as follows [43],

$$d \approx \frac{10^4}{c_i^2} \left(\frac{\text{MeV}}{m_a}\right)^4 \left(\frac{f_s}{\text{GeV}}\right)^2 \left(\frac{|p_a|}{\text{GeV}}\right) \text{ m} , \tag{8.45}$$

3 In the ALP scenario, a solution to the Strong CP problem is not guaranteed and therefore the condition 4 is not required. An additional scenario satisfying conditions 1, 2, and 3, can be considered: in this case, $n_{q_L} = n_{\psi_L} = n_{\psi_R} = n_{\chi_R} = n_{t_R} \pm n_s = n_{\chi_L} \pm n_s$ (with the "+" or "−" are associated to the presence of the z_1 or $\tilde{z}_1$ terms in the Lagrangian, respectively), and the induced renormalisable scalar potential turns out to be the same as in Eq. (8.1).

where c_i are the couplings in Tab. 7.3 and the typical momentum considered is $\gtrsim$ 100 GeV. For the selected benchmark considered, $m_a \sim 1$ GeV and $f_s \sim 200$ TeV, the decay length is of tens of meters for decays into two photons. This axion can therefore avoid detection at colliders, although for a slightly larger masses this is not guaranteed.

For this value of f_s, the heaviest scalar dofs, despite being much smaller than in the previous scenario, are expected to have so large masses and so small couplings that will be very unlikely to detect any signal at present or even future LHC runs. Instead, the model can be tested through deviations from the SM predictions of the Higgs couplings or through pure gauge boson observables.

Finally, the difference with respect to the previous scenario is mainly that a massive axion is likely to give signals at colliders, due to the present sensitivity on its couplings with massive gauge bosons.

8.3.1 *The Fine-Tuning Problem*

The presence of different scales in the scalar potential leads to a fine-tuning problem in the model. As already mentioned, the parameter ξ measures the tension between the EW scale and the $SO(5)$ SSB scale, as shown in Eq. (8.38). In models where axions or ALPs are dynamically originated, a new scale f_s is present and typically much larger than the EW scale. Once the scalar field s develops a VEV, the scale f receives a contribution proportional to $\sqrt{\lambda}_{s\phi} f_s$, as can be read in Eq. (7.21). This leads to $f \approx f_s \gg v$, or $\lambda_{s\phi} \ll 1$: this represents two sides of the same fine-tuning problem.

In the ALP model presented here $f_s \sim 200$ TeV and therefore a value of $\lambda_{s\phi} \lesssim 10^{-4}$ would be necessary to not modify, excessively, the scale f. In generic AMLσM, much larger values for f_s are typically necessary to pass the different experimental bounds on the axion/ALP couplings and then a much stronger fine-tuning on $\lambda_{s\phi}$ has to be invoked. In the next chapter (based on Ref. [184]) an ALP model in the MLσM will be presented where the fine-tuning problem is solved, but at the price of renouncing to one of the assumptions listed in Sect. 7.2.

9 A SINGLE SCALE SOLUTION

A suggestive mechanism to protect the Higgs mass from radiative corrections arises when the Higgs field belongs to the Nambu Goldstone Boson (GB) sector of a model equipped with a global symmetry $\mathcal{G}$ spontaneously broken, by an unknown strongly interacting dynamics, to a subgroup $\mathcal{H}$. In the Composite Higgs (CH) framework, the Standard Model (SM) GBs and the Higgs field parametrise (some of) the coset $\mathcal{G}/\mathcal{H}$ coordinates and are forced to be strictly massless [112–114, 148]. The gauging of the SM symmetries and the introduction of fermionic Yukawa couplings introduce an explicit breaking of $\mathcal{G}$, leading to a non-vanishing mass term for the Higgs and to the spontaneous breaking of the electroweak (EW) symmetry.

The Minimal Linear σ-Model (MLσM) is a renormalisable model that represents a convenient and well-defined framework that, at need, by integrating out the extra scalar degree of freedom (dof) σ, matches the usual effective non-linear MCHM [115, 121–123] Lagrangian, or the more generalHiggs Effective Field Theory Lagrangian [124–143, 172].

As it was shown in the previous chapter, the MLσM provides an optimal framework where to look for an Axion solution to the strong CP problem or, more generally, for an ALP. By extending the MLσM spectrum with an additional complex scalar field s, singlet under SM and $SO(5)$ symmetries, and by supplementing it with an additional global Abelian symmetry *à la* Peccei-Quinn (PQ) [1], $U(1)_{\rm PQ}$, an axion or ALP can be introduced. Such a framework has been dubbed Axion-MLσM (AMLσM) [145, 185].

The tree-level renormalisable scalar potential associated to the AMLσM, describing the spontaneous $SO(5)/SO(4)$ and PQ symmetry breaking, reported in Eq. (7.21), reads:

$$V(\phi,\, s) = \lambda(\phi^T\phi - f^2)^2 + \lambda_s(2s^*s - f_s^2)^2 - 2\lambda_{s\phi}(s^*s)(\phi^T\phi) + \dots\,, \quad (9.1)$$

As in the previous chapter, we parametrise the complex scalar singlet s, in the PQ symmetry broken phase, with an exponential notation,

$$s = \frac{v_r + r}{\sqrt{2}} e^{i\,a/f_a}\,, \quad (9.2)$$

with r the radial component field and a the pseudoscalar field, to be identified with the axion or ALP dof. The axion (or ALP) decay constant $f_a \equiv \langle r\rangle \equiv v_r$ is typically of the order of the PQ breaking scale f_s and may undergo strong constraints arising from the experimental limits on the pseudoscalar coupling to photons. In the case of a being the QCD axion, with mass $m_a < 10$ eV, the bound[1] on the scale f_a is [16, 17, 189]

$$f_a \gtrsim |g_{a\gamma\gamma}| \times 10^7 \text{ GeV}\,, \quad (9.3)$$

1 This analysis [186] shows a preferred region of the parameter space $g_{a\gamma\gamma} \times g_{aee}$, being the latter the effective coupling of the axion with two electrons. When interpreted in terms of the DFSZ [10, 11] or KSVZ [8, 9] axion models, the best fit point is in the border of the perturbative unitarity of the Yukawas, while the fit is inconclusive at more than 2σ. This region will be tested by future ARIADNE [187] and IAXO [188] experiments.

which corresponds to the value of Eq. (8.43) in the specific charge assignment of tab. 7.2. For masses $10\ \text{eV} < m_a < 0.1\ \text{GeV}$ the bounds become even stronger [49]. As it was explained in Sect. 8.3.1, the bound in Eq. (9.3) strongly crashes with the requirement of a natural EW scale. Indeed, either the coupling $\lambda_{s\phi}$ in Eq. (9.1) is unnaturally set to 0, or the "effective" $SO(5)/SO(4)$ breaking scale, labelled f_R, runs to the highest scale, $f_R \approx f_s \approx f_a$, reintroducing a strong fine-tuning between the EW and the CH scale, $\xi = v^2/f_R^2 \ll 1$. This suggests that the AMLσM framework is "natural" only if f_s, and therefore f_a, are at the TeV scale.

To escape the constraint in Eq. (9.3), two approaches can be outlined. The first is still to rely on the QCD axion paradigm, as the solution to the strong CP problem: in this case a specific (*ad hoc*) choice of the PQ charges can be identified such that the $a\gamma\gamma$ coupling is vanishing [190] and consequently the astrophysical constraints are automatically avoided. The second approach consists in abandoning, partially or completely, the QCD ansatz and considering, instead, an ALP particle: then the inverse proportionality relation between the QCD axion mass and its decay constant does not hold anymore and a mass larger than 0.1 GeV can be achieved, relaxing the astrophysics bounds on the $a\gamma\gamma$ coupling, $f_a \gtrsim |g_{a\gamma\gamma}|$ GeV.

In Chap. 7 and 8, a minimal ALP scenario in the AMLσM framework has been considered, assuming that the PQ dynamics does not intervene in the explicit breaking of the $SO(5)$ symmetry, i.e. the two scales f and f_s are independent. The scale f can be taken in the TeV range and the phenomenology associated to the $SO(5)/SO(4)$ sector turns out to be very similar to the one described in the original MLσM in Ref. [24]; the scale f_a, and therefore f_s, can also be taken in the TeV range, opening the possibility to test this model both at colliders and at B-factories. Moreover, no fine-tuning between the two scales f and f_s is necessary in this model. However, in this chapter, the mechanisms behind the PQ and the $SO(5)$ symmetry breaking are instead identified assuming $f_s = f$ around the TeV scale (the possibility of $f_s \approx f$ has already been considered in Ref. [145], where however only the QCD axion scenario has been investigated, with $f_s \approx f \gg$ TeV). This is obtained by replacing the scales appearing in the $SO(5)$ explicit breaking terms with the singlet scalar s: once this field develops a VEV, these terms break $SO(5)$ spontaneously and not explicitly, thus linking f with f_s. In this context, where $SO(5)$ is dynamically broken, alternative constructions with respect to the ALP solution considered in Ref. [185] can be considered. Moreover, these AMLσM realisations can be testable at colliders and flavour factories.

9.1 BUILDING THE AMLσM WITH A SINGLE SCALE f

The construction of the model follows exactly the same approach of Chap. 7. In the single-scale scenario ($f_s \equiv f$) the Lagrangian is almost identical to the one in Sect. 7.1, where the only relevant differences can be found in the fermionic part:

$$\begin{aligned}
\mathcal{L}_{\text{f}} = {} & \overline{q}_L i\not{D} q_L + \overline{t}_R i\not{D} t_R + \overline{b}_R i\not{D} b_R \\
& + \overline{\psi}\left[i\not{D} - M_5\right]\psi + \overline{\chi}\left[i\not{D} - M_1\right]\chi - \left[y_1\,\overline{\psi}_L\,\phi\,\chi_R + y_2\,\overline{\psi}_R\,\phi\,\chi_L + \text{h.c.}\right] \\
& - \left[z_1\,\overline{\chi}_R\,\chi_L\,s + \tilde{z}_1\,\overline{\chi}_R\,\chi_L\,s^* + z_5\,\overline{\psi}_R\,\psi_L\,s + \tilde{z}_5\,\overline{\psi}_R\,\psi_L\,s^* + \text{h.c.}\right] \\
& + \Big[\left(\Lambda_1 + k_1 s + \tilde{k}_1 s^*\right)\left(\overline{q}_L \Delta_{2\times 5}\right)\psi_R + \left(\Lambda_2 + k_2 s + \tilde{k}_2 s^*\right)\overline{\psi}_L\left(\Delta_{5\times 1} t_R\right) + \\
& + \left(\Lambda_3 + k_3 s + \tilde{k}_3 s^*\right)\overline{\chi}_L t_R + \text{h.c.}\Big] + \ldots
\end{aligned} \tag{9.4}$$

where the dots stand for the "primed" part relative to the bottom sector. Unlike Eq. (7.6), now the dimensionful parameters Λ_i, associated with the $SO(5)$ soft-

breaking terms responsible for the partial-compositness mechanism, are allowed to be generate after the spontaneous breaking of the PQ symmetry, like the masses of the exotic fermions:

$$\begin{aligned} \Lambda_i(v_r) &\equiv \Lambda_i + (k_i + \tilde{k}_i)v_r \,, \\ M_i(v_r) &\equiv M_i + (z_i + \tilde{z}_i)v_r \,. \end{aligned} \tag{9.5}$$

With the exotic fermions acquiring masses larger than the EW scale, a fermionic Seesaw mechanism provides the masses for the SM fermions [146,147]and the Leading Order (LO) contribution reads:

$$\begin{aligned} m_t = &\frac{y_1\,\Lambda_1(v_r)\,\Lambda_3(v_r)\,v_h}{M_1(v_r)\,M_5(v_r) - y_1\,y_2\,(v_h^2+v_\sigma^2)} + \\ &- \frac{y_1\,y_2\,\Lambda_1(v_r)\,\Lambda_2(v_r)\,v_h\,v_\sigma}{M_1(v_r)\,M_5^2(v_r) - y_1\,y_2\,M_5(v_r)\,(v_r^2+v_\sigma^2)} \,, \end{aligned} \tag{9.6}$$

where v_h, v_σ and v_r are the VEVs of the physical field h, σ and r, satisfying to $v_h^2 + v_\sigma^2 = f^2$. The same argument about the simultaneous presence of M_i, z_i or $\tilde{z}_i$ of Sect.(7.1.2) still holds in this case, generalised to Λ_i, k_i and $\tilde{k}_i$.

Once the fermionic Lagrangian is fully determined, the computation of the 1-loop contributions to the scalar potential is straightforward: the Coleman-Weinberg (CW) formula [155] allows to extract the divergences generated at 1-loop with internal fermion and gauge boson lines. In general, several divergent contributions arise at one loop that cannot be re-absorbed in the tree-level $SO(5)$ invariant scalar potential in Eq. (9.1). In consequence, to have a renormalisable Lagrangian, consistent with a viable EW symmetry breaking, the corresponding terms need to be added to the tree-level scalar potential. As two is the minimum number of explicit $SO(5)$ breaking terms needed to have a viable EW breaking sector, constructions with only two extra parameters in Eq. (9.1) have been dubbed "minimal".

9.2 VIABLE, NATURAL AND MINIMAL

A proper model should be viable, natural and minimal. In order to build an AMLσM satisfying these three features, the following guiding conditions are required (see Sect. (7.2) for a more detailed discussion): i) third generation SM fermion masses are generated at LO and therefore the expression in Eq. (9.6) must not vanish; ii) no large hierarchy is present between the $SO(5)$ and $U(1)_{\rm PQ}$ breaking scales; iii) the model depends on the minimal possible number of parameters.

In order to identify the PQ charge assignments compatible with these three requirements, it is useful to introduce the following five PQ charges differences: for the top sector,

$$\begin{aligned} &\Delta_{y_1} \equiv n_{\psi_L} - n_{\chi_R} \\ \Delta_{\Lambda_1} \equiv n_{q_L} - n_{\psi_R} \qquad &\Delta_{\Lambda_3} \equiv n_{\chi_L} - n_{t_R} \\ \Delta_\chi \equiv n_{\chi_L} - n_{\chi_R} \qquad &\Delta_\psi \equiv n_{\psi_L} - n_{\psi_R} \,. \end{aligned} \tag{9.7}$$

Similar quantities can be defined for the bottom sector by replacing the unprimed fields with the primed ones.

Condition i) is satisfied by requiring that none among y_1, $\Lambda_1(v_r)$, $\Lambda_3(v_r)$, $M_1(v_r)$ and $M_5(v_r)$ is vanishing. Alternative possibilities with non-vanishing $\Lambda_2(v_r)$ turn out to be non-minimal. In terms of the quantities defined above, this corresponds to

$$\begin{aligned} &\Delta_{y_1} = 0 \,, \qquad \Delta_{\Lambda_1} = \{0, \pm n_s\} \,, \qquad \Delta_{\Lambda_3} = \{0, \pm n_s\} \,, \\ &\Delta_\chi = \{0, \pm n_s\} \,, \qquad \Delta_\psi = \{0, \pm n_s\} \,. \end{aligned}$$

	Conditions on PQ charges	y_1	y_2	Λ_1	k_1	$\tilde{k}_1$	$\tilde{k}_3$	$\tilde{z}_1$	M_5	z_5	$\tilde{z}_5$	Δ_ψ	Δ_χ	Δ_t
$\mathcal{M}_1$	$n_{\psi_L} = n_{\chi_R} = n_{\psi_R} = n_{\chi_L} - n_s = n_{q_L} = n_{t_R} - 2n_s$	✓		✓			✓	✓	✓			0	n_s	$-2n_s$
$\mathcal{M}_2$	$n_{\psi_L} = n_{\chi_R} = n_{\psi_R} = n_{\chi_L} - n_s = n_{q_L} + n_s = n_{t_R} - 2n_s$	✓				✓	✓	✓	✓			0	n_s	$-3n_s$
$\mathcal{M}_3$	$n_{\psi_L} = n_{\chi_R} = n_{\psi_R} + n_s = n_{\chi_L} - n_s = n_{q_L} + 2n_s = n_{t_R} - 2n_s$	✓				✓	✓	✓			✓	n_s	n_s	$-4n_s$
$\mathcal{M}_4$	$n_{\psi_L} = n_{\chi_R} = n_{\psi_R} + n_s = n_{\chi_L} - n_s = n_{q_L} + n_s = n_{t_R} - 2n_s$	✓		✓			✓	✓			✓	n_s	n_s	$-3n_s$
$\mathcal{M}_5$	$n_{\psi_L} = n_{\chi_R} = n_{\psi_R} + n_s = n_{\chi_L} - n_s = n_{q_L} = n_{t_R} - 2n_s$	✓			✓		✓	✓			✓	n_s	n_s	$-2n_s$
$\mathcal{M}_6$	$n_{\psi_L} = n_{\chi_R} = n_{\psi_R} - n_s = n_{\chi_L} - n_s = n_{q_L} - n_s = n_{t_R} - 2n_s$	✓	✓	✓			✓	✓		✓		$-n_s$	n_s	$-n_s$
$\mathcal{M}_7$	$n_{\psi_L} = n_{\chi_R} = n_{\psi_R} = n_{\chi_L} - n_s = n_{q_L} - n_s = n_{t_R} - 2n_s$	✓			✓		✓	✓	✓			0	n_s	$-n_s$

Table 9.1: *List of the viable, natural and minimal AMLσM realisations, defined by the conditions on the PQ charges of the fermion fields written in terms of the charge n_s of the PQ scalar field. The constants allowed in the Lagrangian are indicated with "✓", while all the remaining Lagrangian parameters that are not listed in this table are not allowed for symmetry reasons. On the right side, the corresponding values for Δ_ψ, Δ_χ and Δ_t are listed.*

Whenever one of these quantities vanishes, the corresponding allowed term in the Lagrangian is the constant one: i.e. y_1, Λ_i and M_i. On the other hand, if any of the charge differences is equal to $-n_s$ ($+n_s$), the corresponding term, allowed in the Lagrangian, is proportional to s (s^*). As an example, $\Delta_\chi = 0$ means that χ_L and χ_R transform under $U(1)_{\rm PQ}$ with the same charge and therefore the term $M_1 \overline{\chi}_R \chi_L$ is invariant under $U(1)_{\rm PQ}$ and should be kept in the Lagrangian. If, instead, $\Delta_\chi = -n_s$, then the $z_1\, \overline{\chi}_R\, \chi_L\, s$ term is the invariant one. There are $3^4 = 81$ possible different configurations compatible with condition i) for a single fermion sector, while any value different from 0 or $\pm n_s$ leads to vanishing SM fermion masses.

The naturalness requirement, condition ii), is satisfied only if all the scales in the Lagrangian, except for M_1 and Λ_3, are in the TeV range. The $SO(5)$ and $U(1)_{\rm PQ}$ breaking scales f and f_s need to satisfy to this condition in order to avoid large fine-tunings in the tree-level scalar potential. For the other quantities, such as M_5, Λ_1 and Λ_2, the reason resides in the fact that they correct the scalar potential parameters at one-loop. If these parameters are much larger than the TeV, large fine-tunings would be necessary in order to guarantee a viable EW VEV. M_1 and Λ_3 evade this condition because they do not enter the CW contributions: as already pointed out in Ref. [145], they only need to satisfy $\Lambda_3 / M_1 \sim 1$ in order to provide a viable value for the mass of third generation SM quarks – see Eq. (9.6) – assuming natural Yukawa couplings y_i.

The minimality condition iii) only concerns the number of parameters that enter the scalar potential once considering the 1-loop contributions. Two divergent terms, proportional to h^2 and h^4, arise from the CW potential induced by the gauge bosons: these divergences are independent of the specific PQ charge assignment and therefore the corresponding terms necessarily enter the final scalar potential. Minimal constructions are those where the fermionic CW potential does not introduce any additional divergence that cannot be absorbed by a redefinition of the parameters in Eq. (9.1) or of h^2 or h^4 as discussed in the previous chapter.

Out of the 81 possible AMLσM constructions, only seven satisfy to all three conditions and they are listed in Tab. (9.1), defined by the PQ charges of the fermion fields, written as a function of the charge n_s of the PQ scalar field. In the same table, the parameters entering the Lagrangian are explicitly reported. On the right side, the corresponding values for Δ_ψ, Δ_χ and

$$\Delta_t \equiv n_{q_L} - n_{t_R} \tag{9.8}$$

are listed, as they will be relevant in the phenomenological section that follows. A sibling for each configuration can be found by replacing $n_s \to -n_s$, $\tilde{k}_3 \to k_3$, $z_1 \to \tilde{z}_1$, $k_1 \leftrightarrow \tilde{k}_1$ and $z_5 \leftrightarrow \tilde{z}_5$. A charge assignment and its own sibling, for a given fermion

sector, are completely equivalent. All the remaining Lagrangian parameters that are not listed in this table are not allowed for symmetry reasons. Similar considerations hold for the bottom quark sector, in terms of the PQ charge differences $\Delta_{\psi'}$, $\Delta_{\chi'}$ and

$$\Delta_b \equiv n_{q_L} - n_{b_R} \,. \tag{9.9}$$

The top and bottom sectors are not completely independent as q_L enters simultaneously in the quantities of Eqs. (9.8) and (9.9). The values listed in Tab. (9.1) hold simultaneously for the top and bottom sector, with an extra freedom of a global sign difference between the two. In what follows, the notation $\mathcal{M}_i^+$ has been adopted for the same charge case, defined by $\Delta_\psi = \Delta_{\psi'}$, $\Delta_\chi = \Delta_{\chi'}$ and $\Delta_t = \Delta_b$, while $\mathcal{M}_i^-$ for the opposite charge case, where $\Delta_\psi = -\Delta_{\psi'}$, $\Delta_\chi = -\Delta_{\chi'}$ and $\Delta_t = -\Delta_b$.

The scalar potential associated to all the models listed in Tab. (9.1) has already been thoroughly studied in Chap. (8), together with the phenomenology associated to the exotic fermions and scalar fields. As a consequence, the next section will only focus on the ALP phenomenology.

9.3 THE ALP PHENOMENOLOGY

Performing fermion field redefinitions, the Lagrangian in Eq. (7.6) can be rewritten such that the axion or ALP has only derivative couplings with fermions. In particular, these models predict that the axion or ALP couples to both top and bottom quarks: these interactions can be written as

$$\mathcal{L}_a \supset -c_{a\psi\psi'} \frac{\partial_\mu a}{2f_a} \bar{\psi}\gamma^\mu\gamma_5\psi' \,, \tag{9.10}$$

where the couplings $c_{a\psi\psi'}$ depends on the specific model considered and can be read in Tab. (9.2).

	c_{att}	c_{abb}
$\mathcal{M}_1^+$	$2n_s$	$2n_s$
$\mathcal{M}_1^-$	$2n_s$	$-2n_s$
$\mathcal{M}_2^+$	$3n_s$	$3n_s$
$\mathcal{M}_2^-$	$3n_s$	$-3n_s$
$\mathcal{M}_3^+$	$4n_s$	$4n_s$
$\mathcal{M}_3^-$	$4n_s$	$-4n_s$
$\mathcal{M}_4^+$	$3n_s$	$3n_s$
$\mathcal{M}_4^-$	$3n_s$	$-3n_s$
$\mathcal{M}_5^+$	$2n_s$	$2n_s$
$\mathcal{M}_5^-$	$2n_s$	$-2n_s$
$\mathcal{M}_6^+$	n_s	n_s
$\mathcal{M}_6^-$	n_s	$-n_s$
$\mathcal{M}_7^+$	n_s	n_s
$\mathcal{M}_7^-$	n_s	$-n_s$

Table 9.2: *Values of the coefficients $c_{a\psi\psi'}$ in terms of the charge n_s for the top and bottom quarks.*

Moreover, at the quantum level, the derivative of the axial current is non-vanishing, giving rise to the following effective axion-gauge boson couplings: in the physical basis for the gauge bosons,

$$\begin{aligned}\delta\mathcal{L}_a^{\text{eff}} \supset & -\frac{\alpha_s}{8\pi}\, c_{agg}\, \frac{a}{f_a}\, G^a_{\mu\nu}\widetilde{G}^{a\mu\nu} - \frac{\alpha_{em}}{8\pi}\, c_{a\gamma\gamma}\, \frac{a}{f_a}\, F_{\mu\nu}\widetilde{F}^{\mu\nu} + \\ & - \frac{\alpha_{em}}{8\pi}\, c_{aZZ}\, \frac{a}{f_a}\, Z_{\mu\nu}\widetilde{Z}^{\mu\nu} - \frac{\alpha_{em}}{8\pi}\, c_{a\gamma Z}\, \frac{a}{f_a}\, F_{\mu\nu}\widetilde{Z}^{\mu\nu} + \\ & - \frac{\alpha_{em}}{8\pi}\, c_{aWW}\, \frac{a}{f_a}\, W^+_{\mu\nu}\widetilde{W}^{-\mu\nu}\,,\end{aligned} \tag{9.11}$$

where $\widetilde{X}^{\mu\nu} \equiv \epsilon^{\mu\nu\rho\sigma} X_{\rho\sigma}/2$ and the convention $\epsilon_{1230} = +1$ is used. The mass independent anomaly contributions to the coefficients c_{ai} are explicitly reported in App. (A.2), in terms of the PQ fermionic charges, while in Tab. (9.3) the anomalous coefficients for the seven models summarised in Tab. (9.1) are listed.[2] These coefficients include the contributions of all the fermions that do couple with a.

	c_{agg}	$c_{a\gamma\gamma}$	c_{aZZ}	$c_{a\gamma Z}$	c_{aWW}
$\mathcal{M}_1^+$	$-2n_s$	$-\frac{10}{3}n_s$	$-\frac{1}{3}n_s t_\theta^2 - \frac{3n_s}{t_\theta^2}$	$\frac{2}{3}n_s t_\theta - \frac{6n_s}{t_\theta}$	$-\frac{6n_s}{s_\theta^2}$
$\mathcal{M}_1^-$	0	$-2n_s$	$-2n_s t_\theta^2$	$4n_s t_\theta$	0
$\mathcal{M}_2^+$	$-4n_s$	$-\frac{20}{3}n_s$	$-\frac{13}{6}n_s t_\theta^2 - \frac{9n_s}{2t_\theta^2}$	$\frac{13}{3}n_s t_\theta - \frac{9n_s}{t_\theta}$	$-\frac{9n_s}{s_\theta^2}$
$\mathcal{M}_2^-$	0	$-4n_s$	$-4n_s t_\theta^2$	$8n_s t_\theta$	0
$\mathcal{M}_3^+$	$4n_s$	$\frac{92}{3}n_s$	$\frac{74}{3}n_s t_\theta^2 + \frac{6n_s}{t_\theta^2}$	$-\frac{148}{3}n_s t_\theta + \frac{12n_s}{t_\theta}$	$\frac{12n_s}{s_\theta^2}$
$\mathcal{M}_3^-$	0	$4n_s$	$4n_s t_\theta^2$	$-8n_s t_\theta$	0
$\mathcal{M}_4^+$	$6n_s$	$34n_s$	$\frac{53}{2}n_s t_\theta^2 + \frac{15n_s}{2t_\theta^2}$	$-53n_s t_\theta + \frac{15n_s}{t_\theta}$	$\frac{15n_s}{s_\theta^2}$
$\mathcal{M}_4^-$	0	$6n_s$	$6n_s t_\theta^2$	$-12n_s t_\theta$	0
$\mathcal{M}_5^+$	$8n_s$	$\frac{112}{3}n_s$	$\frac{85}{3}n_s t_\theta^2 + \frac{9n_s}{t_\theta^2}$	$-\frac{170}{3}n_s t_\theta + \frac{18n_s}{t_\theta}$	$\frac{18n_s}{s_\theta^2}$
$\mathcal{M}_5^-$	0	$8n_s$	$8n_s t_\theta^2$	$-16n_s t_\theta$	0
$\mathcal{M}_6^+$	$-10n_s$	$-\frac{122}{3}n_s$	$-\frac{163}{6}n_s t_\theta^2 - \frac{27n_s}{2t_\theta^2}$	$\frac{163}{3}n_s t_\theta - \frac{27n_s}{t_\theta}$	$-\frac{27n_s}{s_\theta^2}$
$\mathcal{M}_6^-$	0	$-10n_s$	$-10n_s t_\theta^2$	$20n_s t_\theta$	0
$\mathcal{M}_7^+$	0	0	$\frac{3}{2}n_s t_\theta^2 - \frac{3n_s}{2t_\theta^2}$	$-3n_s t_\theta - \frac{3n_s}{t_\theta}$	$-\frac{3n_s}{s_\theta^2}$
$\mathcal{M}_7^-$	0	0	0	0	0

Table 9.3: *Values of the coefficients c_{ai} in terms of the charge n_s. t_θ and s_θ stand for the tangent and the sine of the Weinberg angle respectively.*

It is now possible to discuss the phenomenological features of the seven AMLσM constructions presented. Firstly, all models, but $\mathcal{M}_7^\pm$, have a non-vanishing coupling between the ALP and two photons. As a consequence, the strong bound present on this coupling - reported in Eq. (9.3) - translates into a constraint on the scale f_a that should be much larger than the EW scale, introducing a strong Hierarchy problem in the scalar potential (tree and loop level [191]). In order to avoid this fine-tuning problem, $m_a \gtrsim 0.1$ GeV has to be considered for all the models $\mathcal{M}_{1-6}^\pm$. As a

2 Only one generation of SM fermions has been considered here, consistently with the formulation of the AMLσM presented in the previous section. Once extending this study to the realistic case of three generations, the values reported in Tab. (9.3) has to be modified: for example, assuming that the same charges will be adopted for all the fermion generations, the numerical values in the table would have to be multiplied by a factor 3.

drawback, none of these ALP models provide a solution to the Strong CP problem: such a large mass would correspond to an explicit breaking of the shift symmetry, perturbing the QCD potential and preventing the classical solution of the QCD axion models [1, 5, 6, 8–11].

On the other hand, having f_a in the TeV region opens the possibility of direct searches of ALP signatures at present and future experimental facilities [17, 163, 185]. An ALP with mass $m_a \sim 1$ GeV will be considered in the following as an illustration.

For an ALP with a mass in the GeV region several constraints are present on its couplings to gauge bosons. Assuming that the ALP does not decay within the detector and therefore is treated as missing energy in data analyses, there are bounds from collider searches. In particular LEP data [192, 193] has been used to constrain ALP coupling to two photons [21] once the axion is produced through a virtual photon: the corresponding bound on the scale f_a reads

$$\frac{f_a}{|c_{a\gamma\gamma}|} \gtrsim 1 \text{ GeV} . \tag{9.12}$$

This bound may be improved by two order of magnitudes with dedicated analyses based on data from BaBar and from Belle-II [21, 59, 81]. Moreover, a similar sensitivity may be obtained considering the $\Upsilon(nS) \to \gamma +$ inv. decay [59, 194].

Studies on mono-W and mono-Z present LHC data [43] lead to

$$\frac{f_a}{|c_{aWW}|} \gtrsim 0.7 \text{ GeV} , \qquad \frac{f_a}{|c_{aZZ}|} \gtrsim 1.4 \text{ GeV} , \tag{9.13}$$

while LEP data [192, 193] on the radiative Z decays has been used to infer a bound on $a\gamma Z$ one [59]:

$$\frac{f_a}{|c_{a\gamma Z}|} \gtrsim 18 \text{ GeV} . \tag{9.14}$$

Future LHC sensitivity prospects on mono-W and mono-Z considering an integrated luminosity of 3000 fb^{-1} improve the first two bounds of an order of magnitude [43].

On the other side, rare meson decays provide strong constraints on the ALP coupling to two W's. In the case of an invisible ALP, the most stringent bounds arise from Belle limits on $\mathcal{B}(B \to K\nu\bar{\nu})$ [195]. By assuming that only c_{aWW} contributes, it leads to

$$\frac{f_a}{|c_{aWW}|} \gtrsim 10 \text{ GeV} . \tag{9.15}$$

Belle-II expected sensitivity improves this bound of approximately one order of magnitude [81, 196].

Finally, considering the ALP coupling to top and bottom quarks, B and Υ decays provide interesting bounds. Once considering that $B^+ \to K^+ a$ proceeds only via a loop diagram containing the c_{att} coupling, the bound that can be extracted from Belle data [195] for $m_a \approx 1$ GeV reads [83]

$$\frac{f_a}{|c_{att}|} \gtrsim 200 \text{ TeV} , \tag{9.16}$$

while Belle-II may improve this bound of a factor of 5. In general, both c_{aWW} and c_{att} contribute to this decay and may exist part of the parameter space where a cancellation take place, relaxing the bounds in Eqs. (9.15) and (9.16). As discussed in Ref. [83], this cancellation is possible only if both c_{aWW} and c_{att} are loop-induced: this is not the case in the models discussed here, where c_{att} is at tree-level.

Finally, data from BaBar [87, 89] and Belle [88] on $\Upsilon(ns) \to \gamma +$ inv. put bounds on $f_a/|c_{abb}|$, but they are sub-dominant with respect to the previous bound from B decays, reaching a sensitivity of a few TeV [194]: for 10 keV $\lesssim m_a \lesssim$ 5 GeV,

$$\frac{f_a}{|c_{abb}|} \gtrsim 2.5 \text{ TeV}\,, \tag{9.17}$$

Also for $\Upsilon(ns) \to \gamma +$ inv., in general, the branching ratio would depend on both c_{abb} and $c_{a\gamma\gamma}$: however, in the models considered here, $c_{a\gamma\gamma}$ is weighed by loop factors and then its contribution is negligible with respect to the one proportional to c_{abb} (for the generic analysis see Ref. [194]). For heavier ALPs, there are only very weak bounds from colliders or B-factories, that would allow $f_a/|c_{abb}|$ to be in the TeV range. On the other side, for lighter masses, $m_a \lesssim 10$ keV, much stronger bounds from stellar cooling data [197] are obtained:

$$\begin{aligned} \frac{f_a}{|c_{att}|} &\gtrsim 1.2 \times 10^6 \text{ TeV} \qquad \text{for the top} \\ \frac{f_a}{|c_{abb}|} &\gtrsim 6.1 \times 10^2 \text{ TeV} \qquad \text{for the bottom}\,. \end{aligned} \tag{9.18}$$

These constraints have been derived translating the existing bounds on axion coupling to electrons into constraints on the axion emission occurring via a top or bottom loop.

When the ALP decays within the detector, other observables need to be considered. Focussing on the radiative ALP decay, LEP data [192, 193] on the radiative Z decays can again be used to infer a bound on $a\gamma Z$ coupling [59]:

$$\frac{f_a}{|c_{a\gamma Z}|} \gtrsim 1.8 \text{ GeV}\,, \tag{9.19}$$

under the assumption that $\mathcal{B}(a \to \gamma\gamma) = 1$. These bounds may be improved by two order of magnitude with dedicated analyses both at B-factories and at LHC [21, 59, 81].

Although a decays dominantly into photons in the models considered here ($c_{a\gamma\gamma} > c_{agg}$), the coupling with gluons can provide interesting phenomenology and can be bounded considering the BaBar results on the branching ratio of $\Upsilon(2s, 3s) \to \gamma a(\to jj)$ [198]: for $m_a = 1$ GeV,

$$\frac{f_a}{|c_{agg}|} \gtrsim 80 \text{ GeV}\,. \tag{9.20}$$

This bound is expected to reach values of 0.2 TeV at Belle-II [23].

Finally, considering the ALP coupling with bottom quarks, data on $b \to sg$ or $b \to sq\bar{q}$ from CLEO collaboration [199] allows to put bound on $f_a/|c_{abb}|$ [61]: for 0.4 GeV $\lesssim m_a \lesssim$ 4.8 GeV,

$$\frac{f_a}{|c_{abb}|} \gtrsim 2 \text{ TeV}\,. \tag{9.21}$$

On the other side, $B^\pm \to K^\pm a(\to 2\gamma)$ decay, that could be studied at Belle-II, may be extremely useful to improve on these bound and will work as a test for the models presented here. Assuming that Belle-II reached a sensitivity of 10^{-6} on $\mathcal{B}(B \to K\gamma\gamma)$, strong bound can be inferred to aWW and att couplings: values of f_a as large as $|c_{aWW}| \times 60$ GeV and $|c_{att}| \times 300$ TeV could be probed.

To understand which bounds apply to the models listed above, the ALP decay length must be considered. The general formula is given by Eq. (8.45). For an ALP of $m_a \sim 1$ GeV, $f_a \sim 1$ TeV and typical momentum $|p_a| \sim 100$ GeV, the traveling

distance before decaying into two photons (the dominant channel as $|c_{a\gamma\gamma}| \gg |c_{agg}|$) is around $1/c_{a\gamma\gamma}^2$ m, that is in the interval 1 mm $-$ 0.1 m for $n_s = 1$, depending on the specific value of $c_{a\gamma\gamma}$ reported in Tab. 9.3. Therefore, all the ALPs described in the models $\mathcal{M}_{1-6}^{\pm}$ decay within the detector and the bounds in Eqs. (9.19)–(9.21) apply. The models $\mathcal{M}_7^{\pm}$, instead, predict vanishing ALP couplings with both photons and gluons and therefore these ALPs are stable at tree level for masses up to $\sim$ 10 GeV: for these models the bounds in Eqs. (9.12)-(9.17) apply.

Considering the explicit values of the axion coupling, taking $n_s = 1$, the strongest bounds on f_a for each model $\mathcal{M}_{1-6}^{\pm}$ read as follow:

$$\begin{aligned} &\mathcal{M}_1^{\pm} \longrightarrow f_a \gtrsim 4 \text{ TeV}\,, \qquad &&\mathcal{M}_2^{\pm} \longrightarrow f_a \gtrsim 6 \text{ TeV}\,, \\ &\mathcal{M}_3^{\pm} \longrightarrow f_a \gtrsim 8 \text{ TeV}\,, \qquad &&\mathcal{M}_4^{\pm} \longrightarrow f_a \gtrsim 6 \text{ TeV}\,, \\ &\mathcal{M}_5^{\pm} \longrightarrow f_a \gtrsim 4 \text{ TeV}\,, \qquad &&\mathcal{M}_6^{\pm} \longrightarrow f_a \gtrsim 2 \text{ TeV}\,. \end{aligned} \tag{9.22}$$

For all these cases, f_a can be in the TeV range, where the $SO(5)$ breaking mechanism is expected to occur.

On the other side, to summarise the most relevant constraints for $\mathcal{M}_7^{\pm}$, the plots in Fig. 9.1 are shown. As can be seen, pretty strong constraints are present for $m_a \lesssim 4.8$ GeV: in this case, $f_a \gtrsim 200$ TeV and therefore a mild tuning is present in the scalar potential of the models $\mathcal{M}_7^{\pm}$. For masses larger than this value, but up to 10 GeV the constraints are milder and $f_a \sim \mathcal{O}(1)$ TeV, avoiding any tuning in the scalar potential. The plots in Fig. 9.1 are computed taking into account the discussion of part ii for what concerns the bounds from the Υ meson decay.

Finally, it is possible to comment *a posteriori* on the assumed value for m_a. The ALP Lagrangian is written as an expansion in inverse powers of f_a, and for the EFT description to be meaningful, the ALP should be lighter than f_a. The benchmark scenario of $m_a = 1$ GeV enters in this range of values.

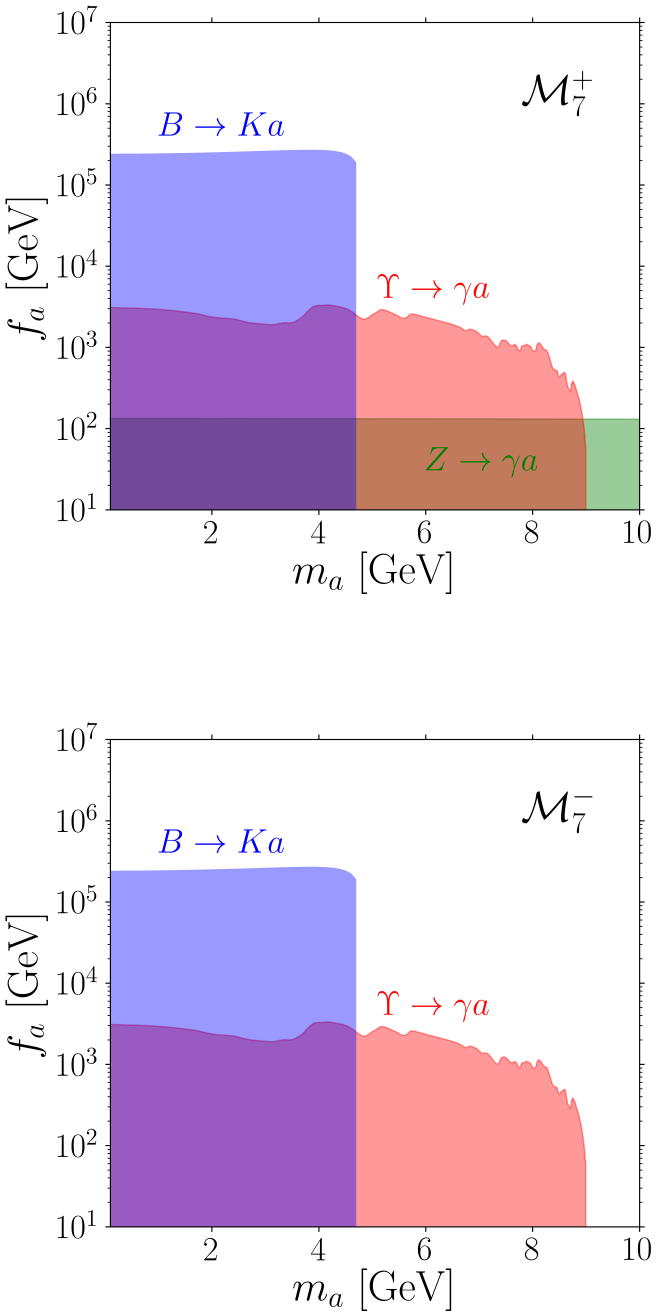

Figure 9.1: *Exclusions regions for the models $\mathcal{M}_7^{\pm}$. The blue region corresponds to the bound from $B^+ \to K^+ a$ in Eq. (9.16). The red region to the bound from $\Upsilon(ns) \to \gamma + \text{inv.}$ in Eq. (9.17). The green region to the collider bound from the radiative Z decay in Eq. (9.14). The latter does not apply to the $\mathcal{M}_7^-$ model because ALP only couples at tree level to bottom and top quarks.*

10 CONCLUSIONS

The AMLσM [145] represents a class of models that extend the MLσM [24] by the introduction of a complex scalar singlet, that allows to supplement the $SO(5)$ and EW symmetries with an extra $U(1)_{\rm PQ}$.

The spectrum of the AMLσM encodes: i) the SM gauge bosons and fermions; ii) three real scalar dofs, one of them, the Higgs particle, being the only uneaten GB of the $SO(5)/SO(4)$ breaking; iii) two types of vectorial exotic fermions respectively in the fundamental and in the singlet representation of $SO(5)$; iv) the PQ GB originated by the spontaneous breaking of the $U(1)_{\rm PQ}$ symmetry. The scale f of the $SO(5)/SO(4)$ breaking is expected to be in the TeV region, in order to solve the Higgs hierarchy problem, while the PQ–breaking scale, f_s, is in principle independent from f, spanning over a large range of values.

A detailed analysis of the scalar potential and its minima has been presented. The appearance of possible $SO(5)$ and PQ explicit breaking terms arising from 1-loop fermionic and gauge contributions has been extensively discussed. The type and number of the additional terms required by renormalisability depends on the PQ charges assigned to the fields of the model.

A minimal AMLσM has been identified by introducing few general requirements with the intent to minimize the number of parameters in the whole Lagrangian. In particular, the parameter space of the minimal AMLσM scalar sector is determined by 7 parameters. Two of them can be fixed by identifying one scalar dof with the physical Higgs particle and its VEV with the EW scale. The remaining free parameters correspond to: the quartic couplings λ and λ_s that control the linearity of the EWSB and the PQ symmetry breaking mechanisms, respectively; the scales f and f_s related to the symmetry breaking; the mixed quartic coupling $\lambda_{s\phi}$ that represents the portal between the EW and PQ sectors. Simplified analytical expressions can be obtained for the scalar sector by integrating out the highest mass dof, either in the strongly interacting regime, $\lambda_s \gg 1$, keeping free the scales f_s and f either in the perturbative regime, $\lambda_s \lesssim 1$, but assuming instead a large hierarchy between the scales, $f_s \gg f$. Interesting analytical expression for the scalar sector in the regime $f_s \sim f$ can be obtained also in the limit $\beta, \lambda_{s\phi} \ll 1$.

The analytical and numerical analysis of the parameter space points out that for f, $f_s \gtrsim 1$ TeV the heavier scalar dofs are unlikely to give signals at the present and future LHC run, while only the non-linearity of the EWSB mechanism would lead to interesting deviations from the SM predictions in Higgs and gauge boson sectors.

The analysis of the PQ GB phenomenology reveals two possible scenarios: a light QCD axion or a heavy ALP. In the first case, the axion mass is expected in the range [meV, keV] and the strong bounds present on the axion coupling to two photons require that its characteristic scale $f_a \sim f_s$ must be larger than 10^5 TeV, strongly suppressing all its interactions. This model represents a minimal invisible axion construction, where the EWSB mechanism is non-linearly realised and the physical Higgs particle arises as a GB. As can be realised from Eqs. (8.6)-(8.25), invisible axion models are, in general, strongly fine-tuned. In fact, the typical $SO(5)/SO(4)$ breaking scale of the effective theory obtained integrating out the heavy degrees of freedom "naturally runs" to the highest scale, $f_R \sim f_s$, reintroducing the EW hierarchy problem, $\xi \ll 1$. Alternatively, the tuning $\lambda_{s\phi} = 0$ can be introduced: this is, however, rather unnatural as no symmetry protects it.

In the second scenario, the ALP typically has a much larger mass, independent from the value of its characteristic scale. The benchmark $m_a = 1\,\text{GeV}$ and $f_s = 200\,\text{TeV}$ has been considered for concreteness. Such an ALP would be free from the strong bounds on $a\gamma\gamma$ and it is likely to be detected at LHC, the best sensitivity being on the aWW and aZZ couplings, while no signals are expected in flavour observables such as meson decays.

From the numerical analysis of the scalar potential it comes out clearly that the strong bounds on axion/ALP couplings to photons and electrons imply very high values for the PQ breaking scale f_a. This represents the origin of a hierarchy problem present in most of the axion models: the quartic coupling in the potential between the Higgs field and the complex scalar field, associated to the axion, can be hardly ever prevented by symmetry arguments. As a consequence, avoiding fine-tuning among parameters, any other energy scale tends to be close to f_a. To try to solve this problem, differently from the first version of the AMLσM, the $SO(5)$ breaking scale and the PQ one are taken to be equal ($f_s \equiv f$). After adding this condition to the minimality requirements, seven possible scenarios have been identified.

For ALPs with masses larger than $10\,\text{MeV}$, the aforementioned astrophysical bounds on couplings to photons and electrons are avoided. For concreteness, a mass of $1\,\text{GeV}$ has been considered. This value is within the expected range of values for an ALP, that naturally has a mass larger than Λ_{QCD} but smaller then f_a. In six of the models, the ALP decays within the detector and the most relevant bounds come from CLEO: they can be translated into constraints of the scale of the ALP, $f_a \gtrsim 2 \div 8\,\text{TeV}$. For the seventh model, the ALP does not decay and the strongest constraints arise from $B^+ \to K^+ a$ decay, the radiative Υ decay and collider analysis on radiative Z decay: in this case, for ALP with masses up to $4.5\,\text{GeV}$, $f_a = f \sim 200\,\text{TeV}$, while for larger masses up to $\sim 10\,\text{GeV}$ much weaker bounds are present and $f_a = f \sim \mathcal{O}(1)\,\text{TeV}$. Therefore, in all the realisations presented, the PQ and $SO(5)$ breaking scales can satisfy to $f_a = f \approx \mathcal{O}(1)\,\text{TeV}$ and then these models have the possibilities to be tested soon both at colliders and at Belle-II (the only exception is $\mathcal{M}_7^{\pm}$ and for ALP masses up to $\sim 4.8\,\text{GeV}$). In conclusion, these are testable and natural AMLσM, free from any fine-tuning in the scalar potential, and where the typical hierarchy problem that affects axion and ALP models is avoided.

Part IV

GENERAL CONCLUSIONS

11 GENERAL CONCLUSIONS

The scope of this thesis work is to investigate some particular aspects of ALP models, both from an experimental and theoretical point of view. In part i the axion mechanism and its peculiarities are revised, integrating with a more general perspective on ALPs and on the different effective approaches commonly used in this context. In part ii we revisited the production of ALPs at B-factories via the process $e^+e^- \to \gamma a$. To this purpose, the relevant cross-section is computed via an effective Lagrangian, described in chap. 3, with simultaneous ALP couplings to b-quarks and photons. The interference between the two decay channels for the Υ meson is computed for the first time. We noticed that this interference can be destructive, creating an unconstrained flat-direction in the parameter space. While the non-resonant contribution is always dominant, the resonant contribution is shown to be relevant for experiments operating at $\sqrt{s} = m_{\Upsilon(nS)}$, with $n = 1, 2, 3$. On the other side, only the non-resonant component of the cross-section is relevant at the $\Upsilon(4S)$ resonance. These effects imply that the experimental searches performed at different Υ resonances can be sensitive to complementary combinations of ALP couplings. To show this result, constraints from existing Babar and Belle data on ALPs decaying into invisible final states are computed, and the prospects for the Belle-II experiment are discussed.

In part iii we focus on a specific model-building case, creating an environment where an axion/ALP can arise consistently from a composite Higgs scenario. The minimal $SO(5)/SO(4)$ linear σ model is extended including an additional complex scalar field, singlet under the global $SO(5)$ and the SM gauge symmetries. This scalar field creates the conditions to generate a KSVZ-like axion, providing a solution to the strong-CP problem, or an ALP. Different choices for the PQ charges are possible and lead to physically distinct Lagrangians. For consistency reasons, we studied the scalar potential describing $SO(5) \to SO(4)$, electroweak and PQ symmetry breaking. A single minimal scenario is identified and the associated scalar potential is minimised including counter-terms needed to ensure one-loop renormalizability. In the allowed parameter space, we illustrated some phenomenological features of the scalar degrees of freedom, of the exotic fermions and of the axion/ALP. We noticed that, in this framework, an axion model consistent with the experimental bounds would require a scale larger than $\sim 10^8$ GeV. However, from the analysis of the potential clearly emerges that such a large scale unavoidably affects the Higgs potential. Therefore, within this context, every QCD axion model of this type is fine-tuned. A possible way-out is described at the end of part iii. Considering just ALPs, a viable and natural solution can be identified in the case where the PQ breaking scale and the compositeness scale coincide ($f_s \approx f$). The parameter space of the model is bounded using the prescriptions discussed in part ii.

11.1 FUTURE PROSPECTS

The phenomenological study of more general scenarios, where the ALP can decay visibly into SM particles as well as displaced vertices, is the target of future works. Concerning B-factories, we are considering both the cases of ALP production via $\Upsilon(nS)$ decay and rare mesons decay such $B \to Ka$ and $K \to \pi a$. The most interesting final state is the 3γ, where the ALP disintegrates into two photos, and the first data about this final state are soon to be revealed by the Belle-II collaboration. Many

other possible final states can be introduced, letting the ALP decay for example into a pair of leptons or into two jets, and the interplay between these different searches can be useful to tighten the allowed parameter space. However, including all these new couplings means adding more free parameters to our model and, as a consequence, some assumptions on the underlying UV structure must be considered. On a mid-term perspective, the target is to enlarge the analysis to collider experiments, such as LHCb, CMS and ATLAS. Even though the couplings with the SM model vector bosons are widely studied at the LHC, the coupling with fermions and the interplay between them is still an unexplored field.

I had the possibility to contribute to some other projects during my PhD. One is the paper "Setting Limits on EFT: the case of Dark Matter" [200], whose target is to develop a new statistical tool to study effective field theories at collider, where the energy cut-off of the model is unknown. Now I am currently collaborating for a project called "*the flavour of the invisible universe*", whose target is to study how a lepto-quark can act as a portal to a dark sector and how it impacts the cosmological and astrophysical observables like the relic density or the gamma ray bursts. These topic were intentionally left outside this work because of their incompatibility with the main topic of the thesis.

APPENDIX

AXION LAGRANGIAN

The axion or ALP Lagrangian in the basis where axion-fermion couplings are only derivative is given by

$$\mathcal{L}_a = -\frac{\partial_\mu a}{2f_a}\left[\Delta_\psi \bar{\psi}\gamma^\mu\psi + \Delta_\chi \bar{\chi}\gamma^\mu\chi + \Delta_{\psi'}\bar{\psi}'\gamma^\mu\psi' + \Delta_{\chi'}\bar{\chi}'\gamma^\mu\chi' + \Delta_t \bar{t}\gamma^\mu t + \Delta_b \bar{b}\gamma^\mu b\right]. \tag{A.1}$$

The axion or ALP couplings with gauge bosons arise due to the anomalous nature of the PQ symmetry. They can be read out in the following effective Lagrangian that encodes the traditional 1-loop contributions of all the fermions:

$$\begin{aligned}
\delta\mathcal{L}_a^{\text{eff}} \supset & -\frac{\alpha_s}{8\pi}\left[5\left(\Delta_\psi + \Delta_{\psi'}\right) + \Delta_\chi + \Delta_{\chi'} + \Delta_t + \Delta_b\right] G_{\mu\nu}\widetilde{G}^{\mu\nu} + \\
& - \frac{\alpha_{em}}{8\pi}\left[6\Delta_\psi\left(1 + 2\left(Y_K^2 + Y_Q^2\right) + Y_{T_5}^2\right) + 6\Delta_{\psi'}\left(1 + 2\left(Y_{K'}^2 + Y_{Q'}^2\right) + Y_{B_5}^2\right) + \right. \\
& \left. + 6\left(\Delta_\chi Y_{T_1}^2 + \Delta_{\chi'} Y_{B_1}^2\right) + 6\left(\Delta_t Y_{t_R}^2 + \Delta_b Y_{b_R}^2\right)\right] F_{\mu\nu}\widetilde{F}^{\mu\nu} + \\
& - \frac{\alpha_{em}}{8\pi}\frac{6}{\sin^2\theta_W}\left[2\left(\Delta_\psi + \Delta_{\psi'}\right) + \frac{\Delta_t + \Delta_b}{4}\right] W_{\mu\nu}^+ \widetilde{W}^{-\mu\nu} + \\
& - \frac{\alpha_{em}}{8\pi}\left[6\Delta_\psi\left(\frac{1}{\tan^2\theta_W} + \tan^2\theta_W\left(2\left(Y_K^2 + Y_Q^2\right) + Y_{T_5}^2\right)\right) + 6\Delta_\chi \tan^2\theta_W Y_{T_1}^2 + \right. \\
& + 6\Delta_{\psi'}\left(\frac{1}{\tan^2\theta_W} + \tan^2\theta_W\left(2\left(Y_{K'}^2 + Y_{Q'}^2\right) + Y_{B_5}^2\right)\right) + 6\Delta_{\chi'}\tan^2\theta_W Y_{B_1}^2 + \\
& \left. + 3\frac{\Delta_t + \Delta_b}{4}\left(\frac{1}{\tan^2\theta_W} - \tan^2\theta_W\right) + 6\tan^2\theta_W\left(\Delta_t Y_t^2 + \Delta_b Y_b^2\right)\right] Z_{\mu\nu}\widetilde{Z}^{\mu\nu} + \\
& - \frac{\alpha_{em}}{8\pi}\left[12\Delta_\psi\left(\frac{1}{\tan\theta_W} - \tan\theta_W\left(2\left(Y_K^2 + Y_Q^2\right) + Y_{T_5}^2\right)\right) - 12\tan\theta_W\Delta_\chi Y_{T_1}^2 + \right. \\
& + 12\Delta_{\psi'}\left(\frac{1}{\tan\theta_W} - \tan\theta_W\left(2\left(Y_{K'}^2 + Y_{Q'}^2\right) + Y_{B_5}^2\right)\right) - 12\tan\theta_W\Delta_{\chi'}Y_{B_1}^2 + \\
& \left. + 3\frac{\Delta_t + \Delta_b}{2}\left(\frac{1}{\tan\theta_W} + \tan\theta_W\right) - 12\tan\theta_W\left(\Delta_t Y_t^2 + \Delta_b Y_b^2\right)\right] F_{\mu\nu}\widetilde{Z}^{\mu\nu}.
\end{aligned} \tag{A.2}$$

In the previous expression, Δ_f are defined in Eqs. (9.7), (9.8) and (9.9), while n_f is the PQ charge of the generic field f that are reported for simplicity in Tab. A.1.

$\mathcal{M}_1^+$	$n_{\psi_L} = n_{\chi_R} = n_{\psi_R} = n_{\chi_L} - n_s = n_{q_L} = n_{t_R} - 2n_s = n_{\psi'_L} = n_{\chi'_R} = n_{\psi'_R} = n_{\chi'_L} - n_s = n_{b_R} - 2n_s$
$\mathcal{M}_1^-$	$n_{\psi_L} = n_{\chi_R} = n_{\psi_R} = n_{\chi_L} - n_s = n_{q_L} = n_{t_R} - 2n_s = n_{\psi'_L} = n_{\chi'_R} = n_{\psi'_R} = n_{\chi'_L} + n_s = n_{b_R} + 2n_s$
$\mathcal{M}_2^+$	$n_{\psi_L} = n_{\chi_R} = n_{\psi_R} = n_{\chi_L} - n_s = n_{q_L} + n_s = n_{t_R} - 2n_s = n_{\psi'_L} = n_{\chi'_R} = n_{\psi'_R} = n_{\chi'_L} - n_s = n_{q_L} + n_s = n_{b_R} - 2n_s$
$\mathcal{M}_2^-$	$n_{\psi_L} = n_{\chi_R} = n_{\psi_R} = n_{\chi_L} - n_s = n_{q_L} + n_s = n_{t_R} - 2n_s = n_{\psi'_L} + 2n_s = n_{\chi'_R} + 2n_s = n_{\psi'_R} + 2n_s = n_{\chi'_L} + 3n_s = n_{b_R} + 4n_s$
$\mathcal{M}_3^+$	$n_{\psi_L} = n_{\chi_R} = n_{\psi_R} + n_s = n_{\chi_L} - n_s = n_{q_L} + 2n_s = n_{t_R} - 2n_s = n_{\psi'_L} = n_{\chi'_R} = n_{\psi'_R} + n_s = n_{\chi'_L} - n_s = n_{b_R} - 2n_s$
$\mathcal{M}_3^-$	$n_{\psi_L} = n_{\chi_R} = n_{\psi_R} + n_s = n_{\chi_L} - n_s = n_{q_L} + 2n_s = n_{t_R} - 2n_s = n_{\psi'_L} + 4n_s = n_{\chi'_R} + 4n_s = n_{\psi'_R} + 3n_s = n_{\chi'_L} + 5n_s = n_{b_R} + 6n_s$
$\mathcal{M}_4^+$	$n_{\psi_L} = n_{\chi_R} = n_{\psi_R} + n_s = n_{\chi_L} - n_s = n_{q_L} + n_s = n_{t_R} - 2n_s = n_{\psi'_L} = n_{\chi'_R} = n_{\psi'_R} + n_s = n_{\chi'_L} - n_s = n_{b_R} - 2n_s$
$\mathcal{M}_4^-$	$n_{\psi_L} = n_{\chi_R} = n_{\psi_R} + n_s = n_{\chi_L} - n_s = n_{q_L} + n_s = n_{t_R} - 2n_s = n_{\psi'_L} + 2n_s = n_{\chi_R} + 2n_s = n_{\psi_R} + n_s = n_{\chi_L} + 3n_s = n_{b_R} + 4n_s$
$\mathcal{M}_5^+$	$n_{\psi_L} = n_{\chi_R} = n_{\psi_R} + n_s = n_{\chi_L} - n_s = n_{q_L} = n_{t_R} - 2n_s = n_{\psi'_L} = n_{\chi'_R} = n_{\psi'_R} + n_s = n_{\chi'_L} - n_s = n_{b_R} - 2n_s$
$\mathcal{M}_5^-$	$n_{\psi_L} = n_{\chi_R} = n_{\psi_R} + n_s = n_{\chi_L} - n_s = n_{q_L} = n_{t_R} - 2n_s = n_{\psi'_L} = n_{\chi'_R} = n_{\psi'_R} - n_s = n_{\chi'_L} + n_s = n_{b_R} + 2n_s$
$\mathcal{M}_6^+$	$n_{\psi_L} = n_{\chi_R} = n_{\psi_R} - n_s = n_{\chi_L} - n_s = n_{q_L} - n_s = n_{t_R} - 2n_s = n_{\psi'_L} = n_{\chi'_R} = n_{\psi'_R} - n_s = n_{\chi'_L} - n_s = n_{b_R} - 2n_s$
$\mathcal{M}_6^-$	$n_{\psi_L} = n_{\chi_R} = n_{\psi_R} - n_s = n_{\chi_L} - n_s = n_{q_L} - n_s = n_{t_R} - 2n_s = n_{\psi'_L} - 2n_s = n_{\chi'_R} - 2n_s = n_{\psi'_R} - n_s = n_{\chi'_L} - n_s = n_{b_R}$
$\mathcal{M}_7^+$	$n_{\psi_L} = n_{\chi_R} = n_{\psi_R} = n_{\chi_L} - n_s = n_{q_L} - n_s = n_{t_R} - 2n_s = n_{\psi'_L} = n_{\chi'_R} = n_{\psi'_R} = n_{\chi'_L} - n_s = n_{b_R} - 2n_s$
$\mathcal{M}_7^-$	$n_{\psi_L} = n_{\chi_R} = n_{\psi_R} = n_{\chi_L} - n_s = n_{q_L} - n_s = n_{t_R} - 2n_s = n_{\psi'_L} - 2n_s = n_{\chi'_R} - 2n_s = n_{\psi'_R} - 2n_s = n_{\chi'_L} - n_s = n_{b_R}$

Table A.1: *Definition of all the models in terms of the PQ charges of the fields as a function of* n_s.

B

$\Upsilon(nS)$ DECAY

In this appendix the full computation of the $\Upsilon(nS) \to \gamma a$ branching ratio in Eq. (4.15) is presented. The starting point is the effective Lagrangian in Eq. (4.3), using the results in [58, 100] as benchmarks for everything that concerns assumptions and techniques. The computation will be split into three sections: the first and the second will regard the single channels, proportional to $g_{a\gamma\gamma}$ and g_{abb} alone, while in the last section the interference term between the two contribution will be computed.

B.1 PHOTONIC CHANNEL

In this section the contribution to the $\Upsilon(nS) \to \gamma a$ branching ratio due to the ALP-photon coupling will be presented (diagram in Fig. B.1).

The amplitude of the process is the following:

$$i\mathcal{M}_{\gamma\gamma} = \frac{e}{3}\langle 0|\bar{b}\gamma_\rho b|\Upsilon(p)\rangle \left(-i\frac{\eta^{\rho\nu}}{q^2}\right) i\, g_{a\gamma\gamma}\, \epsilon_{\mu\nu\alpha\beta} q^\mu \epsilon^\beta(k) k^\alpha \,, \tag{B.1}$$

where p,q,k are respectively the momenta of the Υ meson (for momentum-energy conservation $q \equiv p$), the internal photon and the external photon. The anti-symmetric tensor is conventionally defined by $\epsilon_{1230} = +1$. The expression inside the bra-ket contains the non-perturbative QCD part of the amplitude and can be parametrised as:

$$\langle 0|\bar{b}\gamma_\rho b|\Upsilon(p)\rangle \equiv m_\Upsilon f_\Upsilon e_\rho(p) \,, \tag{B.2}$$

where f_Υ is the Υ decay constant and $e^\mu(p)$ is the polarisation vector (not to confuse with the polarisation $\epsilon^\beta(k)$ of the outgoing photon). After this parametrisation, the amplitude takes the form:

$$i\mathcal{M}_{\gamma\gamma} = \frac{e}{3} f_\Upsilon m_\Upsilon \frac{f_\Upsilon m_\Upsilon}{q^2}\, g_{a\gamma\gamma}\, \epsilon_{\mu\nu\alpha\beta} q^\mu e^\nu(q) k^\alpha \epsilon^\beta(k) \,. \tag{B.3}$$

After averaging on the initial state and summing on the possible final states the result is:

$$\begin{aligned}\frac{1}{3}\overline{|\mathcal{M}_{\gamma\gamma}|}^2 &= \frac{1}{3}\frac{e^2}{9}\left(\frac{f_\Upsilon m_\Upsilon}{q^2}\right)^2 g_{a\gamma\gamma}^2\, \epsilon_{\mu\nu\alpha\beta}\epsilon_{\mu'\nu'\alpha'\beta'} q^\mu k^\alpha q^{\mu'} k^{\alpha'} \times \\ &\quad \times \left(-\eta^{\beta\beta'}\right)\left(-\eta^{\nu\nu'} + \frac{q^\nu q^{\nu'}}{q^2}\right) \\ &= -\frac{2}{27}e^2\left(\frac{f_\Upsilon m_\Upsilon}{q^2}\right)^2 g_{a\gamma\gamma}^2\, q^\mu k^\alpha q^{\mu'} k^{\alpha'} (\delta_{\alpha\alpha'}\delta_{\mu\mu'} - \delta_{\alpha\mu'}\delta_{\mu\alpha'}) \,,\end{aligned} \tag{B.4}$$

where we enforced the anti-simmetry of the Levi-Civita tensor $\epsilon_{\mu\nu\alpha\beta} q^\mu q^\nu = 0$ and the contraction between two completely anti-symmetric tensors

$$\epsilon_{\beta\nu\alpha\mu}\epsilon^{\beta\nu}{}_{\alpha'\mu'} = -2\left(\delta_{\alpha\alpha'}\delta_{\mu\mu'} - \delta_{\alpha\mu'}\delta_{\mu\alpha'}\right) \,. \tag{B.5}$$

The expression for the amplitude is obtained contracting the indices:

$$\frac{1}{3}\overline{|\mathcal{M}_{\gamma\gamma}|}^2 = \frac{2}{27}e^2\left(\frac{f_\Upsilon m_\Upsilon}{q^2}\right)^2 g_{a\gamma\gamma}^2\, (q\cdot k)^2 \,, \tag{B.6}$$

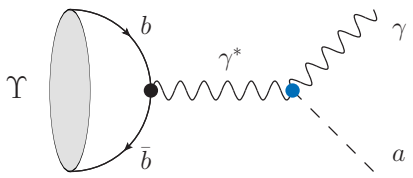

Figure B.1: *Diagrams of the photon channel of the process* $\Upsilon(nS) \to \gamma a$.

reminding that $k^2 = 0$ and $q^2 = m_\Upsilon^2$. In the rest frame of the $\Upsilon(nS)$ meson

$$q \cdot k = \frac{m_\Upsilon^2 - m_a^2}{2}\,, \tag{B.7}$$

so the expression of partial decay width is:

$$\begin{aligned}\Gamma(\Upsilon \to \gamma a)_{\text{bos}} &= \frac{1}{16\pi m_\Upsilon^3}\left(m_\Upsilon^2 - m_a^2\right)\frac{1}{3}\overline{|\mathcal{M}_{\gamma\gamma}|}^2 \\ &= \frac{\alpha_{\text{em}}}{216} m_\Upsilon f_\Upsilon^2 g_{a\gamma\gamma}^2 \left(1 - \frac{m_a^2}{m_\Upsilon^2}\right)^3 .\end{aligned} \tag{B.8}$$

B.2 FERMIONIC CHANNEL

The diagrams in Fig. B.2 represent the fermionic channel for the decay of the Υ meson. Differently from the previous case, some quite strong assumptions are required to deal with the non-perturbative QCD part of the amplitude. The expression is a bit more complicated:

$$i\mathcal{M}_{bb} = 2\frac{e}{3} m_b\, g_{abb}\, \epsilon^\beta(k) \langle 0|\bar{b}(p_2)\gamma_5 \frac{\not{p}_1 - \not{k} + m_b}{(p_1 - k)^2 - m_b^2}\gamma_\beta b(p_1)|\Upsilon(p)\rangle \tag{B.9}$$

where the presence of two diagrams is represented by the factor of 2 in the front.

The first assumption consists in considering a non-relativistic framework, so that the momenta of the two b quarks are approximately half of the momentum of the Υ and m_Υ is twice the mass of the b quark:

$$p_1 = p_2 \simeq \frac{p}{2}, \qquad m_\Upsilon \simeq 2m_b\,. \tag{B.10}$$

The approximate amplitude reads:

$$i\mathcal{M}_{bb} = -\frac{e}{3} m_\Upsilon\, g_{abb}\, \epsilon^\beta(k) \frac{\left(\frac{p}{2} - k\right)^\nu}{p \cdot k} \langle 0|\bar{b}(p_2)\gamma_5\gamma_\nu\gamma_\beta b|\Upsilon(p)\rangle\,. \tag{B.11}$$

The term in Eq. (B.9) proportional to the quark mass vanishes for parity reasons. A dedicated discussion is necessary to treat the non-perturbative part. A useful property of the gamma matrices is the following:

$$\gamma_5\gamma_\nu\gamma_\beta = \gamma_5\eta_{\nu\beta} + \frac{1}{2}\epsilon_{\nu\beta\alpha\rho}\sigma^{\alpha\rho}\,. \tag{B.12}$$

Again, for parity reasons, the term proportional to γ_5 is forbidden so, after replacing the expression of Eq. (B.12) into the non-perturbative term, we get:

$$\frac{1}{2}\langle 0|\bar{b}\sigma^{\alpha\rho}b|\Upsilon(p)\rangle \equiv \frac{1}{2} f_\Upsilon^T \left(e^\alpha(p)p^\rho - e^\rho(p)p^\alpha\right)\,, \tag{B.13}$$

where $e^\alpha(p)$ is the polarisation vector of the Υ meson and f_Υ^T is the tensorial decay constant. Within the non-relativistic approach considered here, it is reasonable to

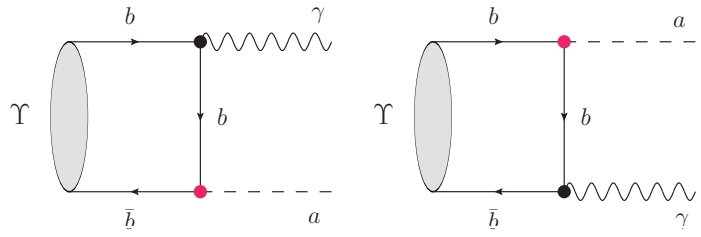

Figure B.2: *Diagrams of the fermionic channel of the process* $\Upsilon(nS) \to \gamma a$.

consider $f_\Upsilon^T \simeq f_\Upsilon$. However, for a more precise computation, f_Υ^T should be properly evaluated on the lattice. The final form of the amplitude is:

$$i\mathcal{M}_{bb} = -\frac{e}{6} m_\Upsilon f_\Upsilon \, g_{abb} \, \epsilon^\beta(k) \frac{\left(\frac{p}{2}-k\right)^\nu}{p\cdot k} \left(e^\alpha(p)p^\rho - e^\rho(p)p^\alpha\right)\epsilon_{\nu\beta\alpha\rho} \,. \quad \text{(B.14)}$$

Squaring the amplitude and using the anti-symmetric properties of the Levi-Civita tensor one gets:

$$\begin{aligned}\mathcal{M}_{bb} = \frac{e^2}{9} m_\Upsilon^2 f_\Upsilon^2 \, g_{abb}^2 \, \frac{1}{(p\cdot q)^2} p^\nu p^{\nu'} \left(\frac{p}{2}-k\right)^\alpha \left(\frac{p}{2}-k\right)^{\alpha'} \times \\ \times \, \epsilon^\beta(k)\epsilon^{\beta'}(k) e^\mu(p) e^{\mu'}(p) \epsilon_{\mu\nu\alpha\beta}\epsilon_{\mu'\nu'\alpha'\beta'} \,,\end{aligned} \quad \text{(B.15)}$$

The computation is similar to the previous case, so, averaging and summing:

$$\frac{1}{3}\overline{|\mathcal{M}_{bb}|}^2 = \frac{2}{27} e^2 m_\Upsilon^2 f_\Upsilon^2 \, g_{abb}^2 \,. \quad \text{(B.16)}$$

In the Υ rest frame the fermionic partial decay width is:

$$\Gamma(\Upsilon \to \gamma a)_{\text{ferm}} = \frac{\alpha_{\text{em}}}{54} m_\Upsilon f_\Upsilon^2 \, g_{abb}^2 \left(1 - \frac{m_a^2}{m_\Upsilon^2}\right) \quad \text{(B.17)}$$

B.3 INTERFERENCE TERM

The last piece to complete the computation of the branching ratio in Eq. (4.15) is the interference between the two channels. The starting point is the combination of Eq. (B.3) and Eq. (B.14). The interference amplitude is:

$$\begin{aligned}\mathcal{M}_{\text{int}}^2 &= \mathcal{M}_{bb}^\dagger \mathcal{M}_{\gamma\gamma} + \mathcal{M}_{\gamma\gamma}^\dagger \mathcal{M}_{bb} = \\ &= \frac{e^2}{9} m_\Upsilon f_\Upsilon^2 \, g_{a\gamma\gamma} \, g_{abb} \, \frac{q^\mu}{q^2} k^\alpha \frac{\left(\frac{p}{2}-k\right)^{\alpha'}}{p\cdot k} \epsilon_{\mu'\nu'\alpha'\beta'}\epsilon_{\mu\nu\alpha\beta} \times \\ &\quad \times \, \epsilon^\beta(k)\epsilon^{\beta'}(k) e^\nu(q) \left(e^{\mu'}(p)p^{\nu'} - e^{\nu'}(p)p^{\mu'}\right) \,.\end{aligned} \quad \text{(B.18)}$$

Remembering that $q \equiv p$, $q^2 = m_\Upsilon^2$ and using the anti-symmetric properties of the tensor structure we get:

$$\begin{aligned}\mathcal{M}_{\text{int}}^2 = \frac{e^2}{9} f_\Upsilon^2 \, g_{a\gamma\gamma} \, g_{abb} \, p^\mu k^\alpha \frac{\left(\frac{p}{2}-k\right)^{\alpha'}}{p\cdot k} \times \\ \times \, \epsilon_{\mu'\nu'\alpha'\beta'}\epsilon_{\mu\nu\alpha\beta} 2\epsilon^\beta(k)\epsilon^{\beta'}(k) e^\nu(p) e^{\mu'}(p) p^{\nu'} \,.\end{aligned} \quad \text{(B.19)}$$

The computation here is very similar to the previous cases, so the averaged amplitude is:

$$\frac{1}{3}\overline{\mathcal{M}_{\text{int}}^2} = -\frac{4}{27} e^2 f_\Upsilon^2 \, g_{a\gamma\gamma} \, g_{abb} \, p\cdot k \,. \quad \text{(B.20)}$$

The last step consists in putting together the three amplitude components:

$$|\mathcal{M}_{\text{tot}}|^2 = |\mathcal{M}_{\gamma\gamma}|^2 + |\mathcal{M}_{bb}|^2 + \mathcal{M}_{bb}^\dagger \mathcal{M}_{\gamma\gamma} + \mathcal{M}_{\gamma\gamma}^\dagger \mathcal{M}_{bb}\,. \tag{B.21}$$

After averaging and summing:

$$\begin{aligned}\frac{1}{3}\overline{|\mathcal{M}_{\text{tot}}|}^2 &= \frac{e^2}{54} f_\Upsilon^2 m_\Upsilon^2 \left[4\, g_{abb}^2 - 4\, g_{a\gamma\gamma}\, g_{abb} \left(1 - \frac{m_a^2}{m_\Upsilon^2}\right) + g_{a\gamma\gamma}^2 \left(1 - \frac{m_a^2}{m_\Upsilon^2}\right)^2\right] \\ &= \frac{e^2}{54} f_\Upsilon^2 m_\Upsilon^2 \left[g_{a\gamma\gamma} \left(1 - \frac{m_a^2}{m_\Upsilon^2}\right) - 2\, g_{abb}\right]^2 ,\end{aligned} \tag{B.22}$$

where we moved into the Υ rest frame. The formula in Eq. (4.15) now is obtained simply by plugging the amplitude into the decay width formula:

$$\begin{aligned}\Gamma(\Upsilon \to \gamma a)_{\text{tot}} &= \frac{1}{16\pi m_\Upsilon^3} (m_\Upsilon^2 - m_a^2) \frac{1}{3} \overline{|\mathcal{M}_{\text{tot}}|}^2 \\ &= \frac{\alpha_{\text{em}}}{216} m_\Upsilon f_\Upsilon^2 \left(1 - \frac{m_a^2}{m_\Upsilon^2}\right) \left[g_{a\gamma\gamma} \left(1 - \frac{m_a^2}{m_\Upsilon^2}\right) - 2\, g_{abb}\right]^2 .\end{aligned} \tag{B.23}$$

COLOPHON

This document was typeset using the typographical look-and-feel classicthesis developed by André Miede. The style was inspired by Robert Bringhurst's seminal book on typography "*The Elements of Typographic Style*". classicthesis is available for both LaTeX and LyX:

http://code.google.com/p/classicthesis/

Happy users of classicthesis usually send a real postcard to the author, a collection of postcards received so far is featured here:

http://postcards.miede.de/

Final Version as of January 13, 2020 (classicthesis version 1.0).

BIBLIOGRAPHY

[1] R. D. Peccei and H. R. Quinn, *"CP Conservation in the Presence of Instantons"*, Phys. Rev. Lett. 38, 1440 (1977).

[2] T. Schäfer and E. V. Shuryak, *"Instantons in QCD"*, Rev. Mod. Phys. 70, 323 (1998), hep-ph/9610451.

[3] R. J. Crewther, P. Di Vecchia, G. Veneziano and E. Witten, *"Chiral Estimate of the Electric Dipole Moment of the Neutron in Quantum Chromodynamics"*, Phys. Lett. 88B, 123 (1979), [Erratum: Phys. Lett.91B,487(1980)].

[4] J. M. Pendlebury et al., *"Revised experimental upper limit on the electric dipole moment of the neutron"*, Phys. Rev. D92, 092003 (2015), arXiv:1509.04411.

[5] F. Wilczek, *"Problem of Strong P and T Invariance in the Presence of Instantons"*, Phys. Rev. Lett. 40, 279 (1978).

[6] S. Weinberg, *"A New Light Boson?"*, Phys. Rev. Lett. 40, 223 (1978).

[7] E. M. Riordan et al., *"A Search for Short Lived Axions in an Electron Beam Dump Experiment"*, Phys. Rev. Lett. 59, 755 (1987).

[8] J. E. Kim, *"Weak Interaction Singlet and Strong CP Invariance"*, Phys. Rev. Lett. 43, 103 (1979).

[9] M. A. Shifman, A. I. Vainshtein and V. I. Zakharov, *"Can Confinement Ensure Natural CP Invariance of Strong Interactions?"*, Nucl. Phys. B166, 493 (1980).

[10] M. Dine, W. FisCHLer and M. Srednicki, *"A Simple Solution to the Strong CP Problem with a Harmless Axion"*, Phys. Lett. B104, 199 (1981).

[11] A. R. Zhitnitsky, *"On Possible Suppression of the Axion Hadron Interactions. (In Russian)"*, Sov. J. Nucl. Phys. 31, 260 (1980), [Yad. Fiz.31,497(1980)].

[12] M. B. Gavela, M. Ibe, P. Quilez and T. T. Yanagida, *"Automatic Peccei–Quinn symmetry"*, Eur. Phys. J. C79, 542 (2019), arXiv:1812.08174.

[13] M. K. Gaillard, M. B. Gavela, R. Houtz, P. Quilez and R. Del Rey, *"Color unified dynamical axion"*, Eur. Phys. J. C78, 972 (2018), arXiv:1805.06465.

[14] L. D. Duffy and K. van Bibber, *"Axions as Dark Matter Particles"*, New J. Phys. 11, 105008 (2009), arXiv:0904.3346.

[15] K. Freese, J. A. Frieman and A. V. Olinto, *"Natural inflation with pseudo - Nambu-Goldstone bosons"*, Phys. Rev. Lett. 65, 3233 (1990).

[16] J. Jaeckel and M. Spannowsky, *"Probing MeV to 90 GeV Axion-Like Particles with Lep and Lhc"*, Phys. Lett. B753, 482 (2016), arXiv:1509.00476.

[17] M. Bauer, M. Neubert and A. Thamm, *"Collider Probes of Axion-Like Particles"*, arXiv:1708.00443.

[18] T. Banks and N. Seiberg, *"Symmetries and Strings in Field Theory and Gravity"*, Phys. Rev. D83, 084019 (2011), arXiv:1011.5120.

[19] CAST Collaboration, M. Arik et al., *"Search for Solar Axions by the CERN Axion Solar Telescope with ^{3}He Buffer Gas: Closing the Hot Dark Matter Gap"*, Phys. Rev. Lett. 112, 091302 (2014), arXiv:1307.1985.

[20] ADMX Collaboration, N. Du et al., *"A Search for Invisible Axion Dark Matter with the Axion Dark Matter Experiment"*, Phys. Rev. Lett. 120, 151301 (2018), arXiv:1804.05750.

[21] K. Mimasu and V. Sanz, *"Alps at Colliders"*, JHEP 1506, 173 (2015), arXiv:1409.4792.

[22] Belle-II Collaboration, W. Altmannshofer et al., *"The Belle II Physics Book"*, edited by E. Kou and P. Urquijo, arXiv:1808.10567.

[23] X. Cid Vidal, A. Mariotti, D. Redigolo, F. Sala and K. Tobioka, *"New Axion Searches at Flavor Factories"*, arXiv:1810.09452.

[24] F. Feruglio, B. Gavela, K. Kanshin, P. A. N. Machado, S. Rigolin and S. Saa, *"The Minimal Linear Sigma Model for the Goldstone Higgs"*, JHEP 1606, 038 (2016), arXiv:1603.05668.

[25] A. Ringwald, *"Exploring the Role of Axions and Other WISPs in the Dark Universe"*, Phys. Dark Univ. 1, 116 (2012), arXiv:1210.5081.

[26] D. J. E. Marsh, *"Axion Cosmology"*, Phys. Rept. 643, 1 (2016), arXiv:1510.07633.

[27] S. Coleman, *"Aspects of Symmetry"*, Cambridge University Press 643, S. Coleman (1988).

[28] R. Bott, *"An application of the Morse theory to the topology of Lie-groups"*, Bulletin de la Société Mathématique de France 84, 251 (1956).

[29] Particle Data Group Collaboration, M. Tanabashi et al., *"Review of Particle Physics"*, Phys. Rev. D98, 030001 (2018).

[30] C. Vafa and E. Witten, *"Parity Conservation in QCD"*, Phys. Rev. Lett. 53, 535 (1984).

[31] ATLAS Collaboration, G. Aad et al., *"Observation of a new particle in the search for the Standard Model Higgs boson with the ATLAS detector at the LHC"*, Phys. Lett. B716, 1 (2012), arXiv:1207.7214.

[32] CMS Collaboration, S. Chatrchyan et al., *"Observation of a New Boson at a Mass of 125 GeV with the CMS Experiment at the LHC"*, Phys. Lett. B716, 30 (2012), arXiv:1207.7235.

[33] G. 't Hooft, *"Computation of the Quantum Effects Due to a Four-Dimensional Pseudoparticle"*, Phys. Rev. D14, 3432 (1976), [,70(1976)].

[34] L. F. Urrutia and J. D. Vergara, *"Anomalies in the Fujikawa method using parameter dependent regulators"*, Phys. Rev. D45, 1365 (1992).

[35] M. Srednicki, *"Axion Couplings to Matter. 1. CP Conserving Parts"*, Nucl. Phys. B260, 689 (1985).

[36] C. G. Callan, Jr., R. F. Dashen and D. J. Gross, *"The Structure of the Gauge Theory Vacuum"*, Phys. Lett. B63, 334 (1976), [,357(1976)].

[37] J. E. Kim, *"Light Pseudoscalars, Particle Physics and Cosmology"*, Phys. Rept. 150, 1 (1987).

[38] L. Calibbi, F. Goertz, D. Redigolo, R. Ziegler and J. Zupan, *"Minimal Axion Model from Flavor"*, Phys. Rev. D95, 095009 (2017), arXiv:1612.08040.

[39] Y. Ema, K. Hamaguchi, T. Moroi and K. Nakayama, *"Flaxion: a Minimal Extension to Solve Puzzles in the Standard Model"*, JHEP 1701, 096 (2017), arXiv:1612.05492.

[40] C. Boehm, M. J. Dolan, C. McCabe, M. Spannowsky and C. J. Wallace, *"Extended gamma-ray emission from Coy Dark Matter"*, JCAP 1405, 009 (2014), arXiv:1401.6458.

[41] C. Gordon and O. Macias, *"Dark Matter and Pulsar Model Constraints from Galactic Center Fermi-LAT Gamma Ray Observations"*, Phys. Rev. D88, 083521 (2013), arXiv:1306.5725, [Erratum: Phys. Rev.D89,no.4,049901(2014)].

[42] W. J. Marciano, A. Masiero, P. Paradisi and M. Passera, *"Contributions of Axionlike Particles to Lepton Dipole Moments"*, Phys. Rev. D94, 115033 (2016), arXiv:1607.01022.

[43] I. Brivio, M. B. Gavela, L. Merlo, K. Mimasu, J. M. No, R. del Rey and V. Sanz, *"Alps Effective Field Theory and Collider Signatures"*, arXiv:1701.05379.

[44] P. W. Graham and S. Rajendran, *"New Observables for Direct Detection of Axion Dark Matter"*, Phys. Rev. D88, 035023 (2013), arXiv:1306.6088.

[45] G. Alonso-Álvarez, M. B. Gavela and P. Quilez, *"Axion couplings to electroweak gauge bosons"*, Eur. Phys. J. C79, 223 (2019), arXiv:1811.05466.

[46] L. Harland–Lang, J. Jaeckel and M. Spannowsky, *"A fresh look at ALP searches in fixed target experiments"*, Phys. Lett. B793, 281 (2019), arXiv:1902.04878.

[47] C. Baldenegro, S. Fichet, G. von Gersdorff and C. Royon, *"Searching for axion-like particles with proton tagging at the LHC"*, JHEP 1806, 131 (2018), arXiv:1803.10835.

[48] D. Cadamuro and J. Redondo, *"Cosmological bounds on pseudo Nambu-Goldstone bosons"*, JCAP 1202, 032 (2012), arXiv:1110.2895.

[49] M. Millea, L. Knox and B. Fields, *"New Bounds for Axions and Axion-Like Particles with Kev-Gev Masses"*, Phys. Rev. D92, 023010 (2015), arXiv:1501.04097.

[50] L. Di Luzio, F. Mescia and E. Nardi, *"Redefining the Axion Window"*, Phys. Rev. Lett. 118, 031801 (2017), arXiv:1610.07593.

[51] I. G. Irastorza and J. Redondo, *"New experimental approaches in the search for axion-like particles"*, Prog. Part. Nucl. Phys. 102, 89 (2018), arXiv:1801.08127.

[52] R. Essig et al., *"Working Group Report: New Light Weakly Coupled Particles"*, arXiv:1311.0029, in: *"Proceedings, 2013 Community Summer Study on the Future of U.S. Particle Physics: Snowmass on the Mississippi (CSS2013): Minneapolis, MN, USA, July 29-August 6, 2013"*, http://www.slac.stanford.edu/econf/C1307292/docs/IntensityFrontier/NewLight-17.pdf.

[53] NA62 Collaboration, E. Cortina Gil et al., *"The Beam and detector of the NA62 experiment at CERN"*, JINST 12, P05025 (2017), arXiv:1703.08501.

[54] S. Alekhin et al., *"A facility to Search for Hidden Particles at the CERN SPS: the SHiP physics case"*, Rept. Prog. Phys. 79, 124201 (2016), arXiv:1504.04855.

[55] LHCb Collaboration, R. Aaij et al., *"Search for hidden-sector bosons in $B^0 \to K^{*0}\mu^+\mu^-$ decays"*, Phys. Rev. Lett. 115, 161802 (2015), arXiv:1508.04094.

[56] LHCb Collaboration, R. Aaij et al., *"Search for long-lived scalar particles in $B^+ \to K^+\chi(\mu^+\mu^-)$ decays"*, Phys. Rev. D95, 071101 (2017), arXiv:1612.07818.

[57] BaBar, Belle Collaboration, A. J. Bevan et al., *"The Physics of the B Factories"*, Eur. Phys. J. C74, 3026 (2014), arXiv:1406.6311.

[58] E. Masso and R. Toldra, *"On a light spinless particle coupled to photons"*, Phys. Rev. D52, 1755 (1995), hep-ph/9503293.

[59] M. J. Dolan, T. Ferber, C. Hearty, F. Kahlhoefer and K. Schmidt-Hoberg, *"Revised Constraints and Belle II Sensitivity for Visible and Invisible Axion-Like Particles"*, arXiv:1709.00009.

[60] P. deNiverville, H.-S. Lee and M.-S. Seo, *"Implications of the dark axion portal for the muon g-2, B-factories, fixed target neutrino experiments and beam dumps"*, Phys. Rev. D98, 115011 (2018), arXiv:1806.00757.

[61] M. J. Dolan, F. Kahlhoefer, C. McCabe and K. Schmidt-Hoberg, *"A Taste of Dark Matter: Flavour Constraints on Pseudoscalar Mediators"*, JHEP 1503, 171 (2015), arXiv:1412.5174, [Erratum: JHEP07,103(2015)].

[62] BaBar Collaboration, J. P. Lees et al., *"Evidence for an excess of $\bar{B} \to D^{(*)}\tau^-\bar{\nu}_\tau$ decays"*, Phys. Rev. Lett. 109, 101802 (2012), arXiv:1205.5442.

[63] BaBar Collaboration, J. P. Lees et al., *"Measurement of an Excess of $\bar{B} \to D^{(*)}\tau^-\bar{\nu}_\tau$ Decays and Implications for Charged Higgs Bosons"*, Phys. Rev. D88, 072012 (2013), arXiv:1303.0571.

[64] Belle Collaboration, M. Huschle et al., *"Measurement of the branching ratio of $\bar{B} \to D^{(*)}\tau^-\bar{\nu}_\tau$ relative to $\bar{B} \to D^{(*)}\ell^-\bar{\nu}_\ell$ decays with hadronic tagging at Belle"*, Phys. Rev. D92, 072014 (2015), arXiv:1507.03233.

[65] LHCb Collaboration, R. Aaij et al., *"Measurement of the ratio of branching fractions $\mathcal{B}(\bar{B}^0 \to D^{*+}\tau^-\bar{\nu}_\tau)/\mathcal{B}(\bar{B}^0 \to D^{*+}\mu^-\bar{\nu}_\mu)$"*, Phys. Rev. Lett. 115, 111803 (2015), arXiv:1506.08614, [Erratum: Phys. Rev. Lett.115,no.15,159901(2015)].

[66] Belle Collaboration, S. Hirose et al., *"Measurement of the τ lepton polarization and $R(D^*)$ in the decay $\bar{B} \to D^*\tau^-\bar{\nu}_\tau$"*, Phys. Rev. Lett. 118, 211801 (2017), arXiv:1612.00529.

[67] Belle Collaboration, Y. Sato et al., *"Measurement of the branching ratio of $\bar{B}^0 \to D^{*+}\tau^-\bar{\nu}_\tau$ relative to $\bar{B}^0 \to D^{*+}\ell^-\bar{\nu}_\ell$ decays with a semileptonic tagging method"*, Phys. Rev. D94, 072007 (2016), arXiv:1607.07923.

[68] Belle Collaboration, A. Abdesselam et al., *"Measurement of the branching ratio of $\bar{B}^0 \to D^{*+}\tau^-\bar{\nu}_\tau$ relative to $\bar{B}^0 \to D^{*+}\ell^-\bar{\nu}_\ell$ decays with a semileptonic tagging method"*, arXiv:1603.06711, in: *"Proceedings, 51st Rencontres de Moriond on Electroweak Interactions and Unified Theories: La Thuile, Italy, March 12-19, 2016"*.

[69] HFLAV Collaboration, Y. Amhis et al., *"Averages of b-hadron, c-hadron, and τ-lepton properties as of summer 2016"*, Eur. Phys. J. C77, 895 (2017), arXiv:1612.07233.

[70] MILC Collaboration, J. A. Bailey et al., *"$B \to Dl\nu$ form factors at nonzero recoil and $|V_{cb}|$ from 2+1-flavor lattice QCD"*, Phys. Rev. D92, 034506 (2015), arXiv:1503.07237.

[71] HPQCD Collaboration, H. Na, C. M. Bouchard, G. P. Lepage, C. Monahan and J. Shigemitsu, *"$B \to Dl\nu$ form factors at nonzero recoil and extraction of $|V_{cb}|$"*, Phys. Rev. D92, 054510 (2015), arXiv:1505.03925, [Erratum: Phys. Rev.D93,no.11,119906(2016)].

[72] S. Aoki et al., *"Review of lattice results concerning low-energy particle physics"*, Eur. Phys. J. C77, 112 (2017), arXiv:1607.00299.

[73] D. Bigi, P. Gambino and S. Schacht, *"$R(D^*)$, $|V_{cb}|$, and the Heavy Quark Symmetry relations between form factors"*, JHEP 1711, 061 (2017), arXiv:1707.09509.

[74] F. U. Bernlochner, Z. Ligeti, M. Papucci and D. J. Robinson, *"Combined analysis of semileptonic B decays to D and D^*: $R(D^{(*)})$, $|V_{cb}|$, and new physics"*, Phys. Rev. D95, 115008 (2017), arXiv:1703.05330, [erratum: Phys. Rev.D97,no.5,059902(2018)].

[75] LHCb Collaboration, R. Aaij et al., *"Measurement of the ratio of branching fractions $\mathcal{B}(B_c^+ \to J/\psi\tau^+\nu_\tau)/\mathcal{B}(B_c^+ \to J/\psi\mu^+\nu_\mu)$"*, Phys. Rev. Lett. 120, 121801 (2018), arXiv:1711.05623.

[76] LHCb Collaboration, R. Aaij et al., *"Test of lepton universality using $B^+ \to K^+\ell^+\ell^-$ decays"*, Phys. Rev. Lett. 113, 151601 (2014), arXiv:1406.6482.

[77] LHCb Collaboration, R. Aaij et al., *"Test of lepton universality with $B^0 \to K^{*0}\ell^+\ell^-$ decays"*, JHEP 1708, 055 (2017), arXiv:1705.05802.

[78] M. Bordone, G. Isidori and A. Pattori, *"On the Standard Model predictions for R_K and R_{K^*}"*, Eur. Phys. J. C76, 440 (2016), arXiv:1605.07633.

[79] J. E. Kim and G. Carosi, *"Axions and the Strong CP Problem"*, Rev. Mod. Phys. 82, 557 (2010), arXiv:0807.3125.

[80] M. Freytsis, Z. Ligeti and J. Thaler, *"Constraining the Axion Portal with $B \to Kl^+l^-$"*, Phys. Rev. D81, 034001 (2010), arXiv:0911.5355.

[81] E. Izaguirre, T. Lin and B. Shuve, *"A New Flavor of Searches for Axion-Like Particles"*, Phys. Rev. Lett. 118, 111802 (2017), arXiv:1611.09355.

[82] B. Döbrich, F. Ertas, F. Kahlhoefer and T. Spadaro, *"Model-independent bounds on light pseudoscalars from rare B-meson decays"*, Phys. Lett. B790, 537 (2019), arXiv:1810.11336.

[83] M. B. Gavela, R. Houtz, P. Quilez, R. del Rey and O. Sumensari, *"Flavor-Changing Constraints on Electroweak Alp Couplings"*, arXiv:1901.02031.

[84] G. Arcadi, *"2HDM portal for Singlet-Doublet Dark Matter"*, Eur. Phys. J. C78, 864 (2018), arXiv:1804.04930.

[85] BaBar Collaboration, J. P. Lees et al., *"Search for a light Higgs boson decaying to two gluons or $s\bar{s}$ in the radiative decays of $\Upsilon(1S)$"*, Phys. Rev. D88, 031701 (2013), arXiv:1307.5306.

[86] BaBar Collaboration, J. P. Lees et al., *"Search for a light Higgs resonance in radiative decays of the Y(1S) with a charm tag"*, Phys. Rev. D91, 071102 (2015), arXiv:1502.06019.

[87] BaBar Collaboration, P. del Amo Sanchez et al., *"Search for Production of Invisible Final States in Single-Photon Decays of $\Upsilon(1S)$"*, Phys. Rev. Lett. 107, 021804 (2011), arXiv:1007.4646.

[88] Belle Collaboration, I. S. Seong et al., *"Search for a Light Cp-Odd Higgs Boson and Low-Mass Dark Matter at the Belle Experiment"*, arXiv:1809.05222.

[89] BaBar Collaboration, B. Aubert et al., *"Search for Invisible Decays of a Light Scalar in Radiative Transitions $\upsilon_{3S} \to \gamma$ A0"*, arXiv:0808.0017, in: *"Proceedings, 34th International Conference on High Energy Physics (ICHEP 2008): Philadelphia, Pennsylvania, July 30-August 5, 2008"*, http://www-public.slac.stanford.edu/sciDoc/docMeta.aspx?slacPubNumber=slac-pub-13328.

[90] BaBar Collaboration, B. Aubert et al., *"Search for Dimuon Decays of a Light Scalar Boson in Radiative Transitions $\Upsilon \to \gamma A_0$"*, Phys. Rev. Lett. 103, 081803 (2009), arXiv:0905.4539.

[91] BaBar Collaboration, J. P. Lees et al., *"Search for di-muon decays of a low-mass Higgs boson in radiative decays of the $\Upsilon(1S)$"*, Phys. Rev. D87, 031102 (2013), arXiv:1210.0287, [Erratum: Phys. Rev.D87,no.5,059903(2013)].

[92] BaBar Collaboration, J. P. Lees et al., *"Search for a low-mass scalar Higgs boson decaying to a tau pair in single-photon decays of $\Upsilon(1S)$"*, Phys. Rev. D88, 071102 (2013), arXiv:1210.5669.

[93] H. Koiso, A. Morita, Y. Ohnishi, K. Oide and K. Satoh, *"Lattice of the KEKB colliding rings"*, PTEP 2013, 03A009 (2013).

[94] Y. Ohnishi et al., *"Accelerator design at SuperKEKB"*, PTEP 2013, 03A011 (2013).

[95] BaBar Collaboration, B. Aubert et al., *"A measurement of the total width, the electronic width, and the mass of the $\Upsilon(10580)$ resonance"*, Phys. Rev. D72, 032005 (2005), hep-ex/0405025.

[96] S. Eidelman, D. Epifanov, M. Fael, L. Mercolli and M. Passera, *"τ dipole moments via radiative leptonic τ decays"*, JHEP 1603, 140 (2016), arXiv:1601.07987.

[97] A. Gray, I. Allison, C. T. H. Davies, E. Dalgic, G. P. Lepage, J. Shigemitsu and M. Wingate, *"The Upsilon spectrum and m(b) from full lattice QCD"*, Phys. Rev. D72, 094507 (2005), hep-lat/0507013.

[98] R. Lewis and R. M. Woloshyn, *"Excited Upsilon Radiative Decays"*, Phys. Rev. D84, 094501 (2011), arXiv:1108.1137.

[99] A. Abada, D. Bečirević, M. Lucente and O. Sumensari, *"Lepton flavor violating decays of vector quarkonia and of the Z boson"*, Phys. Rev. D91, 113013 (2015), arXiv:1503.04159.

[100] F. Wilczek, *"Decays of Heavy Vector Mesons Into Higgs Particles"*, Phys. Rev. Lett. 39, 1304 (1977).

[101] J. R. Ellis, M. K. Gaillard, D. V. Nanopoulos and C. T. Sachrajda, *"Is the Mass of the Higgs Boson About 10-GeV?"*, Phys. Lett. 83B, 339 (1979).

[102] J. T. Pantaleone, M. E. Peskin and S. H. H. Tye, *"Bound State Effects in $\Upsilon \to \gamma$ + Resonance"*, Phys. Lett. 149B, 225 (1984).

[103] H. E. Haber, G. L. Kane and T. Sterling, *"The Fermion Mass Scale and Possible Effects of Higgs Bosons on Experimental Observables"*, Nucl. Phys. B161, 493 (1979).

[104] P. Fayet, *"U(1)(A) Symmetry in two-doublet models, U bosons or light pseudoscalars, and psi and Upsilon decays"*, Phys. Lett. B675, 267 (2009), arXiv:0812.3980.

[105] L. S. Dulian and A. Yu. Khodjamirian, *"LIGHT PSEUDOSCALAR AND SCALAR PARTICLES IN QUARKONIUM RADIATIVE DECAYS: QCD SUM RULES ESTIMATES"*, Z. Phys. C42, 243 (1989).

[106] BaBar Collaboration, B. Aubert et al., *"A Search for Invisible Decays of the Upsilon(1S)"*, Phys. Rev. Lett. 103, 251801 (2009), arXiv:0908.2840.

[107] B. McElrath, *"Invisible quarkonium decays as a sensitive probe of dark matter"*, Phys. Rev. D72, 103508 (2005), hep-ph/0506151.

[108] R. Dermisek, J. F. Gunion and B. McElrath, *"Probing NMSSM Scenarios with Minimal Fine-Tuning by Searching for Decays of the Upsilon to a Light CP-Odd Higgs Boson"*, Phys. Rev. D76, 051105 (2007), hep-ph/0612031.

[109] F. Domingo, U. Ellwanger, E. Fullana, C. Hugonie and M.-A. Sanchis-Lozano, *"Radiative Upsilon decays and a light pseudoscalar Higgs in the NMSSM"*, JHEP 0901, 061 (2009), arXiv:0810.4736.

[110] BaBar Collaboration, J. P. Lees et al., *"Search for Invisible Decays of a Dark Photon Produced in e^+e^- Collisions at BaBar"*, Phys. Rev. Lett. 119, 131804 (2017), arXiv:1702.03327.

[111] R. Essig, P. Schuster and N. Toro, *"Probing Dark Forces and Light Hidden Sectors at Low-Energy e+e- Colliders"*, Phys. Rev. D80, 015003 (2009), arXiv:0903.3941.

[112] D. B. Kaplan, H. Georgi and S. Dimopoulos, *"Composite Higgs Scalars"*, Phys. Lett. B136, 187 (1984).

[113] D. B. Kaplan and H. Georgi, *"$SU(2) \times$ U(1) Breaking by Vacuum Misalignment"*, Phys. Lett. B136, 183 (1984).

[114] T. Banks, *"Constraints on $SU(2) \times$ U(1) Breaking by Vacuum Misalignment"*, Nucl. Phys. B243, 125 (1984).

[115] K. Agashe, R. Contino and A. Pomarol, *"The Minimal Composite Higgs Model"*, Nucl. Phys. B719, 165 (2005), hep-ph/0412089.

[116] B. Gripaios, A. Pomarol, F. Riva and J. Serra, *"Beyond the Minimal Composite Higgs Model"*, JHEP 0904, 070 (2009), arXiv:0902.1483.

[117] J. Mrazek, A. Pomarol, R. Rattazzi, M. Redi, J. Serra and A. Wulzer, *"The Other Natural Two Higgs Doublet Model"*, Nucl. Phys. B853, 1 (2011), arXiv:1105.5403.

[118] R. Barbieri, B. Bellazzini, V. S. Rychkov and A. Varagnolo, *"The Higgs Boson from an Extended Symmetry"*, Phys. Rev. D76, 115008 (2007), arXiv:0706.0432.

[119] H. Gertov, A. Meroni, E. Molinaro and F. Sannino, *"Theory and Phenomenology of the Elementary Goldstone Higgs Boson"*, Phys. Rev. D92, 095003 (2015), arXiv:1507.06666.

[120] M. B. Gavela, K. Kanshin, P. A. N. Machado and S. Saa, *"The Linear/Non-Linear Frontier for the Goldstone Higgs"*, Eur. Phys. J. C76, 690 (2016), arXiv:1610.08083.

[121] R. Alonso, I. Brivio, B. Gavela, L. Merlo and S. Rigolin, *"Sigma Decomposition"*, JHEP 1412, 034 (2014), arXiv:1409.1589.

[122] G. Panico and A. Wulzer, *"The Composite Nambu-Goldstone Higgs"*, Lect. Notes Phys. 913, pp.1 (2016), arXiv:1506.01961.

[123] I. M. Hierro, L. Merlo and S. Rigolin, *"Sigma Decomposition: the Cp-Odd Lagrangian"*, JHEP 1604, 016 (2016), arXiv:1510.07899.

[124] F. Feruglio, *"The Chiral Approach to the Electroweak Interactions"*, Int. J. Mod. Phys. A8, 4937 (1993), hep-ph/9301281, in: *"International Conference on Mossbauer Effect Vancouver, British Columbia, Canada, September 1-3, 1993"*, 4937-4972p.

[125] B. Grinstein and M. Trott, *"A Higgs-Higgs Bound State Due to New Physics at a TeV"*, Phys. Rev. D76, 073002 (2007), arXiv:0704.1505.

[126] R. Contino, C. Grojean, M. Moretti, F. Piccinini and R. Rattazzi, *"Strong Double Higgs Production at the Lhc"*, JHEP 1005, 089 (2010), arXiv:1002.1011.

[127] R. Alonso, M. B. Gavela, L. Merlo, S. Rigolin and J. Yepes, *"The Effective Chiral Lagrangian for a Light Dynamical "Higgs Particle""*, Phys. Lett. B722, 330 (2013), arXiv:1212.3305, [Erratum: Phys. Lett.B726,926(2013)].

[128] R. Alonso, M. B. Gavela, L. Merlo, S. Rigolin and J. Yepes, *"Minimal Flavour Violation with Strong Higgs Dynamics"*, JHEP 1206, 076 (2012), arXiv:1201.1511.

[129] R. Alonso, M. B. Gavela, L. Merlo, S. Rigolin and J. Yepes, *"Flavor with a Light Dynamical "Higgs Particle""*, Phys. Rev. D87, 055019 (2013), arXiv:1212.3307.

[130] G. Buchalla, O. CatÃ and C. Krause, *"Complete Electroweak Chiral Lagrangian with a Light Higgs at Nlo"*, Nucl. Phys. B880, 552 (2014), arXiv:1307.5017, [Erratum: Nucl. Phys.B913,475(2016)].

[131] I. Brivio, T. Corbett, O. J. P. Aboli, M. B. Gavela, J. Gonzalez-Fraile, M. C. Gonzalez-Garcia, L. Merlo and S. Rigolin, *"Disentangling a Dynamical Higgs"*, JHEP 1403, 024 (2014), arXiv:1311.1823.

[132] I. Brivio, O. J. P. Aboli, M. B. Gavela, M. C. Gonzalez-Garcia, L. Merlo and S. Rigolin, *"Higgs Ultraviolet Softening"*, JHEP 1412, 004 (2014), arXiv:1405.5412.

[133] M. B. Gavela, J. Gonzalez-Fraile, M. C. Gonzalez-Garcia, L. Merlo, S. Rigolin and J. Yepes, *"CP Violation with a Dynamical Higgs"*, JHEP 1410, 044 (2014), arXiv:1406.6367.

[134] M. B. Gavela, K. Kanshin, P. A. N. Machado and S. Saa, *"On the Renormalization of the Electroweak Chiral Lagrangian with a Higgs"*, JHEP 1503, 043 (2015), arXiv:1409.1571.

[135] R. Alonso, E. E. Jenkins and A. V. Manohar, *"A Geometric Formulation of Higgs Effective Field Theory: Measuring the Curvature of Scalar Field Space"*, Phys. Lett. B754, 335 (2016), arXiv:1511.00724.

[136] B. M. Gavela, E. E. Jenkins, A. V. Manohar and L. Merlo, *"Analysis of General Power Counting Rules in Effective Field Theory"*, Eur. Phys. J. C76, 485 (2016), arXiv:1601.07551.

[137] R. Alonso, E. E. Jenkins and A. V. Manohar, *"Sigma Models with Negative Curvature"*, Phys. Lett. B756, 358 (2016), arXiv:1602.00706.

[138] O. J. P. Aboli and M. C. Gonzalez Garcia, *"Classifying the Bosonic Quartic Couplings"*, Phys. Rev. D93, 093013 (2016), arXiv:1604.03555.

[139] I. Brivio, J. Gonzalez-Fraile, M. C. Gonzalez-Garcia and L. Merlo, *"The Complete Heft Lagrangian After the Lhc Run I"*, Eur. Phys. J. C76, 416 (2016), arXiv:1604.06801.

[140] R. Alonso, E. E. Jenkins and A. V. Manohar, *"Geometry of the Scalar Sector"*, JHEP 1608, 101 (2016), arXiv:1605.03602.

[141] LHC Higgs Cross Section Working Group Collaboration, D. de Florian et al., *"Handbook of Lhc Higgs Cross Sections: 4. Deciphering the Nature of the Higgs Sector"*, arXiv:1610.07922.

[142] L. Merlo, S. Saa and M. SacristÃ¡n-Barbero, *"Baryon Non-Invariant Couplings in Higgs Effective Field Theory"*, Eur. Phys. J. C77, 185 (2017), arXiv:1612.04832.

[143] R. Alonso, K. Kanshin and S. Saa, *"Renormalization Group Evolution of Higgs Effective Field Theory"*, arXiv:1710.06848.

[144] G. Buchalla, O. Cata, A. Celis, M. Knecht and C. Krause, *"Complete One-Loop Renormalization of the Higgs-Electroweak Chiral Lagrangian"*, arXiv:1710.06412.

[145] I. Brivio, M. B. Gavela, S. Pascoli, R. del Rey and S. Saa, *"The Axion and the Goldstone Higgs"*, arXiv:1710.07715.

[146] D. B. Kaplan, *"Flavor at Ssc Energies: a New Mechanism for Dynamically Generated Fermion Masses"*, Nucl. Phys. B365, 259 (1991).

[147] R. Contino and A. Pomarol, *"Holography for Fermions"*, JHEP 0411, 058 (2004), hep-th/0406257.

[148] M. J. Dugan, H. Georgi and D. B. Kaplan, *"Anatomy of a Composite Higgs Model"*, Nucl. Phys. B254, 299 (1985).

[149] J. Galloway, J. A. Evans, M. A. Luty and R. A. Tacchi, *"Minimal Conformal Technicolor and Precision Electroweak Tests"*, JHEP 1010, 086 (2010), arXiv:1001.1361.

[150] G. D'Ambrosio, G. F. Giudice, G. Isidori and A. Strumia, *"Minimal Flavor Violation: an Effective Field Theory Approach"*, Nucl. Phys. B645, 155 (2002), hep-ph/0207036.

[151] V. Cirigliano, B. Grinstein, G. Isidori and M. B. Wise, *"Minimal Flavor Violation in the Lepton Sector"*, Nucl. Phys. B728, 121 (2005), hep-ph/0507001.

[152] S. Davidson and F. Palorini, *"Various Definitions of Minimal Flavour Violation for Leptons"*, Phys. Lett. B642, 72 (2006), hep-ph/0607329.

[153] R. Alonso, G. Isidori, L. Merlo, L. A. Munoz and E. Nardi, *"Minimal Flavour Violation Extensions of the Seesaw"*, JHEP 1106, 037 (2011), arXiv:1103.5461.

[154] D. N. Dinh, L. Merlo, S. T. Petcov and R. Vega-Alvarez, *"Revisiting Minimal Lepton Flavour Violation in the Light of Leptonic CP Violation"*, JHEP 1707, 089 (2017), arXiv:1705.09284.

[155] S. R. Coleman and E. J. Weinberg, *"Radiative Corrections as the Origin of Spontaneous Symmetry Breaking"*, Phys. Rev. D7, 1888 (1973).

[156] S. Dimopoulos and L. Susskind, *"Mass without Scalars"*, Nucl. Phys. B155, 237 (1979), in: *"Proceedings: International Conference on High Energy Physics, Geneva, Switzerland, Jun 27 - Jul 4, 1979: in 2 Volumes"*, 237-252p, [2,930(1979)].

[157] G. F. Giudice, R. Rattazzi and A. Strumia, *"Unificaxion"*, Phys. Lett. B715, 142 (2012), arXiv:1204.5465.

[158] M. Redi and A. Strumia, *"Axion-Higgs Unification"*, JHEP 1211, 103 (2012), arXiv:1208.6013.

[159] M. Redi and R. Sato, *"Composite Accidental Axions"*, JHEP 1605, 104 (2016), arXiv:1602.05427.

[160] M. Farina, D. Pappadopulo, F. Rompineve and A. Tesi, *"The Photo-Philic QCD Axion"*, JHEP 1701, 095 (2017), arXiv:1611.09855.

[161] L. Di Luzio, F. Mescia and E. Nardi, *"The Window for Preferred Axion Models"*, arXiv:1705.05370.

[162] R. Coy, M. Frigerio and M. Ibe, *"Dynamical Clockwork Axions"*, arXiv:1706.04529.

[163] F. Arias-Aragon and L. Merlo, *"The Minimal Flavour Violating Axion"*, arXiv:1709.07039.

[164] A. Manohar and H. Georgi, *"Chiral Quarks and the Nonrelativistic Quark Model"*, Nucl. Phys. B234, 189 (1984).

[165] B. Bellazzini, C. CsÃ¡ki and J. Serra, *"Composite Higgses"*, Eur. Phys. J. C74, 2766 (2014), arXiv:1401.2457.

[166] ATLAS, CMS Collaboration, G. Aad et al., *"Measurements of the Higgs Boson Production and Decay Rates and Constraints on Its Couplings from a Combined Atlas and Cms Analysis of the Lhc PP Collision Data at $\sqrt{s} = 7$ and 8 TeV"*, JHEP 1608, 045 (2016), arXiv:1606.02266.

[167] CMS Collaboration, C. Collaboration, *"Combined measurements of the Higgs boson's couplings at $\sqrt{s} = 13$ TeV"*.

[168] M. Carena, L. Da Rold and E. Pontan, *"Minimal Composite Higgs Models at the Lhc"*, JHEP 1406, 159 (2014), arXiv:1402.2987.

[169] M. E. Peskin and T. Takeuchi, *"Estimation of Oblique Electroweak Corrections"*, Phys. Rev. D46, 381 (1992).

[170] G. Altarelli and R. Barbieri, *"Vacuum Polarization Effects of New Physics on Electroweak Processes"*, Phys. Lett. B253, 161 (1991).

[171] I. Brivio, M. B. Gavela, L. Merlo, K. Mimasu, J. M. No, R. del Rey and V. Sanz, *"Non-Linear Higgs Portal to Dark Matter"*, JHEP 1604, 141 (2016), arXiv:1511.01099.

[172] P. Hernandez-Leon and L. Merlo, *"The Complete Bosonic Basis for a Higgs-Like Dilaton"*, arXiv:1703.02064.

[173] D. Espriu and B. Yencho, *"Longitudinal WW Scattering in Light of the Higgs Boson Discovery"*, Phys. Rev. D87, 055017 (2013), arXiv:1212.4158.

[174] D. Espriu, F. Mescia and B. Yencho, *"Radiative Corrections to Wl Wl Scattering in Composite Higgs Models"*, Phys. Rev. D88, 055002 (2013), arXiv:1307.2400.

[175] R. L. Delgado, A. Dobado and F. J. Llanes-Estrada, *"One-Loop W_LW_L and Z_LZ_L Scattering from the Electroweak Chiral Lagrangian with a Light Higgs-Like Scalar"*, JHEP 1402, 121 (2014), arXiv:1311.5993.

[176] R. L. Delgado, A. Dobado, M. J. Herrero and J. J. Sanz-Cillero, *"One-Loop $\gamma\gamma \to W_L^+W_L^-$ and $\gamma\gamma \to Z_LZ_L$ from the Electroweak Chiral Lagrangian with a Light Higgs-Like Scalar"*, JHEP 1407, 149 (2014), arXiv:1404.2866.

[177] R. L. Delgado, A. Dobado, D. Espriu, C. García-Garcia, M. J. Herrero, X. Marcano and J. J. Sanz-Cillero, *"Production of Vector Resonances at the LHC via WZ-Scattering: a Unitarized ECHL Analysis"*, arXiv:1707.04580.

[178] S. M. Barr and D. Seckel, *"Planck Scale Corrections to Axion Models"*, Phys. Rev. D46, 539 (1992).

[179] M. Kamionkowski and J. March-Russell, *"Planck Scale Physics and the Peccei-Quinn Mechanism"*, Phys. Lett. B282, 137 (1992), hep-th/9202003.

[180] R. Holman, S. D. H. Hsu, T. W. Kephart, E. W. Kolb, R. Watkins and L. M. Widrow, *"Solutions to the Strong CP Problem in a World with Gravity"*, Phys. Lett. B282, 132 (1992), hep-ph/9203206.

[181] R. Alonso and A. Urbano, *"Wormholes and Masses for Goldstone Bosons"*, arXiv:1706.07415.

[182] W. A. Bardeen, S. H. H. Tye and J. A. M. Vermaseren, *"Phenomenology of the New Light Higgs Boson Search"*, Phys. Lett. 76B, 580 (1978).

[183] P. Di Vecchia and G. Veneziano, *"Chiral Dynamics in the Large N Limit"*, Nucl. Phys. B171, 253 (1980).

[184] J. Alonso-González, L. Merlo, F. Pobbe, S. Rigolin and O. Sumensari, *"Testable Axion-Like Particles In The Minimal Linear σ Model"*, arXiv:1807.08643.

[185] L. Merlo, F. Pobbe and S. Rigolin, *"The Minimal Axion Minimal Linear σ Model"*, Eur. Phys. J. C78, 415 (2018), arXiv:1710.10500.

[186] M. Giannotti, I. G. Irastorza, J. Redondo, A. Ringwald and K. Saikawa, *"Stellar Recipes for Axion Hunters"*, JCAP 1710, 010 (2017), arXiv:1708.02111.

[187] A. Arvanitaki and A. A. Geraci, *"Resonantly Detecting Axion-Mediated Forces with Nuclear Magnetic Resonance"*, Phys. Rev. Lett. 113, 161801 (2014), arXiv:1403.1290.

[188] E. Armengaud et al., *"Conceptual Design of the International Axion Observatory (Iaxo)"*, JINST 9, T05002 (2014), arXiv:1401.3233.

[189] CAST Collaboration, V. Anastassopoulos et al., *"New Cast Limit on the Axion-Photon Interaction"*, Nature Phys. 13, 584 (2017), arXiv:1705.02290.

[190] N. Craig, A. Hook and S. Kasko, *"The Photophobic Alp"*, arXiv:1805.06538.

[191] A. de Gouvea, D. Hernandez and T. M. P. Tait, *"Criteria for Natural Hierarchies"*, Phys. Rev. D89, 115005 (2014), arXiv:1402.2658.

[192] L3 Collaboration, M. Acciarri et al., *"Search for Anomalous Z –≫ Gamma Gamma Gamma Events at Lep"*, Phys. Lett. B345, 609 (1995).

[193] DELPHI Collaboration, E. Anashkin et al., *"An Analysis of E+ E- –≫ Gamma Gamma (Gamma) at Lep at S(1/2) Approximately 189-Gev"*, in: *"Proceedings, International Europhysics Conference on High Energy Physics (Eps-Hep 1999): Tampere, Finland, July 15-21, 1999"*, http://cdsweb.cern.ch/search.py?sysno=000339520cer.

[194] L. Merlo, F. Pobbe, S. Rigolin and O. Sumensari, *"Revisiting the production of ALPs at B-factories"*, JHEP 1906, 091 (2019), arXiv:1905.03259.

[195] Belle Collaboration, J. Grygier et al., *"Search for $B \to h\nu\bar{\nu}$ decays with semileptonic tagging at Belle"*, Phys. Rev. D96, 091101 (2017), arXiv:1702.03224, [Addendum: Phys. Rev.D97,no.9,099902(2018)].

[196] S. Cunliffe, *"Prospects for Rare B Decays at Belle II"*, arXiv:1708.09423, in: *"Meeting of the Aps Division of Particles and Fields (Dpf 2017) Batavia, Illinois, Usa, July 31-August 4, 2017"*, http://inspirehep.net/record/1620904/files/arXiv:1708.09423.pdf.

[197] J. L. Feng, T. Moroi, H. Murayama and E. Schnapka, *"Third Generation Familons, B Factories, and Neutrino Cosmology"*, Phys. Rev. D57, 5875 (1998), hep-ph/9709411.

[198] BaBar Collaboration, J. P. Lees et al., *"Search for hadronic decays of a light Higgs boson in the radiative decay $\Upsilon \to \gamma A^0$"*, Phys. Rev. Lett. 107, 221803 (2011), arXiv:1108.3549.

[199] CLEO Collaboration, T. E. Coan et al., *"Flavor - Specific Inclusive B Decays to Charm"*, Phys. Rev. Lett. 80, 1150 (1998), hep-ex/9710028.

[200] F. Pobbe, A. Wulzer and M. Zanetti, *"Setting limits on Effective Field Theories: the case of Dark Matter"*, JHEP 1708, 074 (2017), arXiv:1704.00736.